# Heavy Quark Threshold Dynamics in Higher Order

Dissertation
zur Erlangung des Doktorgrades
des Departments Physik
der Universität Hamburg

vorgelegt von
Jan Heinrich Piclum
aus Krefeld

Hamburg
2007

| | |
|---|---|
| Gutachter der Dissertation: | Prof. Dr. Matthias Steinhauser<br>Prof. Dr. Bernd A. Kniehl<br>Prof. Dr. Thomas Gehrmann |
| Gutachter der Disputation: | Prof. Dr. Matthias Steinhauser<br>Prof. Dr. Jochen Bartels |
| Datum der Disputation: | 24. April 2007 |
| Vorsitzende<br>des Prüfungsausschusses: | Prof. Dr. Caren Hagner |
| Vorsitzender<br>des Promotionsausschusses: | Prof. Dr. Günther Huber |
| Departmentleiter: | Prof. Dr. Robert Klanner |
| Dekan der Fakultät für Mathematik,<br>Informatik und Naturwissenschaften: | Prof. Dr. Arno Frühwald |

## Abstract

In this work we discuss an important building block for the next-to-next-to-next-to leading order corrections to the pair production of top quarks at threshold. Specifically, we explain the calculation of the third order strong corrections to the matching coefficient of the vector current in non-relativistic Quantum Chromodynamics and provide the result for the fermionic part, containing at least one loop of massless quarks. As a byproduct, we obtain the matching coefficients of the axial-vector, pseudo-scalar and scalar current at the same order. Furthermore, we calculate the three-loop corrections to the quark renormalisation constants in the on-shell scheme in the framework of dimensional regularisation and dimensional reduction. Finally, we compute the third order strong corrections to the chromomagnetic interaction in Heavy Quark Effective Theory. The calculational methods are discussed in detail and results for the master integrals are given.



## Zusammenfassung

In dieser Arbeit wird ein wichtiger Baustein der Korrekturen der nächst-nächst-nächst-führenden Ordnung zur Paarerzeugung von Topquarks an der Schwelle behandelt. Insbesondere wird die Berechnung der starken Korrekturen dritter Ordnung zum Anpassungskoeffizienten des Vektorstroms in der nichtrelativistischen Quantenchromodynamik besprochen und das Ergebnis für die fermionischen Korrekturen mit mindestens einer masselosen Quarkschleife angegeben. Als Nebenprodukt erhalten wir die Anpassungskoeffizienten des pseudoskalaren, skalaren und des Axialvektorstroms zur gleichen Ordnung. Außerdem berechnen wir die Dreischleifenkorrekturen für die Quark-Renormierungskonstanten im Onshell-Schema in dimensionaler Regularisierung und dimensionaler Reduktion. Schlussendlich berechnen wir auch die starken Korrekturen dritter Ordnung zur chromomagnetischen Wechselwirkung in der Heavy Quark Effective Theory. Die Rechenmethoden werden im Detail erläutert und Ergebnisse für die Masterintegrale angegeben.

# Contents

# Introduction

The top quark was discovered at the Tevatron in 1995. To date it is the heaviest elementary particle with a mass of $170.9 \pm 1.8$ GeV [1]. Since this is much larger than the mass of any other fermion and also roughly twice as large as the mass of the electroweak gauge bosons, one can wonder whether or not the top quark really is an elementary particle. Furthermore, if it is elementary, can its mass be generated by the same mechanism than the mass of the other particles? After all, its mass is almost six orders of magnitude larger than the electron mass. On the other hand, the top quark is also essential for our understanding of the standard model itself. The reason is that precision observables like the W-boson mass or the effective weak mixing angle depend on the top-quark mass through radiative corrections. If we want to reduce the errors on these quantities, it is therefore necessary to reduce the error on the top-quark mass as well.

To address these and other issues, it is necessary to perform precision measurements of the top-quark properties. Next to its mass, its total decay width and Yukawa coupling are of special interest. Concerning the mass, it is expected that the uncertainty will be reduced to about 1 GeV at the Large Hadron Collider (LHC). However, the width and Yukawa coupling cannot be measured to a very good accuracy either at the Tevatron or at the LHC. This would change at a future International Linear Collider (ILC). Such a collider offers the unique ability to perform a scan of the pair production threshold and thus to measure the corresponding cross section with a very high experimental accuracy [2]. Next to an unrivalled determination of the top-quark properties, this also provides the possibility to extract the strong coupling constant, $\alpha_s$, with high precision. For example, it is expected that the top-quark mass can be measured with better than 100 MeV accuracy. However, in order to extract these quantities from the measured cross section, it is mandatory to have a theoretical prediction for the cross section which equals the measurement in precision.

From a theoretical point of view, the calculation of the cross section is very interesting, since the top quark pairs behave non-relativistically at threshold. It is therefore necessary to employ the framework of a non-relativistic effective theory to perform the calculations. This, in turn, offers the possibility to test this concept. Furthermore, due to its large width, the top quark system is essentially perturbative, meaning that non-perturbative effects are suppressed and perturbative calculations

should work very well.

The status of the theoretical evaluation of the top-anti-top production cross section at threshold is as follows. The next-to-next-to leading order (NNLO) calculation was performed by several groups and the results were compiled in Ref. [3]. It turned out that the NNLO correction is very large. Using so-called threshold mass definitions one obtains a stable peak position. However, the overall normalisation is by far not good enough to perform precise extractions of the width and the Yukawa coupling. Furthermore, the results have a large scale dependence and also vary between the different calculational frameworks.

As a consequence, it is necessary to calculate even higher order corrections. This can be done in two ways. On the one hand, one can calculate the cross section to one order higher in fixed order perturbation theory, namely at next-to-next-to-next-to leading order ($N^3LO$), and on the other hand one can go beyond fixed order perturbation theory and resum logarithms to next-to-next-to leading logarithmic (NNLL) order. Partial results exist for both approaches. At the moment, the uncertainty is estimated to be 6% [4] or 10% [5]. This number should be reduced to about 3% in order to meet the expected experimental precision [2].

In this work we consider the third order strong corrections to the matching coefficient of the vector current in non-relativistic Quantum Chromodynamics (NRQCD). In particular, we evaluate the fermionic part, containing at least one closed loop of massless quarks. As a byproduct, we obtain the corrections to the matching coefficients of the axial-vector, pseudo-scalar and scalar current at the same order. Parts of the results have been published in Refs. [6, 7]

The quark mass and wave function renormalisation constants in the on-shell scheme are crucial inputs not only for our calculation of the matching coefficients, but also for many other calculations. In particular, the relation between the pole and minimally subtracted mass is an important quantity. While the former is the appropriate definition for processes where the energy scale is much larger than the quark mass, the latter is important for threshold processes. Therefore, it is necessary to relate both mass definitions with high accuracy.

Both renormalisation constants and the relation between the pole and minimally subtracted mass are known to third order in Quantum Chromodynamics (QCD) [8–11] in the framework of dimensional regularisation (DREG). However, they are not applicable in the context of supersymmetric theories, since DREG breaks supersymmetry. It is therefore desirable to know these quantities also in a regularisation scheme which preserves supersymmetry. A first step was done in Refs. [12, 13], where the on-shell mass renormalisation constant was considered in the framework of dimensional regularisation (DRED).

In this work we consider the third order QCD corrections to the quark on-shell mass and wave function renormalisation constants in the framework of DREG and DRED. The former constitutes an independent check on the analytical results in the literature, while the latter is interesting in the context of supersymmetry. Our

results for the former and the relation between the pole and minimally subtracted mass in DRED have been published in Ref. [14].

The anomalous magnetic moment of the electron and the muon belong to the most precisely measured quantities in particle physics [15, 16]. The former agrees very well with the theoretical prediction, which leads to a very precise determination of the fine structure constant $\alpha$ [17]. However, in the case of the muon, the theoretical and experimental values disagree by more than three standard deviations (see Ref. [18] for a recent review). If this behaviour remains in future experiments, it is a strong hint for physics beyond the standard model.

The magnetic moments of heavy quarks can of course not be determined to such accuracy. However, the couplings of top quarks to photons or Z bosons, are very interesting due to the large mass of the top quark. This makes them very susceptible to contributions from physics beyond the standard model. Furthermore, due to their colour charges, quarks have a chromomagnetic moment as well. This quantity is interesting in the context of Heavy Quark Effective Theory (HQET), where it enters the matching coefficient of the chromomagnetic interaction. As such it can be tested in lattice simulations.

Here we determine the third order QCD corrections to the chromomagnetic moment of heavy quarks. This computation also provides us with the matching coefficient and anomalous dimension of the chromomagnetic interaction in HQET. As byproducts we recalculate the three-loop contribution to the electron magnetic moment in Quantum Electrodynamics and determine the three-loop QCD correction to the quark magnetic moment.

The structure of this work is as follows. In Chapter 1 NRQCD is introduced, the calculation of the matching coefficients is explained in detail and the results are given. Chapter 2 is concerned with the calculation of the quark mass and wave function renormalisation constants in the on-shell scheme. In Chapter 3 we explain the calculation of the chromomagnetic moment of a heavy quark. Our conclusions are presented in Chapter 4 together with an outlook of what remains to be done. In the Appendix we explain some of the calculational techniques in more detail. The used program packages are introduced and we provide results for all needed master integrals.

# Chapter 1

# Matching Coefficients

This chapter contains the main result of this thesis, namely the fermionic three-loop corrections to the matching coefficient of the vector current. It is presented in Section 1.2.3. Furthermore, the results for the matching coefficients of the axial-vector, pseudo-scalar and scalar current are given to the same order in Sections 1.3–1.5. Part of the results given in this chapter have been published in Refs. [6, 7].

## 1.1 NRQCD

In this section we explain the theoretical framework which is used to describe the behaviour of top-anti-top quark pairs at the production threshold, non-relativistic Quantum Chromodynamics (NRQCD) [19, 20] (see Ref. [21] for a recent review). We explain why it is necessary to turn to an effective theory, how the theory is constructed and how the cross section is calculated within this theory.

### 1.1.1 Why NRQCD?

If we consider the production of heavy quarks at threshold, we find that the relative velocity of quark and anti-quark is of the order of the strong coupling evaluated at the scale given by the quark mass times the velocity, $v \sim \alpha_s(m_Q v)$. Thus, for heavy quarks the velocity is small. This leads to a problem when we calculate processes like the threshold production cross section of heavy quarks, since two small parameters are involved, the strong coupling and the relative velocity. In general, we will encounter corrections proportional to $(\alpha_s/v)^n$, where $n$ is the number of loops of the considered diagram. Since numerator and denominator are of the same order, the contributions of higher loop orders cannot be neglected. This spoils the perturbative expansion.

On the other hand, the fact that the relative velocity is small, provides us with the opportunity to apply the framework of an effective theory. This is based on the

observation that the relevant scales of the problem, the quark mass ($m_Q$), the quark momentum ($\sim m_Q v$) and the kinetic energy ($\sim m_Q v^2$), are well separated. They adhere to the hierarchy

$$m_Q \gg m_Q v \gg m_Q v^2 \gg \Lambda_{\mathrm{QCD}}\,, \tag{1.1}$$

where $\Lambda_{\mathrm{QCD}}$ is the typical hadronic scale.

By "integrating out" the hard modes of order $m_Q$ from QCD, we turn to an effective theory which describes the behaviour of heavy quarks and anti-quarks at energy scales which are smaller than their masses. In this theory the contributions proportional to $(\alpha_s/v)^n$ are automatically resummed to all orders in perturbation theory.

### 1.1.2 Construction of (p)NRQCD

The symmetries of NRQCD are SU(3) gauge symmetry, rotational symmetry, charge conjugation and parity. Additionally, there is a heavy-quark phase symmetry, which imposes separate conservation of heavy quark and anti-quark number. Up to corrections of order $v^2$, there is also a heavy-quark spin symmetry, which independently mixes the two spin components of the heavy quark and anti-quark. Since we are dealing with a non-relativistic theory, NRQCD is of course not Lorentz invariant, but only has the rotational symmetry mentioned above.

The Lagrangian of NRQCD is ordered in powers of $1/m_Q$. Each order can be constructed by writing down all operators, which describe the low energy behaviour of QCD (with respect to the hierarchy of Eq. (1.1)) at the specified order and are allowed by the theory's symmetries. Each operator is multiplied by a coupling constant of the effective theory, the so-called Wilson or matching coefficient. These coefficients are determined by requiring that NRQCD exactly reproduces the QCD results at each order in the $1/m_Q$ expansion.

There is, however, another way to construct the Lagrangian, which is more intuitive. It is based on expansion-by-region in the form of the so-called threshold expansion [22, 23]. With this method, the effective theory can be constructed by considering expansions of QCD diagrams around the threshold region. The relevant momentum regions are

$$\begin{aligned}
&\text{hard:} && k_0 \sim m_Q\,, && k_i \sim m_Q\,, && (1.2)\\
&\text{soft:} && k_0 \sim m_Q v\,, && k_i \sim m_Q v\,, && (1.3)\\
&\text{potential:} && k_0 \sim m_Q v^2\,, && k_i \sim m_Q v\,, && (1.4)\\
&\text{ultrasoft:} && k_0 \sim m_Q v^2\,, && k_i \sim m_Q v^2\,, && (1.5)
\end{aligned}$$

where $k$ is a loop momentum of the considered diagram and $i \in \{1,2,3\}$. The hierarchy of the scales is given by Eq. (1.1). The full result of a Feynman integral is

given by the sum over the integrals of all momentum regions, where the integrands are expanded accordingly.

The full theory, QCD, contains all momentum regions, whereas NRQCD does not contain contributions from the hard region. In this way, it is easy to see that the matching coefficients are determined entirely by the hard momentum region. To illustrate this, let us consider an example with only two scales, hard and soft (an example of such a theory is Heavy Quark Effective Theory (HQET) [24]). In the full theory the Greens function $\Gamma$, corresponding to some operator, receives contributions from both regions, while the Greens function $\tilde{\Gamma}$, corresponding to the same operator in the effective theory, receives only soft contributions. The matching equation is given by

$$\Gamma = C\,\tilde{\Gamma}\,. \tag{1.6}$$

At next-to leading order (NLO) we have

$$\begin{aligned} 1+\Gamma_h+\Gamma_s+\ldots &= (1+C^{\mathrm{NLO}}+\ldots)(1+\Gamma_s+\ldots) \\ &= 1+C^{\mathrm{NLO}}+\Gamma_s+\ldots\,, \end{aligned} \tag{1.7}$$

where the ellipses denote higher order terms and the subscripts label the contributions from different regions. Thus, at NLO we immediately see that $C = 1+\Gamma_h$. Starting at next-to-next-to leading order (NNLO), there are interference terms on the right hand side. In the full theory there are contributions where some loop momenta are hard and some are soft. These mixed terms correspond exactly to each other, so that the matching coefficient is determined to all orders by the hard contributions of the full theory.

The construction of the effective theory with the method of expansion-by-region is particularly useful since it also provides an implicit definition of NRQCD within dimensional regularisation. This is especially important for the matching, since most calculations in QCD are performed within this framework.

So far, we have only used the fact that the scale given by the heavy-quark mass is much larger than all other scales. However, if we consider a physical process with a typical scale of the order of the binding energy, $m_Q v^2$, NRQCD still contains degrees of freedom, which cannot appear as physical states. From the effective theory point of view, these scales should also be integrated out. The corresponding theory is called potential NRQCD (pNRQCD) [25]. Next to the hard mode, the soft quarks and gluons and the potential gluons are integrated out as well. The matching to QCD is performed in two steps. In a first step pNRQCD is matched to NRQCD at the soft scale and in a second step NRQCD is matched to QCD at the hard scale. It is interesting to note that the potentials of the non-relativistic Schrödinger equation appear as matching coefficients of four-quark operators in pNRQCD (hence the name of the theory).

Let us for completeness mention that another effective theory, velocity NRQCD (vNRQCD), was proposed in Ref. [26]. The theory contains potential heavy quarks

and soft and ultrasoft gluons and light quarks. Only ultrasoft energies and momenta are treated as continuous variables, while soft energies and momenta are treated as discreet indices. For example, the heavy quark energy and momentum are written as $E = k_0$ and $P_i = p_i + k_i$, respectively, where $p_i \sim m_Q v$ and $k_0, k_i \sim m_Q v^2$. An important difference to pNRQCD is the fact that vNRQCD is matched directly to QCD.

### 1.1.3 $t\bar{t}$ Cross Section in NRQCD

Let us first specify the power counting corresponding to the cross section in the effective theory. At leading order (LO) the cross section is proportional to $v$ due to the phase space integral. Furthermore, it contains all terms proportional to $(\alpha_s/v)^n$, $n = 0, 1, 2, \ldots$, due to the resummation of these terms in NRQCD. The NLO cross section contains all additional terms of order $\mathcal{O}(\alpha_s)$ and $\mathcal{O}(v)$. At NNLO terms of order $\mathcal{O}(\alpha_s^2)$, $\mathcal{O}(\alpha_s v)$ and $\mathcal{O}(v^2)$ have to be included as well.

To calculate the production cross section of top-quark pairs at threshold, it is convenient to employ the optical theorem. Accordingly, the total cross section is proportional to the imaginary part of current correlators. In particular, the cross section for virtual photon and $Z$-boson exchange reads [3]

$$\begin{aligned}
\sigma_{\text{tot}}^{\gamma,Z}(q^2) &= \sigma_{\text{tot}}(e^+e^- \to \gamma^*, Z^* \to t\bar{t}) \\
&= \frac{4\pi\alpha^2}{3q^2}\Bigg\{ \left[ Q_t^2 - \frac{2q^2}{q^2 - M_Z^2} v_e v_t Q_t + \left(\frac{q^2}{q^2 - M_Z^2}\right)^2 \left(v_e^2 + a_e^2\right) v_t^2 \right] R_v(q^2) \\
&\qquad + \left(\frac{q^2}{q^2 - M_Z^2}\right)^2 \left(v_e^2 + a_e^2\right) a_t^2 R_a(q^2) \Bigg\} . \qquad (1.8)
\end{aligned}$$

where the vector and axial-vector coupling of the $Z$ boson to a fermion $f$ are given by

$$v_f = \frac{T_3^f - 2Q_f \sin^2\theta_w}{2\sin\theta_w \cos\theta_w} , \qquad (1.9)$$

$$a_f = \frac{T_3^f}{2\sin\theta_w \cos\theta_w} . \qquad (1.10)$$

$\alpha$ is Sommerfeld's fine-structure constant, $\theta_w$ is the weak mixing angle and $M_Z$ is the $Z$-boson mass. $Q_f$ and $T_3^f$ denote the charge in units of the positron charge and the third component of the weak isospin of fermion $f$, respectively. $R_v$ and $R_a$ are given by

$$R_k(q^2) = \frac{4\pi}{q^2}\text{Im}\left[ -i \int \mathrm{d}^4x\, e^{i\,q\cdot x} \langle 0|\mathcal{T}\, j_{k\mu}(x) j_k^\mu(0)|0\rangle \right] , \qquad (1.11)$$

where $k \in \{v, a\}$, $\mathcal{T}$ denotes the time-ordered product and $j_v^\mu$ and $j_a^\mu$ are the vector and axial-vector current, respectively.

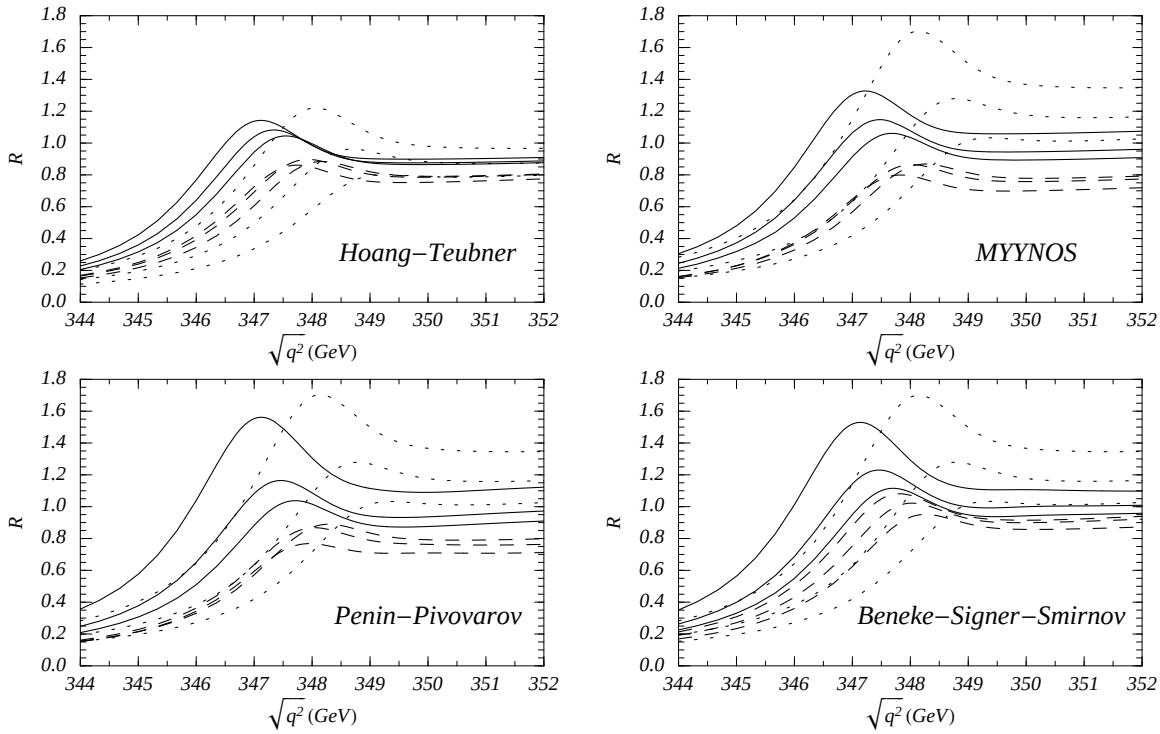


Figure 1.1: Total photon-induced cross section at threshold using the pole mass. Dotted, dashed and solid curves correspond to LO, NLO and NNLO results, respectively. The different lines of same order correspond to different values of the soft scale. The plots are taken from Ref. [3].

Going to the effective theory, we have to replace the currents by their NRQCD counterparts times the corresponding matching coefficients. Thus, to calculate the cross section, we essentially need two ingredients: the matching coefficients and the current correlators in NRQCD. The former are determined by a calculation in the full theory, while it can be shown (see for example §125 of Ref. [27]) that the latter correspond to the solution of the Schrödinger equation in the effective theory.

At the moment, the production cross section of top-quark pairs at threshold is known at NNLO. The corresponding calculation was done by several groups [28–34], both in velocity and potential NRQCD, and is summarised in Ref. [3]. Their results for the total photon-induced cross section in the pole mass scheme are depicted in Fig. 1.1. In the following, we briefly discuss the findings of Ref. [3].

The general shape of the cross section can be understood as being the remnant of a would-be 1S toponium state. Due to its large width, which is of the order of the ultrasoft scale, the top quark decays before it can form bound states. Therefore, there is only one peak in the threshold region, in contrast with charm or bottom quarks. Additionally, the peak is smeared out. The peak position is given by twice the top-quark mass minus the binding energy of the top-anti-top system and can thus be used to determine the top-quark mass. The shape, on the other hand,

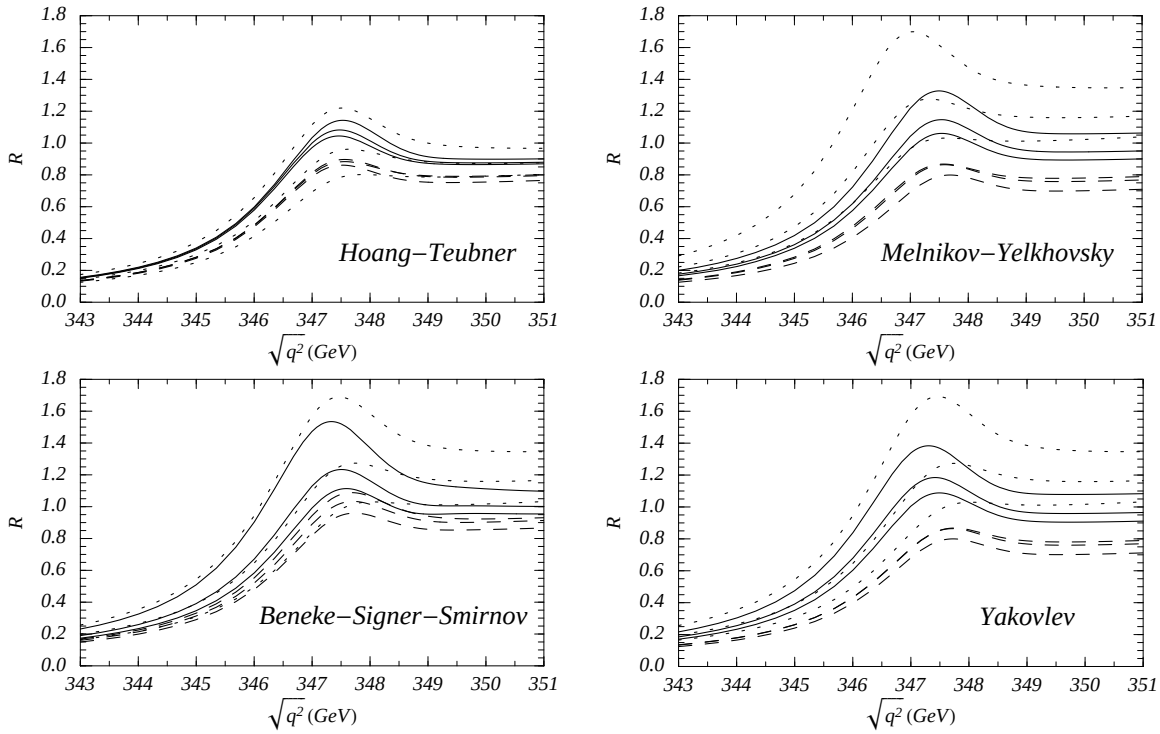


Figure 1.2: Total photon-induced cross section at threshold using the 1S (Hoang-Teubner), the kinetic (Melnikov-Yelkhovsky) and the potential-subtracted (Beneke-Signer-Smirnov and Yakovlev) mass. The plots are taken from Ref. [3].

depends on the total width, the Yukawa coupling to the Higgs boson and $\alpha_s$.

The different plots of Fig. 1.1 show that the NNLO result suffers from a large dependence on the so-called soft scale, $\mu_s$. In particular, this scale dependence grows when one goes from NLO to NNLO. Furthermore, the convergence is quite bad. The scale variation of the NLO result clearly underestimates the NNLO correction. This also leads to a large uncertainty in the normalisation, which is estimated to be 20% [3]. In turn, this would lead to large theoretical errors in the extraction of the top-quark parameters and $\alpha_s$.

The peak position also receives large corrections at higher orders. In Ref. [3] it is therefore estimated that an extraction of the pole mass would have an uncertainty of about 300 MeV, which is larger than the expected experimental uncertainty [2]. The uncertainty due to the different calculational methods is estimated to be about 80 MeV at NNLO. While this number is quite large, it is not the dominating error source.

The problem with the pole mass is that it receives large corrections from energy (distance) scales which are smaller (larger) than the physically relevant scale. This is known as the renormalon problem [35, 36]. As a result, any determination of the pole mass will have an error of at least $\Lambda_{\rm QCD}$. To circumvent this problem, one can turn to mass definitions which are better suited for short-distance physics.

For the $t\bar{t}$ production at threshold, there are several possibilities to define a so-called threshold mass. The ones which were used for the NNLO calculation are the 1S mass [29], the potential-subtracted (PS) mass [37] and the kinetic mass [38]. The results are shown in Fig. 1.2. Compared to Fig. 1.1, the peak position is now more stable. Thus, an extraction of those masses is far more precise. The uncertainty is estimated in Ref. [3] to be about 100 MeV. Since the relationships between the threshold masses and the mass defined in the modified minimal subtraction ($\overline{\text{MS}}$) scheme [39] are known to high precision[1], it is also possible to obtain the latter with a similar uncertainty.

The overall normalisation and scale dependence of the cross section also improves when one turns to threshold mass definitions. However, both are still not good enough to match the experimental precision in the extraction of the top-quark Yukawa coupling, total width and $\alpha_s$. As a consequence, it is mandatory to calculate even higher order corrections. There are basically two approaches to do this. On the one hand, one can evaluate the next term in fixed order perturbation theory and calculate the cross section at N$^3$LO, and on the other hand one can go beyond fixed order perturbation theory and resum logarithms to next-to-next-to leading logarithmic (NNLL) order. In the end, it could very well be that both calculations are necessary.

In recent years, quite a lot of effort has gone into the calculation of higher order contributions, leading to quite a lot of results. Concerning the NNLL calculation, there are partial results in the framework of vNRQCD [40, 41] and pNRQCD [5, 42]. These results already show a better scale dependence. However, the convergence of the different orders is still not satisfactory. At N$^3$LO, the pNRQCD Hamiltonian was found in Ref. [43]. Corrections to the energy levels and the wave function were calculated in Refs. [44–46].

Another important point is the correct inclusion of the top-quark width [47] and of electroweak effects. The former has been addressed in Refs. [48, 49], where absorptive parts of the matching coefficients were calculated. Concerning the latter, the order $\mathcal{O}(\alpha)$ corrections were calculated in Ref. [50] and the full Higgs mass dependence of order $\mathcal{O}(\alpha\alpha_s)$ of the matching coefficient of the vector current was evaluated in Ref. [51].

To date, there are still some important ingredients missing. Next to the NNLL corrections, the electroweak corrections of order $\mathcal{O}(\alpha\alpha_s)$ have to be completed. For the three-loop static potential there exists only a rough estimate [52] based on a Padé approximation. Even though the contribution seems to be small, it is of course desirable to have an exact calculation. At N$^3$LO, ultrasoft corrections to the wave function appear for the first time. The results for these contributions are still not known. Furthermore, the matching coefficients of the vector and axial-vector current are needed to order $\mathcal{O}(\alpha_s^3)$ and $\mathcal{O}(\alpha_s)$, respectively. These corrections are

[1] An essential ingredient in these relationships is the relation between the pole and the $\overline{\text{MS}}$ mass (see for example Ref. [37]), which is discussed in Chapter 2.

considered in the following.

## 1.2 The Vector Current

In this section we discuss the matching coefficient of the vector current. After the definition of the currents in the full and effective theory in Section 1.2.1, Sections 1.2.2 and 1.2.3 explain the calculation and provide the results, respectively. A discussion of the phenomenological impact of the result is given in Section 1.2.4.

### 1.2.1 The Matching Procedure

In the full theory, QCD, the vector current in coordinate space is defined as

$$j_v^\mu = \overline{\psi}\,\gamma^\mu\,\psi\,, \tag{1.12}$$

where $\psi$ is a four-component Dirac spinor. To find the corresponding operator in the effective theory, this expression has to be expanded in the relative velocity $v = p/m_Q$ of the quarks. This is most conveniently done in momentum space, where the vector current is given by

$$J_v^\mu = \overline{v}\,(-\vec{p})\;\gamma^\mu\,u\,(\vec{p})\;. \tag{1.13}$$

$v$ and $u$ are Dirac spinors in momentum space. They can be decomposed into two-component Pauli spinors in the form

$$\begin{aligned} v\,(\vec{p}) &= \sqrt{\frac{E+m_Q}{2m_Q}}\begin{pmatrix} \frac{\vec{p}\cdot\vec{\sigma}}{E+m_Q}\phi \\ \phi \end{pmatrix}, \\ u\,(\vec{p}) &= \sqrt{\frac{E+m_Q}{2m_Q}}\begin{pmatrix} \chi \\ \frac{\vec{p}\cdot\vec{\sigma}}{E+m_Q}\chi \end{pmatrix}, \end{aligned} \tag{1.14}$$

where $E = \sqrt{p^2+m_Q^2}$ is the energy of the quark and $\chi$ and $\phi$ are Pauli spinors representing the quark and the anti-quark, respectively. Expanding the spacial components of Eq. (1.13) to order $v^2$, we obtain the leading order operator in the effective theory

$$\begin{aligned} \overline{v}\,(-\vec{p})\;\gamma^i\,u\,(\vec{p}) &= \left(1+\frac{\vec{p}^{\,2}}{4m_Q}\right)\left(\phi^\dagger\,\frac{(-\vec{p}\cdot\vec{\sigma})}{2m_Q},\;\phi^\dagger\right)\;\sigma^i\;\begin{pmatrix} \frac{\vec{p}\cdot\vec{\sigma}}{2m_Q}\chi \\ \chi \end{pmatrix} + \mathcal{O}\left(v^4\right) \\ &= \phi^\dagger\,\sigma^i\,\chi + \frac{1}{2m_Q^2}\phi^\dagger\left(\vec{p}^{\,2}\sigma^i - p^i\,(\vec{p}\cdot\vec{\sigma})\right)\chi + \mathcal{O}\left(v^4\right)\,. \end{aligned} \tag{1.15}$$

The $\sigma^i$ in Eq. (1.15) are the Pauli matrices. The time-like component of Eq. (1.13) is zero up to higher orders in $v$ and is not considered here. The matching coefficient

of the leading operator (first term on the right hand side of Eq. (1.15)) is required to order $\mathcal{O}(\alpha_s^3)$ for the N$^3$LO evaluation of the cross section. Since the sub-leading operators are suppressed by additional powers of $v$, their matching coefficients do not have to be calculated to the same order in $\alpha_s$. In particular, the matching coefficients of the dimension five operators[2] (suppressed by $v^2$) have to be calculated at one-loop only. Since there are no contributions of closed fermion loops at that order, we do not consider them in this work.

In order to obtain the matching coefficient, we compute vertex corrections induced by the current in the full and effective theory. It is convenient to consider renormalised vertex functions with on-shell quarks and perform an expansion around the threshold $q^2 = 4m_Q^2$. Thus, we arrive at the matching equation

$$Z_2^{\mathrm{OS}}\,\Gamma_v = c_v\,\tilde{Z}_2\,\tilde{Z}_v^{-1}\,\tilde{\Gamma}_v + \dots\,, \tag{1.16}$$

where $Z_2^{\mathrm{OS}}$ is the quark wave function renormalisation constant in the on-shell scheme and $\Gamma_v$ denotes the proper structures of the vertex corrections. The corresponding quantities in the effective theory are marked by a tilde and the ellipses denote terms of higher order in $v$. It is understood that the quark mass and the strong coupling are already renormalised in Eq. (1.16). The former is renormalised in the on-shell scheme while we choose the $\overline{\mathrm{MS}}$ scheme for the latter. $\tilde{Z}_2 = 1$ to the order considered in this work.

Since $c_v$ only depends on the degrees of freedom which have been integrated out of the effective theory, it is useful to apply the so-called threshold expansion [22,23] to Eq. (1.16). This means that $\Gamma_v$ is considered as a sum of the contributions from the different momentum regions. With the exception of the hard region, where energy and momentum are of the order of the quark mass $m_Q$, all regions contribute to $\tilde{\Gamma}_v$ as well. As a consequence, these contributions drop out and it suffices to calculate the contribution from the hard region to get $c_v$ (see also Section 1.1.2).

$\tilde{Z}_v$ is an additional renormalisation constant for the vector current in the effective theory. Since the vector current is conserved in the full theory it does not get renormalised (cf. Ref. [53] for a recent discussion of this point). However, starting from two-loop level the matching procedure begins to exhibit infrared divergences. This is a consequence of the threshold expansion in dimensional regularisation. An alternative would be to choose a cut-off for the momentum integrations. This would result in a factorisation scale separating the soft and hard momenta. Here, we absorb the infrared poles into the additional renormalisation constant $\tilde{Z}_v$, which we define in the $\overline{\mathrm{MS}}$ scheme. Due to this, the matching coefficient becomes scale dependent. In physical quantities this scale dependence is cancelled against the corresponding contributions from the effective theory. Of course it is necessary to choose the same regularisation method for the calculation of the effective theory quantities as well.

Let us now determine the structures of the vertex function $\Gamma^\mu$ which contribute to $\Gamma_v$. The general tensor structure of a quark-anti-quark vector boson vertex at

[2] See for example Ref. [40] for an accurate definition of the two dimension five operators.

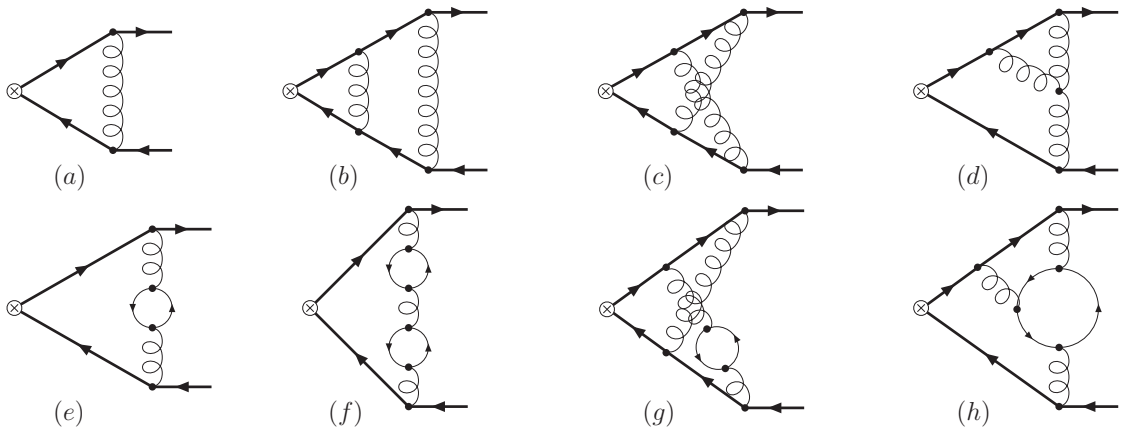


Figure 1.3: Sample Feynman diagrams contributing to the matching coefficient. Bold lines denote massive quarks with mass $m_Q$, thin lines denote massless quarks and curly lines denote gluons. $\otimes$ denotes the coupling of the external current.

threshold is

$$\Gamma^\mu = \gamma^\mu F_1 + \frac{[\gamma^\mu, \not{q}\,]}{4m_Q} F_2 + \frac{\not{q}\, q^\mu}{q^2} F_3 \,. \tag{1.17}$$

Of these three form factors only those contribute which produce the correct structure in the non-relativistic expansion. This is obviously true for $F_1$ as we know from Eq. (1.15). Performing the analogous calculations with the other two tensor structures, we find that $\Gamma_v = F_1 + F_2$.

### 1.2.2 Calculation

From the last section we know that we have to calculate vertex corrections induced by the vector current. Sample Feynman diagrams are shown in Fig. 1.3[3]. However, from these diagrams we only need certain parts, namely the form factors $F_1$ and $F_2$ of Eq. (1.17). The most convenient way to extract them is to use projection operators. Since we do not need both form factors separately, we can use the projector

$$\hat{P}_\mu^{(v)} = \frac{1}{8(d-1)m_Q^2} \left( -\frac{\not{q}}{2} + m_Q \right) \gamma_\mu \left( \frac{\not{q}}{2} + m_Q \right) . \tag{1.18}$$

Multiplying $\Gamma^\mu$ from the left with $\hat{P}_\mu$ and taking the trace gives the sum of $F_1$ and $F_2$. Furthermore, after application of the projector, we only have to deal with scalar quantities.

A further simplification of the diagrams can be achieved by taking advantage of the special kinematics at threshold. Since we have on-shell quarks with momenta $q_1^2 = q_2^2 = m_Q^2$ and $q^2 = (q_1 + q_2)^2 = 4m_Q^2$, $q_1$ and $q_2$ can be replaced by $q/2$. This

[3] All Feynman diagrams in this work were drawn with `JaxoDraw` [54].

in turn allows to use partial fractioning to get rid of some massive lines. Let us consider the scalar one-loop integral corresponding to Fig. 1.3($a$) as an example. We have

$$\begin{aligned}
&\int \frac{\mathrm{d}^d k}{((k+q_1)^2-m_Q^2)\,((k-q_2)^2-m_Q^2)\,k^2} \\
&= \int \frac{\mathrm{d}^d k}{((k+q/2)^2-m_Q^2)\,((k-q/2)^2-m_Q^2)\,k^2} \\
&= \int \frac{\mathrm{d}^d k}{(k^2+q\cdot k)\,(k^2-q\cdot k)\,k^2} \\
&= \frac{1}{2}\left(\int \frac{\mathrm{d}^d k}{(k^2+q\cdot k)\,(k^2)^2} + \int \frac{\mathrm{d}^d k}{(k^2-q\cdot k)\,(k^2)^2}\right), \qquad (1.19)
\end{aligned}$$

where the two integrals in the last line are actually equal since they depend only on $q^2$. Thus, the vertex integral is effectively reduced to an on-shell propagator integral, which, however, has an additional power of the massless propagator.

This procedure can also be applied at the two- and three-loop level. However, since there are different types of diagrams we encounter more integral classes. In particular, we can no longer neglect the sign of the external momentum, which means that there will also be vertex integrals. All occurring integrals can be mapped on the following functions:

$$\begin{aligned}
J^{(1)}(n_1,n_2) &= \frac{\mu^{2\epsilon}}{i\pi^{d/2}} \int \frac{\mathrm{d}^d k}{(k^2)^{n_1}(k^2+q\cdot k)^{n_2}}\,, \\
J^{(2)}_{\pm}(n_1,\ldots,n_5) &= \\
&\left(\frac{\mu^{2\epsilon}}{i\pi^{d/2}}\right)^2 \int \frac{\mathrm{d}^d k\,\mathrm{d}^d l}{(k^2)^{n_1}(l^2)^{n_2}((k-l)^2)^{n_3}(k^2+q\cdot k)^{n_4}(l^2\pm q\cdot l)^{n_5}}\,, \\
L^{(2)}_{\pm}(n_1,\ldots,n_5) &= \\
&\left(\frac{\mu^{2\epsilon}}{i\pi^{d/2}}\right)^2 \int \frac{\mathrm{d}^d k\,\mathrm{d}^d l}{(k^2)^{n_1}(l^2)^{n_2}((k+l)^2+q\cdot(k+l))^{n_3}(k^2+q\cdot k)^{n_4}(l^2\pm q\cdot l)^{n_5}}\,, \\
J^{(3)}_{\pm}(n_1,\ldots,n_9) &= \left(\frac{\mu^{2\epsilon}}{i\pi^{d/2}}\right)^3 \int \frac{\mathrm{d}^d k\,\mathrm{d}^d l\,\mathrm{d}^d p}{(k^2)^{n_1}(l^2)^{n_2}(p^2)^{n_3}((k-l)^2)^{n_4}((l-p)^2)^{n_5}} \\
&\qquad \times \frac{(l^2+q\cdot l)^{-n_8}}{((p-k)^2)^{n_6}(k^2+q\cdot k)^{n_7}(p^2\pm q\cdot p)^{n_9}}\,, \\
L^{(3,n_l)}_{\pm}(n_1,\ldots,n_9) &= \left(\frac{\mu^{2\epsilon}}{i\pi^{d/2}}\right)^3 \int \frac{\mathrm{d}^d k\,\mathrm{d}^d l\,\mathrm{d}^d p}{(k^2)^{n_1}(l^2)^{n_2}((k+l)^2+q\cdot(k+l))^{n_3}(k^2+q\cdot k)^{n_4}} \\
&\qquad \times \frac{(p^2+q\cdot p)^{-n_9}}{(l^2\pm q\cdot l)^{n_5}(p^2)^{n_6}((p+k)^2)^{n_7}((p-l)^2)^{n_8}}\,. \qquad (1.20)
\end{aligned}$$

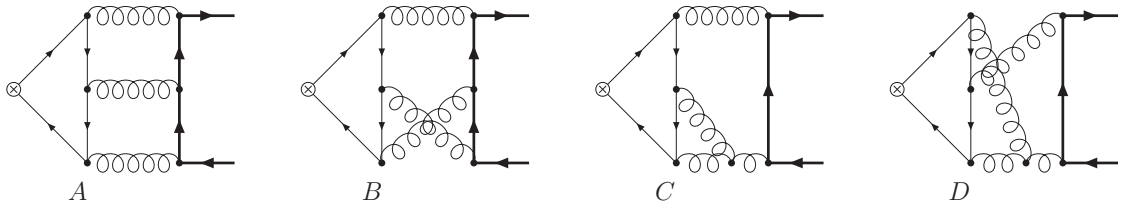


Figure 1.4: The different singlet topologies. The same coding as in Fig. 1.3 is adopted.

The two-loop functions $J_\pm^{(2)}$ and $L_\pm^{(2)}$ have already been defined in Ref. [22]. The three-loop functions $J_\pm^{(3)}$ and $L_\pm^{(3,n_l)}$ contain irreducible scalar products which are shown as numerators in Eq. (1.20). The corresponding indices can only adopt values less or equal to zero. Furthermore, only two out of the three indices $n_6$, $n_7$ and $n_8$ in $L_\pm^{(3,n_l)}$ can have positive values. The integrals $J_+^{(2)}$, $L_+^{(2)}$ and $J_+^{(3)}$ are on-shell propagator integrals whereas the integrals $J_-^{(2)}$, $L_-^{(2)}$, $J_-^{(3)}$ and $L_\pm^{(3,n_l)}$ correspond to vertices at threshold.

A new class of diagrams, which appears first at the three-loop level, are the so-called singlet diagrams. In these diagrams the external quarks do not couple directly to the external current. The different topologies are depicted in Fig. 1.4. Actually, diagrams of this type also appear at the two-loop level. However, the two gluons in these diagrams have to be in a colour-singlet state, which means that Furry's theorem [55] (see also Ref. [56]) is applicable. The sum of the two-loop singlet diagrams is therefore zero.

The singlet integrals pose an additional complication. Since we cannot perform the partial fractioning for these integrals in the way described above, we have to consider the corresponding vertex functions. The topologies of Fig. 1.4 are mapped on the functions

$$\begin{aligned} V_A(n_1,\ldots,n_{12}) &= \left(\frac{\mu^{2\epsilon}}{i\pi^{d/2}}\right)^3 \int \frac{\mathrm{d}^d k\ \mathrm{d}^d l\ \mathrm{d}^d p}{(k^2-m_Q^2)^{n_1}(l^2-m_Q^2)^{n_2}((k-l)^2)^{n_3}((l-p)^2)^{n_4}} \\ &\quad \times \frac{(p^2)^{-n_{10}}((k-q_2)^2)^{-n_{11}}((l+q_1)^2)^{-n_{12}}}{((p-k)^2)^{n_5}((k+q_1)^2)^{n_6}((l-q_2)^2)^{n_7}((p+q_1)^2)^{n_8}((p-q_2)^2)^{n_9}}, \end{aligned}$$

$$\begin{aligned} V_B(n_1,\ldots,n_{12}) &= \left(\frac{\mu^{2\epsilon}}{i\pi^{d/2}}\right)^3 \int \frac{\mathrm{d}^d k\ \mathrm{d}^d l\ \mathrm{d}^d p}{(k^2-m_Q^2)^{n_1}(l^2)^{n_2}((k-l)^2-m_Q^2)^{n_3}((p-k)^2)^{n_4}} \\ &\quad \times \frac{(p^2)^{-n_{12}}}{((l-p+k)^2)^{n_5}((k+q_1)^2)^{n_6}((k-l-q_2)^2)^{n_7}((l+p+q_1)^2)^{n_8}} \\ &\quad \times \frac{1}{((p-l-q_2)^2)^{n_9}((p+q_1)^2)^{n_{10}}((p-q_2)^2)^{n_{11}}}, \end{aligned}$$

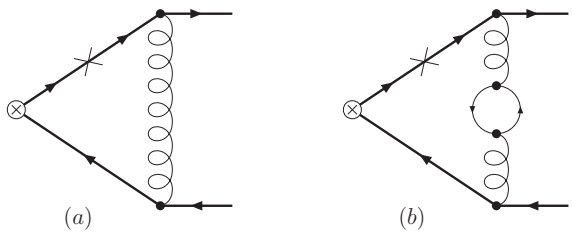


Figure 1.5: Sample diagrams contributing to the mass renormalisation of the matching coefficient. The same coding as in Fig. 1.3 is adopted. The cross denotes the insertion of the quark mass renormalisation constant.

$$
\begin{aligned}
V_C(n_1,\ldots,n_{12}) &= \left(\frac{\mu^{2\epsilon}}{i\pi^{d/2}}\right)^3 \int \frac{\mathrm{d}^d k\,\mathrm{d}^d l\,\mathrm{d}^d p}{(k^2-m_Q^2)^{n_1}((k-l)^2)^{n_2}((l-p)^2)^{n_3}((p-k)^2)^{n_4}} \\
&\quad\times \frac{(l^2)^{-n_{12}}(p^2)^{-n_{12}}}{((k+q_1)^2)^{n_5}((k-q_2)^2)^{n_6}((l+q_1)^2)^{n_7}((l-q_2)^2)^{n_8}((p+q_1)^2)^{n_9}} \\
&\quad\times \frac{1}{((p-q_2)^2)^{n_{10}}}\,, \\
V_D(n_1,\ldots,n_{12}) &= \left(\frac{\mu^{2\epsilon}}{i\pi^{d/2}}\right)^3 \int \frac{\mathrm{d}^d k\,\mathrm{d}^d l\,\mathrm{d}^d p}{(k^2-m_Q^2)^{n_1}((k-l)^2)^{n_2}((l-p)^2)^{n_3}((k+q_1)^2)^{n_4}} \\
&\quad\times \frac{(l^2)^{-n_{10}}(p^2)^{-n_{11}}((p-k)^2)^{-n_{12}}}{((k-q_2)^2)^{n_5}((l-q_2)^2)^{n_6}((k-l+p+q_1)^2)^{n_7}((p+q_1)^2)^{n_8}} \\
&\quad\times \frac{1}{((p-q_2)^2)^{n_9}}\,,
\end{aligned}
\tag{1.21}
$$

respectively. Actually, it is possible to implement the partial fractioning in terms of recurrence relations for the integrals [57]. This is discussed in Section A.4 in the Appendix.

As it was mentioned above, the strong coupling constant and quark mass in $\Gamma_v$ of Eq. (1.16) are already renormalised. The former can be done quite easily by replacing the bare coupling constant by the renormalised one times the corresponding renormalisation constant. The latter is more intricate since we are dealing with on-shell integrals. The problem is due to the fact that we set $(q/2)^2 = m_Q^2$ during the calculation. As a consequence, it is not possible to identify the bare mass, which needs to be renormalised, in the final result.

The solution to this problem is to consider the pole mass in the Lagrangian and to calculate the counterterms explicitly by considering one- and two-loop diagrams with zero momentum insertions. Some sample diagrams are displayed in Fig. 1.5. The one-loop diagram with two counterterm insertions is not needed at the order considered in this work. The vertex denoted by a cross has to be replaced by the

quark mass renormalisation constant in the on-shell scheme. The calculation of this constant is discussed in Chapter 2.

The calculation is performed in dimensional regularisation with $d = 4 - 2\epsilon$. The computation of the diagrams is almost entirely automatised due to the use of the programs `QGRAF` [58], `q2e` [59], `exp` [60, 61] and `MATAD` [62], which are described in Appendix C. In a first step, all occurring integrals are mapped onto the functions defined in Eq. (1.20). The next step is to reduce all occurring integrals to so-called master integrals, using integration-by-parts (IBP) identities [63]. In order to find the solution of the recurrence relations in a systematic way, we used Baikov's method [64, 65] in the formulation of Ref. [66] at the one- and two-loop level, and Laporta's algorithm [67, 68] for the three-loop calculations. In case of the latter method, we used the program `Crusher` [69]. Both methods are explained in detail in Appendix A. For the three-loop fermionic non-singlet contribution to the matching coefficients, we found twelve master integrals. The results are given in Appendix D.3.

The singlet integrals of Eq. (1.21) are significantly more complicated than the non-singlet integrals of Eq. (1.20). Since we have to treat the former as three-point functions, they contain more propagators. Thus, the corresponding IBP relations are harder to solve. Still, the most complicated task is the calculation of the corresponding master integrals. Since there are about 50 master integrals for the singlet integrals alone, this task is not yet completed. The three-loop results in the following are thus only for the non-singlet diagrams. Since both diagram classes are separately finite and gauge independent, they can be considered independently.

All calculations have been carried out in an arbitrary covariant gauge. The cancellation of the gauge parameter, $\xi$, in our final result serves as a welcome check on the correctness of our calculation. Starting from the three-loop level, the wave function renormalisation constant in the on-shell scheme depends on the gauge parameter (cf. Section 2.3). However, all colour factors which are needed here are independent of $\xi$. It is interesting to note that the $\xi$-dependence of the genuine three-loop diagrams is cancelled against terms stemming from the mass renormalisation. The two-loop diagram with one insertion of the one-loop mass renormalisation constant (cf. Fig. 1.5($b$)) is indeed $\xi$-independent. The one-loop diagram (cf. Fig. 1.5($a$)), however, is not. This cancellation can already be observed at the two-loop level.

It is convenient to cast the results for the matching coefficients in the form

$$c_i = 1 + \frac{\alpha_s(\mu)}{\pi}\, c_i^{(1)} + \left(\frac{\alpha_s(\mu)}{\pi}\right)^2 c_i^{(2)} + \left(\frac{\alpha_s(\mu)}{\pi}\right)^3 \left(c_i^{(3,n_l)} + \text{non-}n_l \text{ terms}\right) + \mathcal{O}\left(\alpha_s^4\right) . \tag{1.22}$$

The three-loop term can be further decomposed in terms of the different colour structures

$$c_i^{(3,n_l)} \;=\; C_F T_F n_l \left(C_F\, c_i^{FFL} + C_A\, c_i^{FAL} + T_F n_l\, c_i^{FLL} + T_F c_i^{FHL}\right) , \tag{1.23}$$

where $C_F = (N_c^2 - 1)/(2N_c)$ and $C_A = N_c$ are the eigenvalues of the quadratic Casimir operators of the fundamental and adjoint representation of SU($N_c$), respec-

tively. In the case of QCD we have $N_c = 3$. $T_F = 1/2$ is the index of the fundamental representation, $n_f$ is the number of quark flavours and $n_l = n_f - 1$ is the number of light-quark flavours, which are considered to be massless in our calculation.

### 1.2.3 Results

The known one- [70] and two-loop [71, 72] terms are given by

$$c_v^{(1)} = -2C_F\,, \tag{1.24}$$

$$\begin{aligned} c_v^{(2)} &= \left(\frac{23}{8} - \frac{79}{36}\pi^2 + \pi^2 \ln 2 - \frac{1}{2}\zeta_3\right) C_F^2 \\ &\quad + \left(-\frac{151}{72} + \frac{89}{144}\pi^2 - \frac{5}{6}\pi^2 \ln 2 - \frac{13}{4}\zeta_3\right) C_A C_F \\ &\quad + \left(\frac{11}{18} n_l + \frac{22}{9} - \frac{2}{9}\pi^2\right) C_F T_F - \left[2\,\beta_0 + \pi^2 \left(\frac{1}{6} C_F + \frac{1}{4} C_A\right)\right] C_F \ln \frac{\mu^2}{M_Q^2}\,, \end{aligned} \tag{1.25}$$

where $M_Q$ denotes the pole mass, $\beta_0 = (11C_A/3 - 4Tn_f/3)/4$ is the one-loop coefficient of the strong coupling's $\beta$ function and $\zeta_n$ denotes Riemann's $\zeta$ function with integer argument $n$. The terms proportional to $\beta_0 \ln \frac{\mu^2}{M_Q^2}$ are connected to the choice $\alpha_s(\mu)$ in Eq. (1.22) whereas the ones proportional to $\pi^2 \ln \frac{\mu^2}{M_Q^2}$ originate from the separation of hard and soft scales in the construction of NRQCD. The former vanish if $\alpha_s(M_Q)$ is chosen instead of $\alpha_s(\mu)$. The latter are cancelled by the corresponding terms of the non-relativistic Greens function.

For the renormalisation constant $\tilde{Z}_v$ we obtain

$$\begin{aligned} \tilde{Z}_v &= 1 + \left(\frac{\alpha_s(\mu)}{\pi}\right)^2 \left(\frac{1}{12} C_F^2 + \frac{1}{8} C_F C_A\right) \frac{\pi^2}{\epsilon} \\ &\quad + \left(\frac{\alpha_s(\mu)}{\pi}\right)^3 C_F T n_l \left[\left(\frac{1}{54} C_F + \frac{1}{36} C_A\right) \frac{\pi^2}{\epsilon^2} - \left(\frac{25}{324} C_F + \frac{37}{432} C_A\right) \frac{\pi^2}{\epsilon}\right] \\ &\quad + \dots\,, \end{aligned} \tag{1.26}$$

where the ellipses stand for non-$n_l$ and $\mathcal{O}\left(\alpha_s^4\right)$ terms.

Our final result for $c_v^{(3,n_l)}$ reads

$$\begin{aligned}
c_v^{FFL} &= 46.7(1) + \left(-\frac{17}{12} + \frac{61}{36}\pi^2 - \frac{2}{3}\pi^2\ln 2 + \frac{1}{3}\zeta_3\right) L_\mu + \frac{1}{18}\pi^2 L_\mu^2\,, \\
c_v^{FAL} &= 39.6(1) + \left(\frac{181}{54} - \frac{67}{432}\pi^2 + \frac{5}{9}\pi^2\ln 2 + \frac{13}{6}\zeta_3\right) L_\mu + \left(\frac{11}{9} + \frac{1}{12}\pi^2\right) L_\mu^2\,, \\
c_v^{FLL} &= -\frac{163}{162} - \frac{4}{27}\pi^2 - \frac{11}{27}L_\mu - \frac{2}{9}L_\mu^2\,, \\
c_v^{FHL} &= -\frac{557}{162} + \frac{26}{81}\pi^2 + \left(-\frac{55}{27} + \frac{4}{27}\pi^2\right) L_\mu - \frac{4}{9}L_\mu^2\,,
\end{aligned} \tag{1.27}$$

where $L_\mu = \ln(\mu^2/M_Q^2)$. The uncertainties assigned to the numerical constants in $c_{FFL}$ and $c_{FAL}$ are due to the numerical evaluation of some of the master integrals. The given values correspond to a conservative estimate. We want to stress that the precision of these quantities is more than enough for all phenomenological applications.

The coefficients in Eq. (1.27) correspond to an expansion parameter $\alpha_s(\mu)$, as given in Eq. (1.22). Choosing $\alpha_s(M_Q)$ instead leads to

$$\begin{aligned}
\bar{c}_v^{FFL} &= 46.7(1) + \frac{25}{108}\pi^2 L_\mu - \frac{1}{18}\pi^2 L_\mu^2\,, \\
\bar{c}_v^{FAL} &= 39.6(1) + \frac{37}{144}\pi^2 L_\mu - \frac{1}{12}\pi^2 L_\mu^2\,, \\
\bar{c}_v^{FLL} &= -\frac{163}{162} - \frac{4}{27}\pi^2\,, \\
\bar{c}_v^{FHL} &= -\frac{557}{162} + \frac{26}{81}\pi^2\,.
\end{aligned} \tag{1.28}$$

The dependence on $L_\mu$ in Eq. (1.28) is cancelled against contributions from the effective theory. The $L_\mu$ terms agree with the ones of Ref. [73][4].

### 1.2.4 Phenomenological Analysis

Let us first take a look at numerical values for the individual contributions to the matching coefficient. Inserting the numerical values for the colour factors we obtain for $\mu = M_Q$

$$\begin{aligned}
c_v^{(1)} &\approx -2.6667\,, \\
c_v^{(2)} &\approx -44.551 + 0.4074\, nl\,, \\
c_v^{(3,n_l)} &\approx 121.\, n_l - 0.823\, n_l^2\,.
\end{aligned} \tag{1.29}$$

[4] A typing error in Ref. [73] was pointed out in Ref. [7].

In the case of the bottom quark we have $n_l = 4$. Furthermore, we set $M_b = 5.3$ GeV [44]. To evaluate $\alpha_s$ at the bottom quark mass, we use the program `RunDec` [74]. Starting from $\alpha_s(M_Z) = 0.118$ we obtain $\alpha_s(M_b) = 0.2096$, where both are defined for five active flavours. Using these values, we obtain the following result for the matching coefficient

$$c_v(M_b) = 1 - 0.1780\big|_{\rm NLO} - 0.1911\big|_{\rm NNLO} + 0.139\big|_{\rm N^3LO'}\,, \tag{1.30}$$

where the orders in perturbation theory are indicated by the subscripts. The prime in $\mathrm{N^3LO'}$ reminds us of the fact that only a part of this correction is known. From Eq. (1.30) we see that the second-order correction is larger than the first-order one. It is, however, almost cancelled by our new third-order term. At the moment, the perturbative expansion does not seem to converge. However, this situation may improve when the full third-order correction is known.

In the case of the top quark we have $n_l = 5$ and $M_t = 175$ GeV. For the strong coupling we find $\alpha_s(M_t) = 0.1075$, defined with six active flavours. Thus, the numerical result for the matching coefficient is

$$c_v(M_t) = 1 - 0.0912\big|_{\rm NLO} - 0.0498\big|_{\rm NNLO} + 0.0233\big|_{\rm N^3LO'}\,. \tag{1.31}$$

Also in this case the second- and third-order corrections are large compared to the first-order correction, though not as large as in the bottom quark case. Still, the NNLO correction amounts to more than 50% of the NLO one. This illustrates again why it is necessary to perform the three-loop calculation.

Two important quantities, which depend on the matching coefficient of the vector current, are the leptonic decay width of the $\Upsilon(1S)$ state and the peak of the normalised $t\bar{t}$ cross section, $R = \sigma(e^+e^- \to t\bar{t})/\sigma(e^+e^- \to \mu^+\mu^-)$. Therefore, we want to discuss the impact of our new result on these quantities in the following.

The leptonic decay of the $\Upsilon(1S)$ state can be cast in the form [34, 75–78]

$$\Gamma(\Upsilon(1S) \to l^+l^-) \;=\; \Gamma^{\rm LO}\rho_1\left[c_v^2(M_b) + \frac{C_F^2\alpha_s^2(\mu_s)}{12}c_v(M_b)\,(d_v(M_b)+3)\right] + \dots\,, \tag{1.32}$$

where non-perturbative contributions are ignored. $\Gamma^{\rm LO} = 4\pi N_c Q_b^2\alpha^2|\psi_1^C(0)|^2/(3M_b^2)$, $\rho_1 = |\psi_1(0)|^2/|\psi_1^C(0)|^2$, $Q_b = -1/3$ and $\alpha$ is Sommerfeld's fine-structure constant. The Coulomb wave function is given by $\left|\psi_n^C(0)\right|^2 = C_F^3\alpha_s^3M_Q^3/(8\pi n^3)$. The result for $\rho_1$ is given in Appendix E. $\mu_s$ denotes the so-called soft scale defined by $\mu_s = C_F M_Q\alpha_s(\mu_s)$. Using `RunDec` we obtain $\alpha_s(\mu_s) = 0.2967$ for $\mu_s = 2.0967$ GeV, where $\alpha_s(\mu_s)$ is defined with four active flavours.

Inserting the perturbative expansion for $\rho_1$ and $c_v$ into Eq. (1.32) we obtain

$$\begin{aligned}\Gamma_1 &\approx \Gamma_1^{\rm LO}\left(1-1.70\,\alpha_s(M_b)-7.98\,\alpha_s^2(M_b)+30.0\,\alpha_s^3(M_b)\big|_{n_l}+\ldots\right)\\ &\quad\times\Big[1-0.30\,\alpha_s(\mu_s)+\alpha_s^2(\mu_s)\,(17.2-5.19\ln\alpha_s(\mu_s))\\ &\quad+\alpha_s^3(\mu_s)\left(-14.4\ln^2\alpha_s(\mu_s)+0.17\ln\alpha_s(\mu_s)-34.9\big|_{\beta_0^3}\right)+\ldots\Big] \qquad (1.33)\\ &\approx \Gamma_1^{\rm LO}\left(1-0.446\big|_{\rm NLO}+1.75\big|_{\rm NNLO}-1.20\big|_{\rm N^3LO'}+\ldots\right)\,. \qquad (1.34)\end{aligned}$$

In Eq. (1.34), Eq. (1.33) is expanded and terms of order $\alpha_s^4$ are dropped consistently. Apart from our new contribution to $c_v$ and the known third-order corrections to $\rho_1$ we have also included all interference terms which are proportional to powers of $n_l$. The new corrections are responsible for the reduction of N$^3$LO$'$ terms from $-1.67$ to $-1.20$ which amounts to about 47% of the Born cross section. The perturbative expansion in Eq. (1.34) contains large coefficients, just as in the case of the matching coefficient alone. This makes the application of perturbation theory questionable. Still, for a definite conclusion one has to wait until the complete N$^3$LO corrections are available.

The peak of the normalised $t\bar{t}$ cross section is dominated by the contribution from the would-be toponium ground-state, which can be cast into a form similar to Eq. (1.32)

$$R_1(e^+e^-\to t\bar{t}) = R_1^{\rm LO}\rho_1\left[c_v^2(M_t)+\frac{C_F^2\alpha_s^2(\mu_s)}{12}c_v(M_t)\,(d_v(M_t)+3)\right]+\ldots\,. \qquad (1.35)$$

The leading order term is given by $R_1^{\rm LO}=6\pi N_c Q_t^2|\psi_1^C(0)|^2/(M_t^2\Gamma_t)$. The contributions from the higher Coulomb-like poles and the continuum are not included in Eq. (1.35).

The analog equations to Eqs. (1.33) and (1.34) read

$$\begin{aligned}R_1 &\approx R_1^{\rm LO}\left(1-1.70\,\alpha_s(M_t)-7.89\,\alpha_s^2(M_t)+37.2\,\alpha_s^3(M_t)\big|_{\rm n_l}+\ldots\right)\\ &\quad\times\Big[1-0.43\,\alpha_s(\mu_s)+\alpha_s^2(\mu_s)\,(16.1-5.19\ln\alpha_s(\mu_s))\\ &\quad+\alpha_s^3(\mu_s)\left(-13.8\ln^2\alpha_s(\mu_s)+2.06\ln\alpha_s(\mu_s)-27.2\big|_{\beta_0^3}\right)+\ldots\Big] \qquad (1.36)\\ &\approx R_1^{\rm LO}\left(1-0.243\big|_{\rm NLO}+0.435\big|_{\rm NNLO}-0.195\big|_{\rm N^3LO'}+\ldots\right)\,, \qquad (1.37)\end{aligned}$$

where $\alpha_s(\mu_s)$ is defined with five active flavours. We obtain $\alpha_s(\mu_s)=0.1398$ with $\mu_s=32.625$ GeV. The fermionic corrections to $c_v$ are responsible for a reduction of the third-order coefficient from $-0.268$ to $-0.195$ and thus amount to moderate 7% of the leading order term. Similarly as for the bottom-quark case also for the top quark the perturbative series is alternating and the third-order coefficient tends to stabilise the expansion. It is interesting to note that after the inclusion of our new terms the total correction amounts to less than 1%.

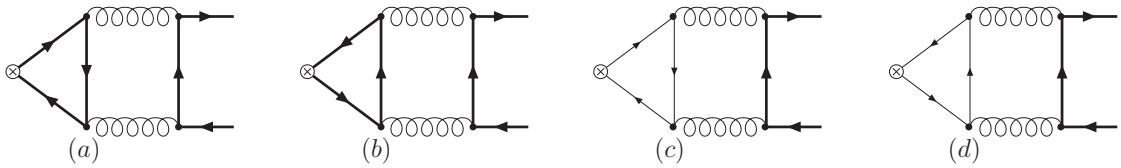


Figure 1.6: The two-loop singlet diagrams contributing to the matching coefficient of the axial-vector current. The same coding as in Fig. 1.3 is adopted.

## 1.3 The Axial-Vector Current

The general approach to the calculation of the axial-vector current, and indeed of the other currents, is the same as for the vector current. Therefore, we will restrict ourselves in this and the following sections to point out only the differences.

The axial-vector current in the full theory is given by

$$j_a^\mu = \overline{\psi}\,\gamma^\mu\gamma_5\,\psi\,. \tag{1.38}$$

The operator in the effective theory corresponding to the spacial components of Eq. (1.38) is

$$\tilde{j}_a^i = \frac{1}{2m_Q}\phi^\dagger\,\left[\sigma^i, \vec{p}\cdot\vec{\sigma}\right]\,\chi + \mathcal{O}\left(v^3\right)\,, \tag{1.39}$$

which is already of order $v$. Contrary to the vector current, there is also a non-zero time-like component at order $v^0$, namely

$$\tilde{j}_a^0 = \phi^\dagger\,\chi + \mathcal{O}\left(v^2\right)\,. \tag{1.40}$$

Since this is the same operator as the one of the pseudo-scalar current, we postpone its discussion to the next section. However, most of what is said in this section about the calculation of the matching coefficient of the spacial component also applies to the time-like component. The matching equation for both cases is similar to the one of the vector current

$$Z_2^{\rm OS}\,\Gamma_a^{(0,i)} = c_a^{(0,i)}\,\tilde{Z}_2\,\tilde{Z}_a^{-1}\,\tilde{\Gamma}_a^{(0,i)} + \ldots\,, \tag{1.41}$$

where $c_a^{(i)} = c_a$ and $c_a^{(0)} = c_p$.

In Section 1.2.2, we noted that there is no contribution from singlet diagrams to the matching coefficient of the vector current at the two-loop level. This statement is not true for the axial-vector current. Here, we get a finite contribution from these diagrams, which are depicted in Fig 1.6. The diagrams can be mapped onto the

following functions

$$\begin{aligned} V_E(n_1,\ldots,n_7) &= \left(\frac{\mu^{2\epsilon}}{i\pi^{d/2}}\right)^2 \int \frac{\mathrm{d}^d k\;\mathrm{d}^d l}{((k-q_2)^2)^{n_1}(k^2-m_Q^2)^{n_2}((k+q_1)^2)^{n_3}((k-l)^2)^{n_4}} \\ &\quad \times \frac{(l^2)^{-n_7}}{((l+q_1)^2)^{n_5}((l-q_2)^2)^{n_6}}\,, \\ V_F(n_1,\ldots,n_7) &= \left(\frac{\mu^{2\epsilon}}{i\pi^{d/2}}\right)^2 \int \frac{\mathrm{d}^d k\;\mathrm{d}^d l}{(k^2)^{n_1}(k^2+2q_2\cdot k)^{n_2}((k+q_1+q_2)^2)^{n_3}} \\ &\quad \times \frac{(l^2)^{-n_7}}{((k-l)^2+2q_2\cdot(k-l))^{n_4}(l^2+2q_1\cdot l)^{n_5}(l^2-2q_2\cdot l)^{n_6}}\,. \end{aligned} \tag{1.42}$$

To reduce these functions to master integrals, we used the program `AIR` [79], which implements Laporta's algorithm. We found seventeen master integrals. If the additional recurrence relations of Appendix A.4 are used, the number of master integrals is reduced to nine. The results for all master integrals are given in Appendix D.2.

To ensure the cancellation of anomaly-like contributions, we have to consider the current

$$j_a^\mu = \bar{t}\,\gamma^\mu\gamma_5\,t - \bar{b}\,\gamma^\mu\gamma_5\,b \tag{1.43}$$

for the singlet contribution, where $t$ and $b$ denote the top and bottom quark, respectively. The contributions from the lighter quarks cancel in the difference of up-type and down-type quarks. Eq. (1.43) also leads to a difference between the matching coefficient for top quarks and the matching coefficient for bottom quarks. The reason is that in both cases the difference of up-type and down-type quarks has to be considered. In the former, the top quark is massive and on-shell while the bottom quark is massless. In the latter case, however, the bottom quark is massive and on-shell but the mass of the top quark cannot be neglected. To evaluate the first term on the left hand side in Eq. (1.43) we perform an asymptotic expansion (see for example Ref. [23]) in $m_t \gg m_b$, keeping only the leading term.

The occurrence of $\gamma_5$ presents an additional complication due to the use of dimensional regularisation, since it is an intrinsically four dimensional object [80, 81]. This means that the two defining properties of $\gamma_5$,

$$\mathrm{Tr}\{\gamma_5\gamma^\mu\gamma^\nu\gamma^\sigma\gamma^\rho\} = -4i\,\varepsilon^{\mu\nu\sigma\rho}\mathbf{1}\,, \tag{1.44}$$

$$\{\gamma_5,\gamma_\mu\} = 0\,, \tag{1.45}$$

where $\mathbf{1}$ is the unit matrix in Dirac space, are incompatible if $d \neq 4$. In the case of the non-singlet diagrams it is safe to use an anti-commuting definition of $\gamma_5$ [82]. For the singlet diagrams, however, this would lead to wrong results, since the property of Eq. (1.44) is essential in the evaluation of these diagrams. Therefore, we use the 't Hooft-Veltman prescription in the formulation of Ref. [83]. This means that we have to perform the replacement

$$\gamma^\mu\gamma_5 \to \frac{1}{3!}\varepsilon^{\mu\alpha\beta\delta}\gamma_\alpha\gamma_\beta\gamma_\delta \tag{1.46}$$

in the vertex corresponding to the external current and in the projector. The $\varepsilon$ tensor of the vertex is then stripped off and absorbed into the projector, where we can use four-dimensional identities for the contraction of $\varepsilon$ tensors to rewrite them in terms of products of metric tensors. Only the $\gamma$ matrices are kept in the actual vertex.

Another important difference to the vector current is the fact that the leading operator of the spacial components is already suppressed by one power of $v$. This poses a complication for the calculation since we now have to expand the diagrams to first order in $v$. In practice this means that we choose $q_1 = q/2 + p$ and $q_2 = q/2 - p$ and expand to first order in $p$. As a consequence, the tensor structure and thus the projector become more complicated as well. The proper structure is projected out by multiplying

$$\begin{aligned}\hat{P}_{\mu}^{(a,i,ac)} &= -\frac{1}{8m_Q^2}\left\{\frac{1}{d-1}\left(\frac{\not{q}}{2}-m_Q\right)\gamma_\mu\gamma_5\left(\frac{\not{q}}{2}-m_Q\right)\right.\\ &\left.+\frac{1}{d-2}\left(\frac{\not{q}}{2}-m_Q\right)\frac{m_Q}{p^2}\left((d-3)p_\mu+\gamma_\mu\not{p}\right)\gamma_5\left(\frac{\not{q}}{2}+m_Q\right)\right\}\end{aligned} \tag{1.47}$$

from the left and taking the trace. Note, that we have chosen a reference frame where $q \cdot p = 0$ [22].

As we pointed out above, it is not possible to use an anti-commuting $\gamma_5$ for the calculation of the singlet diagrams. For the calculation of these diagrams it is therefore necessary to change the projector accordingly. We now have

$$\begin{aligned}\hat{P}_{\alpha\beta\delta}^{(a,i,HV)} &= \frac{1}{8m_Q^2(d-2)}\left\{\left(\frac{\not{q}}{2}-m_Q\right)\left(g_{\nu\alpha}g_{\sigma\beta}g_{\rho\delta}-g_{\nu\alpha}g_{\sigma\delta}g_{\rho\beta}-g_{\nu\beta}g_{\sigma\alpha}g_{\rho\delta}\right.\right.\\ &\qquad\left.+g_{\nu\beta}g_{\sigma\delta}g_{\rho\alpha}+g_{\nu\delta}g_{\sigma\alpha}g_{\rho\beta}-g_{\nu\delta}g_{\sigma\beta}g_{\rho\alpha}\right)\\ &\quad\times\left[\frac{m_Q}{p^2}\frac{1}{(d-3)}\left((d-1)\,\gamma^\nu\gamma^\sigma\gamma^\rho\not{p}+(d-5)\not{p}\,\gamma^\nu\gamma^\sigma\gamma^\rho\right)\right.\\ &\quad\left.\left.\times\left(\frac{\not{q}}{2}-m_Q\right)+\frac{1}{18(d-1)}\gamma^\nu\gamma^\sigma\gamma^\rho\left(\frac{\not{q}}{2}+m_Q\right)\right]\right\},\end{aligned} \tag{1.48}$$

where the indices $\alpha$, $\beta$ and $\delta$ correspond to Eq. (1.46).

Even though it is possible to use an anti-commuting definition of $\gamma_5$ in the non-singlet case, in principle one can use the replacement of Eq. (1.46) and the projector of Eq. (1.48) in this case as well. According to Ref. [83], this requires an additional, finite renormalisation. After this we indeed find the correct result at the one-loop level. At two loops, however, we find a difference in the term proportional to $C_F^2$. This is due to the fact that the prescription of Ref. [83] is only valid for infrared

finite quantities. Since this is not the case here, it would be necessary to modify the additional renormalisation constant.

For the renormalisation constant $\tilde{Z}_a$ we obtain

$$\begin{aligned}\tilde{Z}_a &= 1 + \left(\frac{\alpha_s(\mu)}{\pi}\right)^2 \left(\frac{5}{48}C_F^2 + \frac{1}{24}C_F C_A\right)\frac{\pi^2}{\epsilon} \\ &\quad + \left(\frac{\alpha_s(\mu)}{\pi}\right)^3 C_F T n_l \left[\left(\frac{5}{216}C_F + \frac{1}{108}C_A\right)\frac{\pi^2}{\epsilon^2}\right. \\ &\qquad \left. - \left(0.6321(1)\, C_F + 0.4036(1)\, C_A\right)\frac{\pi^2}{\epsilon}\right] + \ldots ,\end{aligned} \tag{1.49}$$

where the ellipses stand for non-$n_l$ and $\mathcal{O}\left(\alpha_s^4\right)$ terms.

Our one- and two-loop results for the matching coefficient of the axial-vector current read

$$c_a^{(1)} = -C_F\,, \tag{1.50}$$

$$\begin{aligned}c_a^{(2)} &= \left(\frac{23}{24} - \frac{9}{8}\pi^2 + \frac{19}{24}\pi^2 \ln 2 - \frac{27}{16}\zeta_3\right) C_F^2 \\ &\quad + \left(-\frac{101}{72} + \frac{35}{144}\pi^2 - \frac{7}{12}\pi^2 \ln 2 - \frac{9}{8}\zeta_3\right) C_F C_A \\ &\quad + \left(\frac{7}{18}n_l + \frac{20}{9} - \frac{2}{9}\pi^2 + X_{\rm sing}^{(a)}\right) C_F T_F \\ &\quad - \left[\beta_0 + \pi^2\left(\frac{5}{24}C_F + \frac{1}{12}C_A\right)\right] C_F \ln\frac{\mu^2}{M_Q^2}\,,\end{aligned} \tag{1.51}$$

with

$$X_{\rm sing}^{(a)} = -\frac{23}{72}\pi^2 + \frac{2}{3}\pi^2 \ln 2 - 2\ln 2 + \frac{2}{3}\ln^2 2 + i\pi\left(1 - \frac{2}{3}\ln 2\right) \tag{1.52}$$

for top quarks and

$$X_{\rm sing}^{(a)} = \frac{55}{24} + \frac{19}{72}\pi^2 - \frac{2}{3}\pi^2 \ln 2 - \frac{3}{4}\ln\frac{M_b^2}{M_t^2} + \mathcal{O}\left(\frac{M_b^2}{M_t^2}\right) \tag{1.53}$$

for bottom quarks.

The fermionic part of Eq. (1.51) agrees with the result of Ref. [84]. The results for the singlet contribution agree with the results of Ref. [82]. In both of these references the form factors were calculated off threshold. The extraction of the other colour structures of Eq. (1.51) is therefore not so easy since they also contain contributions from other momentum regions.

Our three-loop result reads

$$\begin{aligned}
c_a^{FFL} &= 28.1(1) + 6.6513(1)\, L_\mu + \frac{5}{72}\pi^2 L_\mu^2\,, \\
c_a^{FAL} &= 23.2(1) + 5.2384(1)\, L_\mu + \left(\frac{11}{18} + \frac{1}{36}\pi^2\right) L_\mu^2\,, \\
c_a^{FLL} &= -\frac{65}{162} - \frac{2}{27}\pi^2 - \frac{7}{27} L_\mu - \frac{1}{9} L_\mu^2\,, \\
c_a^{FHL} &= -\frac{415}{162} + \frac{20}{81}\pi^2 + \left(-\frac{47}{27} + \frac{4}{27}\pi^2\right) L_\mu - \frac{2}{9} L_\mu^2\,.
\end{aligned} \tag{1.54}$$

We only give the result for $\alpha_s(\mu)$. The result for $\alpha_s(M_Q)$ or any other scale can be obtained easily with the usual renormalisation group techniques.

## 1.4 The Pseudo-Scalar Current

The pseudo-scalar current is defined as

$$j_p = \overline{\psi}\, i\gamma_5\, \psi\,. \tag{1.55}$$

The corresponding operator in the effective theory is

$$\tilde{j}_p = -i\phi^\dagger\, \chi + \mathcal{O}\left(v^2\right)\,. \tag{1.56}$$

Thus, we have $\tilde{j}_p = -i\,\tilde{j}_a^0$ from Eq. (1.40). Since both currents correspond to the same operator in the effective theory, they must have the same matching coefficient. Still, the calculation in both cases is quite different. The fact that we get the same result is therefore a good check on the correctness of our calculation.

An important difference is the fact that the pseudo-scalar current has an additional renormalisation constant in the full theory. The matching equation therefore reads

$$Z_2^{\rm OS}\, Z_p\, \Gamma_p = c_p\, \tilde{Z}_2\, \tilde{Z}_p^{-1}\, \tilde{\Gamma}_p + \ldots\,. \tag{1.57}$$

$Z_p$, the renormalisation constant of the current in the full theory, is just the mass renormalisation constant. Since we have chosen the on-shell scheme to renormalise the mass in $\Gamma_p$, $Z_p = Z_m^{\rm OS}$.

The projectors for the proper combination of the tensor structures are also different for the two cases. For anti-commuting $\gamma_5$ we have

$$\hat{P}^{(p,ac)} = -\frac{1}{8m_Q^2}\left(\frac{\not{q}}{2} - m_Q\right)\gamma_5\left(\frac{\not{q}}{2} + m_Q\right)\,, \tag{1.58}$$

$$\hat{P}_\mu^{(a,0,ac)} = \frac{1}{8m_Q^2}\left(\frac{\not{q}}{2} - m_Q\right)\gamma_\mu\gamma_5\left(\frac{\not{q}}{2} + m_Q\right)\,, \tag{1.59}$$

respectively. For 't Hooft-Veltman $\gamma_5$ we have to perform the replacement

$$\gamma_5 \to \frac{i}{4!}\varepsilon^{\alpha\beta\rho\sigma}\gamma_\alpha\gamma_\beta\gamma_\rho\gamma_\sigma \tag{1.60}$$

for the pseudo-scalar current. For the time-like component of the axial-vector current the replacement of Eq. (1.46) is performed. The projectors become

$$\begin{aligned}\hat{P}^{(p,HV)}_{\alpha\beta\rho\sigma} &= -\frac{1}{128(d-3)(d-2)(d-1)m_Q^2} \\ &\quad\times\left(\frac{\not{q}}{2}-m_Q\right)(\gamma_\alpha\gamma_\beta\gamma_\rho\gamma_\sigma+\gamma_\sigma\gamma_\rho\gamma_\beta\gamma_\alpha \\ &\qquad -\gamma_\beta\gamma_\rho\gamma_\sigma\gamma_\alpha-\gamma_\alpha\gamma_\sigma\gamma_\rho\gamma_\beta)\left(\frac{\not{q}}{2}+m_Q\right)\end{aligned} \tag{1.61}$$

and

$$\begin{aligned}\hat{P}^{(a,0,HV)}_{\alpha\beta\delta} &= \frac{1}{48(d-3)(d-2)(d-1)m_Q^2} \\ &\quad\times\left(\frac{\not{q}}{2}-m_Q\right)(g_{\nu\alpha}g_{\sigma\beta}g_{\rho\delta}-g_{\nu\alpha}g_{\sigma\delta}g_{\rho\beta}-g_{\nu\beta}g_{\sigma\alpha}g_{\rho\delta} \\ &\qquad +g_{\nu\beta}g_{\sigma\delta}g_{\rho\alpha}+g_{\nu\delta}g_{\sigma\alpha}g_{\rho\beta}-g_{\nu\delta}g_{\sigma\beta}g_{\rho\alpha}) \\ &\quad\times\gamma^\nu\gamma^\sigma\gamma^\rho\left(\frac{\not{q}}{2}+m_Q\right),\end{aligned} \tag{1.62}$$

respectively, where the indices correspond to Eqs. (1.60) and (1.46).

For the pseudo-scalar current we have again contributions from two-loop singlet diagrams. However, the diagrams with light fermions in the loop (cf. Fig 1.6 (*c*) and (*d*)) are suppressed by the mass. Since we set the mass of the light quarks to zero, we only get a contribution from the diagrams with a top quark loop (cf. Fig 1.6 (*a*) and (*b*)). For the zero component of the axial-vector current, we again have to consider the combination of Eq. (1.43). The fact that we have the same result in both cases, is a powerful check on the correctness of our calculation.

For the renormalisation constant $\tilde{Z}_p$ we obtain

$$\begin{aligned}\tilde{Z}_p &= 1+\left(\frac{\alpha_s(\mu)}{\pi}\right)^2\left(\frac{3}{12}C_F^2+\frac{3}{24}C_FC_A\right)\frac{\pi^2}{\epsilon} \\ &\quad+\left(\frac{\alpha_s(\mu)}{\pi}\right)^3 C_FTn_l\left[\left(\frac{1}{18}C_F+\frac{1}{36}C_A\right)\frac{\pi^2}{\epsilon^2}\right. \\ &\qquad\left.-\left(1.0052(1)\,C_F+\frac{37}{432}C_A\right)\frac{\pi^2}{\epsilon}\right]+\ldots,\end{aligned} \tag{1.63}$$

where the ellipses stand for non-$n_l$ and $\mathcal{O}(\alpha_s^4)$ terms. The two-loop contribution agrees with the result of Ref. [85].

The one- and two-loop results for the matching coefficient read

$$c_p^{(1)} = -\frac{3}{2}C_F\,, \tag{1.64}$$

$$\begin{aligned} c_p^{(2)} &= \left(\frac{29}{16} - \frac{79}{48}\pi^2 + \pi^2\ln 2 - \frac{9}{2}\zeta_3\right) C_F^2 \\ &\quad + \left(-\frac{17}{48} + \frac{17}{48}\pi^2 - \pi^2\ln 2 - 3\zeta_3\right) C_F C_A \\ &\quad + \left(\frac{1}{12}n_l + \frac{43}{12} - \frac{1}{3}\pi^2 + X_{\rm sing}^{(p)}\right) C_F T_F \\ &\quad - \left[\frac{3}{2}\beta_0 + \pi^2\left(\frac{1}{2}C_F + \frac{1}{4}C_A\right)\right] C_F\,\ln\frac{\mu^2}{M_Q^2}\,, \end{aligned} \tag{1.65}$$

with

$$X_{\rm sing}^{(p)} = \frac{5}{24}\pi^2 + \frac{1}{2}\pi^2\ln 2 - \frac{21}{8}\zeta_3 + i\frac{1}{8}\pi^3\,. \tag{1.66}$$

The one-loop result has already been obtain in Ref. [86]. The fermionic two-loop part agrees with the results of Refs. [82, 87]. At the two-loop level the matching coefficient has also been considered in the context of the $B_c$ meson in Ref. [88]. Since there are two mass scales involved, the calculation is significantly more complicated. However, the master integrals were evaluated as an expansion in $m_c/m_b$ so that it is not possible to derive the result for the equal mass case. Also, there are no singlet diagrams in the case of the $B_c$ meson.

Our three-loop result reads

$$\begin{aligned} c_p^{FFL} &= 51.9(1) + 12.057(1)\,L_\mu + \frac{1}{6}\pi^2 L_\mu^2\,, \\ c_p^{FAL} &= 39.9(1) + \left(\frac{73}{72} + \frac{1}{48}\pi^2 + \frac{2}{3}\pi^2\ln 2 + 2\zeta_3\right) L_\mu + \left(\frac{11}{12} + \frac{1}{12}\pi^2\right) L_\mu^2\,, \\ c_p^{FLL} &= -\frac{41}{108} - \frac{1}{9}\pi^2 - \frac{1}{18}L_\mu - \frac{1}{6}L_\mu^2\,, \\ c_p^{FHL} &= -\frac{76}{27} + \frac{7}{27}\pi^2 + \left(-\frac{22}{9} + \frac{2}{9}\pi^2\right) L_\mu - \frac{1}{3}L_\mu^2\,. \end{aligned} \tag{1.67}$$

## 1.5 The Scalar Current

In the full theory the scalar current is defined as

$$j_s = \overline{\psi}\,\psi\,. \tag{1.68}$$

The corresponding operator in the effective theory is

$$\tilde{j}_s = -\frac{1}{m_Q}\phi^\dagger\,\vec{p}\cdot\vec{\sigma}\,\chi + \mathcal{O}\left(v^3\right)\,. \tag{1.69}$$

Just as in the case of the axial-vector current, the leading operator is already suppressed by one power of $v$. The matching equation is similar to the pseudo-scalar case and reads

$$Z_2^{\rm OS}\,Z_s\,\Gamma_s = c_s\,\tilde{Z}_2\,\tilde{Z}_s^{-1}\,\tilde{\Gamma}_s + \ldots\,. \tag{1.70}$$

The renormalisation constant of the current in the full theory is again the mass renormalisation constant, $Z_s = Z_m^{\rm OS}$.

The proper combination of tensor structures of the vertex function is projected out by multiplying

$$\hat{P}_{(s)} = \frac{1}{8m_Q^2}\left\{\left(\frac{\not{q}}{2}-m_Q\right)\mathbf{1}\left(\frac{\not{q}}{2}-m_Q\right) - \left(\frac{\not{q}}{2}-m_Q\right)\frac{m_Q}{p^2}\not{p}\,\left(\frac{\not{q}}{2}+m_Q\right)\right\} \tag{1.71}$$

from the left and taking the trace. $\mathbf{1}$ in Eq. (1.71) denotes the unit matrix in Dirac space.

For the renormalisation constant $\tilde{Z}_s$ we obtain

$$\begin{aligned}\tilde{Z}_s &= 1 + \left(\frac{\alpha_s(\mu)}{\pi}\right)^2\left(\frac{1}{6}C_F^2 + \frac{1}{24}C_F C_A\right)\frac{\pi^2}{\epsilon} \\ &\quad + \left(\frac{\alpha_s(\mu)}{\pi}\right)^3 C_F T n_l\left[\left(\frac{1}{27}C_F + \frac{1}{108}C_A\right)\frac{\pi^2}{\epsilon^2}\right. \\ &\qquad \left. - \left(0.8833(1)\,C_F + 0.4036(1)\,C_A\right)\frac{\pi^2}{\epsilon}\right] + \ldots\,,\end{aligned} \tag{1.72}$$

where the ellipses stand for non-$n_l$ and $\mathcal{O}\left(\alpha_s^4\right)$ terms.

The one- and two-loop results for the matching coefficient read

$$c_s^{(1)} = -\frac{1}{2}C_F\,, \tag{1.73}$$

$$\begin{aligned}c_s^{(2)} &= \left(\frac{5}{16} - \frac{37}{48}\pi^2 + \frac{1}{2}\pi^2\ln 2 - \frac{11}{4}\zeta_3\right)C_F^2 \\ &\quad + \left(\frac{49}{144} + \frac{1}{48}\pi^2 - \frac{1}{2}\pi^2\ln 2 - \frac{5}{4}\zeta_3\right)C_F C_A \\ &\quad + \left(-\frac{5}{36}n_l + \frac{121}{36} - \frac{1}{3}\pi^2 + X_{\rm sing}^{(s)}\right)C_F T_F \\ &\quad - \left[\frac{1}{2}\,\beta_0 + \pi^2\left(\frac{1}{3}C_F + \frac{1}{12}C_A\right)\right]C_F\,\ln\frac{\mu^2}{M_Q^2}\,,\end{aligned} \tag{1.74}$$

with

$$X_{\rm sing}^{(s)} = \frac{2}{3} - \frac{29}{72}\pi^2 + \frac{2}{3}\pi^2 \ln 2 - \ln 2 + i\frac{\pi}{2}\,. \tag{1.75}$$

The fermionic two-loop part agrees with the result of Ref. [87].

Our three-loop result reads

$$\begin{aligned}
c_s^{FFL} &= 30.1(1) + 7.5621(1)\, L_\mu + \frac{1}{9}\pi^2 L_\mu^2\,, \\
c_s^{FAL} &= 21.4(1) + 4.0827(1)\, L_\mu + \left(\frac{11}{36} + \frac{1}{36}\pi^2\right) L_\mu^2\,, \\
c_s^{FLL} &= \frac{73}{324} - \frac{1}{27}\pi^2 + \frac{5}{54} L_\mu - \frac{1}{18} L_\mu^2\,, \\
c_s^{FHL} &= -\frac{157}{81} + \frac{5}{27}\pi^2 + \left(-\frac{58}{27} + \frac{2}{9}\pi^2\right) L_\mu - \frac{1}{9} L_\mu^2\,.
\end{aligned} \tag{1.76}$$

# Chapter 2

# Renormalisation Constants

In the last chapter we already pointed out that the quark mass and wave function renormalisation constants in the on-shell scheme are necessary ingredients for the calculation of the matching coefficients. The former is needed to two-loop, the latter even to three-loop order. The results are available in the literature. They have been calculated to two-loops in Refs. [89, 90] and to three-loops in Refs. [8–11] in the framework of dimensional regularisation (DREG). However, the integrals needed for this calculation form a subset of the integrals needed for the calculation of the matching coefficient. The calculation of these renormalisation constants can therefore be used as a check of a part of our implementation. Furthermore, our calculation of the wave function renormalisation constant poses the first independent check of the analytical result in the literature. Additionally, we calculate both renormalisation constants in the framework of dimensional reduction (DRED) to three-loops. These calculations are described in this chapter. Parts of the results have been published in Ref. [14].

## 2.1 General Remarks

In this section we outline the calculation of the renormalisation constants. First, we explain the regularisation schemes, DREG and DRED, and the on-shell, $\overline{\text{MS}}$ and $\overline{\text{DR}}$ renormalisation schemes. The necessary formulae for the calculation are derived in Section 2.1.3. In Section 2.1.4, we discuss the more involved renormalisation procedure of the DRED calculation and provide results for the necessary renormalisation constants.

### 2.1.1 Regularisation Schemes

In order to calculate the divergent integrals, which appear in quantum field theories, it is necessary to specify a regularisation scheme. The most commonly used one is

dimensional regularisation [80]. In this scheme, the number of dimensions is taken to be a complex number $d$, which is different from four. Here, we make the usual choice, $d = 4 - 2\epsilon$. The momentum integrals are then carried out in $d$ dimensions and the limit $\epsilon \to 0$ is only taken in the final result. In this way, the divergencies manifest themselves as poles in $\epsilon$.

While DREG is a very useful calculational framework in non-supersymmetric theories, it has been known for a long time to break supersymmetry (SUSY) (see for example Ref. [91]). The reason is that the number of bosonic and fermionic degrees of freedom in a super-multiplet do not match for $d \neq 4$. To remedy this, DRED was proposed in Ref. [92] (see also Ref. [93]). In this framework, it is assumed that $\epsilon > 0$. Space-time is compactified to $d$ dimensions in such a way that vector fields remain four dimensional. Only the integration momenta are considered to be $d$ dimensional, which is enough to render the loop integrals ultra-violet finite.

It was, however, soon realised that DRED is mathematically inconsistent [94]. In Ref. [95], it was explained that a consistent formulation can be achieved if the four, $d$ and $\epsilon$ dimensional spaces are interpreted as infinite dimensional. This leads again to explicit SUSY breaking. However, it has also been shown that the SUSY restoring counterterms vanish in some calculations [96].

The advantage of DRED in practical applications is that the implementation is very easy at the technical level. It is very convenient to introduce an additional scalar particle, the so-called $\varepsilon$ scalar, by splitting the gauge field into a $d$- and a $2\epsilon$-dimensional part. The actual calculations can now be performed just like in DREG.

However, if DRED is applied to non-supersymmetric theories, for example after some of the heavy SUSY particles have been integrated out, the situation becomes more complicated. In this case the couplings of the $q\bar{q}\varepsilon$ and the four-$\varepsilon$ vertex, the so-called evanescent couplings, renormalise differently from the theory's gauge coupling. Therefore, one has to allow for new couplings in the theory.

In this work we apply DRED to QCD, where we use the implementation of Refs. [97, 98]. In this case, we have to introduce four new couplings. The Yukawa-type coupling of the $\varepsilon$ scalar with a quark and an anti-quark is denoted by $g_e$. The three different four-$\varepsilon$ scalar couplings are denoted by $\lambda_i$, $i \in \{1, 2, 3\}$. The Lagrangian is given by

$$\mathcal{L}^{\text{QCD,DRED}} = \mathcal{L}^d + \mathcal{L}^\epsilon \,, \tag{2.1}$$

where the $d$-dimensional part is the usual QCD Lagrangian in DREG. The (bare) $2\epsilon$-dimensional part is given by [97]

$$\begin{aligned} \mathcal{L}^\epsilon &= \frac{1}{2}\left(\partial_\mu \varepsilon^a_\sigma\right)^2 + g_s\, f^{abc} \partial_\mu \varepsilon^a_\sigma A^{b\mu} \varepsilon^c_\sigma + \frac{1}{2} g_s^2\, f^{abc} f^{ade} A^b_\mu \varepsilon^c_\sigma A^{d\mu} \varepsilon^e_\sigma \\ &\quad - g_e\, \overline{\psi}\, t^a \gamma_\sigma \psi \varepsilon^a_\sigma - \frac{1}{4} \sum_{i=1}^{3} \lambda_i H_i^{abcd} \varepsilon^a_\sigma \varepsilon^b_{\sigma'} \varepsilon^c_\sigma \varepsilon^d_{\sigma'} \,, \end{aligned} \tag{2.2}$$

where $A^a_\mu$ is the gluon field, $\varepsilon^a_\sigma$ denotes the $\varepsilon$-scalar field and $\psi$ is the quark field. $\mu$ is a d-dimensional index, $\sigma$ and $\sigma'$ are $2\epsilon$-dimensional indices and $t^a$ denotes a generator of the fundamental representation of SU(3). The $H_i^{abcd}$ are symmetric under interchange of $(a, b)$ and $(c, d)$. Since the gauge group of QCD is SU(3), there are three independent rank four tensors with this property. Our choice for these tensors is

$$\begin{aligned} H_1^{abcd} &= \frac{1}{2}\left(f^{ace}f^{bde} + f^{ade}f^{bce}\right), \\ H_2^{abcd} &= \delta^{ab}\delta^{cd} + \delta^{ac}\delta^{bd} + \delta^{ad}\delta^{bc}, \\ H_3^{abcd} &= \frac{1}{2}\left(\delta^{ac}\delta^{bd} + \delta^{ad}\delta^{bc}\right) - \delta^{ab}\delta^{cd}. \end{aligned} \tag{2.3}$$

Furthermore, we introduce the notation $\alpha_e = g_e^2/(4\pi)$ and $\eta_i = \lambda_i/(4\pi)$ for the evanescent couplings in analogy with the gauge coupling. Since all terms which involve only the $\varepsilon$ scalars and no gluons are separately gauge independent, the corresponding couplings renormalise differently, as we have already noted above.

### 2.1.2 Renormalisation Schemes

Renormalisation (see for example Ref. [99, 100]) is a necessary procedure in any quantum field theory. It ensures that the parameters of the Lagrangian correspond to the physical observables and that the divergencies are absorbed into unphysical quantities, the so-called bare parameters. There is, however, some freedom in the way how this is achieved. A consistent set of rules for the renormalisation of all parameters of a given theory is called a renormalisation scheme. In the following, we give a brief explanation of the schemes used in this work.

The quark mass and wave function renormalisation constants are defined as

$$m_{Q,0} = Z_m^{\mathrm{OS}}\, M_Q\,, \tag{2.4}$$

$$m_{Q,0} = Z_m^x\, m_Q^x\,, \tag{2.5}$$

$$\psi_0 = \sqrt{Z_2^{\mathrm{OS}}}\,\psi\,, \tag{2.6}$$

where $m_Q$ is the mass of the quark field $\psi$, $M_Q$ is its pole mass, $x \in \{\overline{\mathrm{MS}}, \overline{\mathrm{DR}}\}$ and bare quantities are labelled by a subscript 0. In order to calculate these constants, we have to put certain requirements on the pole position and residual of the quark propagator.

In the on-shell scheme we require the pole of the propagator to be at the position of the renormalised mass. Its residual is required to be equal to $-i$. Thus, the full,

renormalised quark propagator is given by

$$\begin{aligned} S_F(q) &= \frac{-iZ_2^{\mathrm{OS}}}{\not{q} - m_{Q,0} + \Sigma(q, M_Q)} \\ &= \frac{-iZ_2^{\mathrm{OS}}}{\not{q} - Z_m^{\mathrm{OS}} M_Q + \Sigma(q, M_Q)} \qquad (2.7) \\ &\overset{q^2 \to M_Q^2}{\longrightarrow} \frac{-i}{\not{q} - M_Q} \,. \qquad (2.8) \end{aligned}$$

In minimal subtraction (MS) schemes the renormalisation constants are defined in such a way, that they only subtract the divergencies. This has the advantage that the renormalisation constants are mass-independent. In the modified minimal subtraction ($\overline{\mathrm{MS}}$) scheme the $\ln 4\pi$ and $\gamma_E$ terms, which accompany the poles in $\epsilon$, are subtracted as well. The modified minimal subtraction scheme in combination with DRED is called $\overline{\mathrm{DR}}$ scheme.

In DRED we have to deal with an additional mass next to the one of the heavy quark, namely that of the $\varepsilon$ scalars. While there is no $\varepsilon$-scalar mass term in the Lagrangian (cf. Eq. (2.2)), radiative corrections introduce a mass at higher loop order. Here, we renormalise this mass on-shell by requiring that it is zero in every order in perturbation theory. This is the so-called $\overline{\mathrm{DR}}'$ scheme [101]. It has the advantage that the $\varepsilon$-scalar mass completely decouples from physical quantities. For supersymmetric theories, the $\overline{\mathrm{DR}}$ and $\overline{\mathrm{DR}}'$ schemes are the same. The renormalisation of the $\varepsilon$-scalar mass is discussed in more detail in Section 2.1.4.

### 2.1.3 Calculation

Both the mass and the wave function renormalisation constant can be calculated by considering one-particle irreducible quark self-energy diagrams. Sample diagrams are depicted in Fig. 2.1.

The general tensor structure of the quark self-energy diagrams in QCD can be decomposed as

$$\Sigma(q, m_Q) = m_Q \, \Sigma_s(q^2, m_Q) + \not{q} \, \Sigma_v(q^2, m_Q) \,, \qquad (2.9)$$

where $q$ is the momentum of the external quark. Again, it is useful to apply projectors to get the necessary tensor structures. Here, we have

$$\Sigma_s(q^2, m_Q) = \frac{1}{4m_Q} \mathrm{Tr} \left\{ \Sigma(q, m_Q) \right\} \,, \qquad (2.10)$$

$$\Sigma_v(q^2, m_Q) = \frac{1}{4q^2} \mathrm{Tr} \left\{ \not{q} \, \Sigma(q, m_Q) \right\} \,. \qquad (2.11)$$

For the current calculation it is convenient to introduce the functions $\Sigma_1 = \Sigma_s + \Sigma_v$ and $\Sigma_2 = \Sigma_v$. In terms of these functions we can rewrite $\Sigma$ as

$$\Sigma(q, m_Q) = m_Q \, \Sigma_1(q^2, m_Q) + (\not{q} - m_Q) \, \Sigma_2(q^2, m_Q) \,. \qquad (2.12)$$

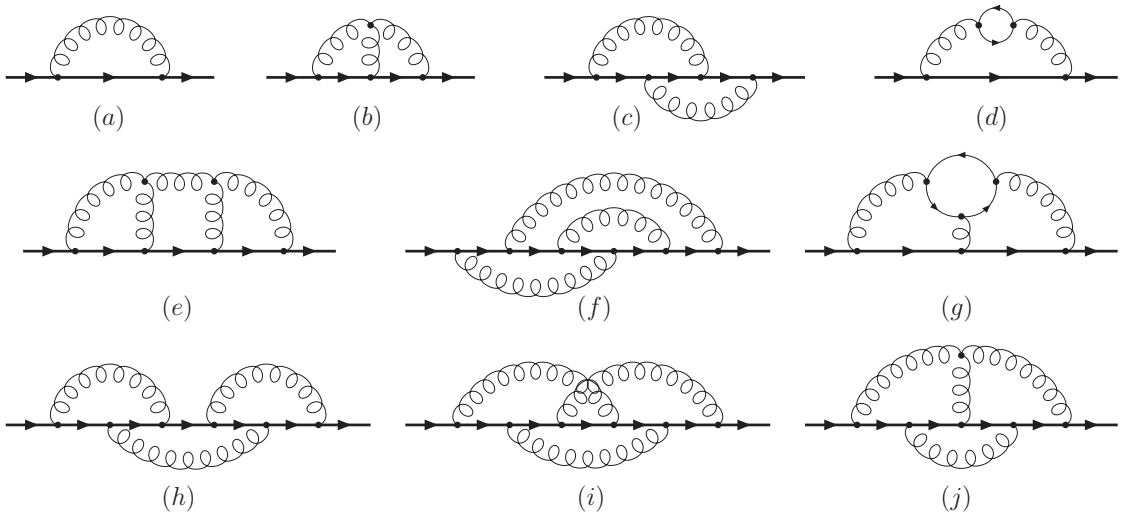


Figure 2.1: Sample self-energy diagrams contributing to the renormalisation constants. Bold lines denote massive quarks with mass $m_Q$ and curly lines denote gluons. In the closed fermion loops all quark flavours have to be considered.

To derive the formulae for the renormalisation constants, we consider, following Ref. [11], the expansion of $\Sigma$ around $q^2 = M_Q^2$. This is given by

$$\begin{aligned}\Sigma(q, M_Q) &\approx M_Q\,\Sigma_1(M_Q^2, M_Q) + (\not{q} - M_Q)\,\Sigma_2(M_Q^2, M_Q) \\ &\quad + M_Q \frac{\partial}{\partial q^2}\Sigma_1(q^2, M_Q)\Big|_{q^2=M_Q^2}(q^2 - M_Q^2) + \dots\,, \end{aligned} \tag{2.13}$$

where the ellipses denote higher order terms. Note that we do not have to take the derivative of the second term in Eq. (2.12) since this is of higher order than the derivative of the first term. Using $q^2 - M_Q^2 = (\not{q} - M_Q)(\not{q} + M_Q)$ and $\not{q} + M_Q \overset{q^2\to M_Q^2}{\longrightarrow} 2M_Q$, we finally obtain

$$\begin{aligned}\Sigma(q, M_Q) &\approx M_Q\,\Sigma_1(M_Q^2, M_Q) \\ &\quad + (\not{q} - M_Q)\left(2M_Q^2 \frac{\partial}{\partial q^2}\Sigma_1(q^2, M_Q)\Big|_{q^2=M_Q^2} + \Sigma_2(M_Q^2, M_Q)\right) \\ &\quad + \dots\,. \end{aligned} \tag{2.14}$$

Inserting Eq. (2.13) into Eq. (2.7) and comparing to Eq. (2.8) we obtain the following formulae for the renormalisation constants

$$Z_m^{\rm OS} = 1 + \Sigma_1(M_Q^2, M_Q)\,, \tag{2.15}$$

$$(Z_2^{\rm OS})^{-1} = 1 + 2M_Q^2 \frac{\partial}{\partial q^2}\Sigma_1(q^2, M_Q)\Big|_{q^2=M_Q^2} + \Sigma_2(M_Q^2, M_Q)\,. \tag{2.16}$$

Thus, to obtain $Z_m$ we only need to calculate the sum of the two tensor structures $\Sigma_s$ and $\Sigma_v$ for $q^2 = M_Q^2$.

A convenient way to obtain $Z_2$ was introduced in Ref. [11]. If we consider the momentum of the external quarks to be $q = Q(1+t)$ with $Q^2 = M_Q^2$, the self-energy can be written as

$$\Sigma(q, M_Q) = M_Q\, \Sigma_1(q^2, M_Q) + (\not{q}\ - M_Q)\, \Sigma_2(q^2, M_Q) + t\, \not{q}\ \Sigma_2(q^2, M_Q)\,. \qquad (2.17)$$

Let us now consider the quantity $\mathrm{Tr}\{\frac{\not{q}\ + M_Q}{4M_Q^2}\Sigma\}$, which is just the sum of $\Sigma_s(M_Q^2, M_Q)$ and $\Sigma_v(M_Q^2, M_Q)$, and expand to first order in $t$

$$\begin{aligned}
\mathrm{Tr}\left\{\frac{\not{q}\ + M_Q}{4M_Q^2}\,\Sigma(q, M_Q)\right\} &= \Sigma_1(q^2, M_Q) + t\,\Sigma_2(q^2, M_Q) \\
&= \Sigma_1(M_Q^2, M_Q) \\
&\quad + \left(2M_Q^2 \frac{\partial}{\partial q^2}\Sigma_1(q^2, M_Q)\Big|_{q^2=M_Q^2} + \Sigma_2(M_Q^2, M_Q)\right) t \\
&\quad + \mathcal{O}\left(t^2\right)\,. \qquad (2.18)
\end{aligned}$$

To calculate $Z_2$ we therefore have to compute the first derivative of the self-energy diagrams and project again on the sum of $\Sigma_s$ and $\Sigma_v$.

Just as in the case of the matching coefficients, the mass renormalisation is taken into account iteratively by calculating one- and two-loop diagrams with zero-momentum insertions.

If we consider only the $n_l$ part at the three-loop level, all occurring diagrams can be mapped onto the "+"-integrals of Eq. (1.20). However, to do the full three-loop calculation, we need seven additional integral classes[1], namely

$$\begin{aligned}
K_1(n_1, \ldots, n_9) &= \\
&\left(\frac{\mu^2}{i\pi^{d/2}}\right)^3 \int \frac{\mathrm{d}^d k\, \mathrm{d}^d l\, \mathrm{d}^d p}{(k^2)^{n_1}(l^2)^{n_2}(p^2)^{n_3}(k^2+2q\cdot k)^{n_4}((k+l)^2+2q\cdot(k+l))^{n_5}} \\
&\quad \times \frac{((p-l)^2)^{-n_9}}{((k+l+p)^2+2q\cdot(k+l+p))^{n_6}((k+l+p)^2)^{n_7}((k+p)^2)^{n_8}}\,, \\
K_2(n_1, \ldots, n_9) &= \left(\frac{\mu^2}{i\pi^{d/2}}\right)^3 \int \frac{\mathrm{d}^d k\, \mathrm{d}^d l\, \mathrm{d}^d p}{(k^2)^{n_1}(l^2)^{n_2}(p^2)^{n_3}((k+l+p)^2+2q\cdot(k+l+p))^{n_4}} \\
&\quad \times \frac{1}{(k^2+2q\cdot k)^{n_5}(p^2+2q\cdot p)^{n_6}((k+l)^2+2q\cdot(k+l))^{n_7}} \\
&\quad \times \frac{1}{((l+p)^2+2q\cdot(l+p))^{n_8}((p-k)^2)^{n_9}}\,,
\end{aligned}$$

[1] These integral classes will appear in the full calculation of the matching coefficient as well. There, however, they will be accompanied by the corresponding vertex integrals.

$$
\begin{aligned}
K_3(n_1,\ldots,n_9) &= \left(\frac{\mu^2}{i\pi^{d/2}}\right)^3 \int \frac{\mathrm{d}^d k\,\mathrm{d}^d l\,\mathrm{d}^d p}{(k^2)^{n_1}(l^2)^{n_2}(p^2)^{n_3}(k^2+2q\cdot k)^{n_4}(l^2+2q\cdot l)^{n_5}} \\
&\quad \times \frac{((p-k)^2)^{-n_9}}{(p^2+2q\cdot p)^{n_6}((k+l)^2+2q\cdot(k+l))^{n_7}((l+p)^2+2q\cdot(l+p))^{n_8}}\,, \\
K_4(n_1,\ldots,n_9) &= \left(\frac{\mu^2}{i\pi^{d/2}}\right)^3 \int \frac{\mathrm{d}^d k\,\mathrm{d}^d l\,\mathrm{d}^d p}{(k^2)^{n_1}(l^2)^{n_2}(p^2)^{n_3}(k^2+2q\cdot k)^{n_4}(l^2+2q\cdot l)^{n_5}} \\
&\quad \times \frac{((p-k)^2)^{-n_9}}{(p^2+2q\cdot p)^{n_6}((k+l)^2+2q\cdot(k+l))^{n_7}((p-l)^2)^{n_8}}\,, \\
K_5(n_1,\ldots,n_9) &= \left(\frac{\mu^2}{i\pi^{d/2}}\right)^3 \int \frac{\mathrm{d}^d k\,\mathrm{d}^d l\,\mathrm{d}^d p}{(k^2)^{n_1}(l^2)^{n_2}(p^2)^{n_3}(k^2+2q\cdot k)^{n_4}(l^2+2q\cdot l)^{n_5}} \\
&\quad \times \frac{((p-l)^2)^{-n_9}}{((k+l)^2+2q\cdot(k+l))^{n_6}((l+p)^2+2q\cdot(l+p))^{n_7}} \\
&\quad \times \frac{1}{((k+l+p)^2+2q\cdot(k+l+p))^{n_8}}\,, \\
K_6(n_1,\ldots,n_9) &= \left(\frac{\mu^2}{i\pi^{d/2}}\right)^3 \int \frac{\mathrm{d}^d k\,\mathrm{d}^d l\,\mathrm{d}^d p}{(k^2)^{n_1}(l^2)^{n_2}(p^2)^{n_3}(k^2+2q\cdot k)^{n_4}(l^2+2q\cdot l)^{n_5}} \\
&\quad \times \frac{((p-l)^2)^{-n_9}}{((k+l)^2+2q\cdot(k+l))^{n_6}((l+p)^2+2q\cdot(l+p))^{n_7}((p-k)^2)^{n_8}}\,, \\
K_7(n_1,\ldots,n_9) &= \left(\frac{\mu^2}{i\pi^{d/2}}\right)^3 \int \frac{\mathrm{d}^d k\,\mathrm{d}^d l\,\mathrm{d}^d p}{(k^2)^{n_1}(l^2)^{n_2}(p^2)^{n_3}((p-k)^2)^{n_4}(k^2+2q\cdot k)^{n_6}} \\
&\quad \times \frac{((k-l)^2)^{-n_5}}{(p^2+2q\cdot p)^{n_7}((k+l)^2+2q\cdot(k+l))^{n_8}((l+p)^2+2q\cdot(l+p))^{n_9}}\,,
\end{aligned}
\tag{2.19}
$$

where $q^2 = m_Q^2$ and only one index out of $n_8$ and $n_9$ of $K_2$ can adopt positive values. Furthermore, the index $n_8$ of $J_+^{(3)}$ can now adopt positive values as well.

The results for the on-shell renormalisation constants in DREG can be cast into the following form

$$
\begin{aligned}
Z_i^{\mathrm{OS}} &= 1 + \frac{\alpha_s(\mu)}{\pi}\left(\frac{e^{\gamma_E}}{4\pi}\right)^{-\epsilon}\delta Z_i^{(1)} + \left(\frac{\alpha_s(\mu)}{\pi}\right)^2\left(\frac{e^{\gamma_E}}{4\pi}\right)^{-2\epsilon}\delta Z_i^{(2)} \\
&\quad + \left(\frac{\alpha_s(\mu)}{\pi}\right)^3\left(\frac{e^{\gamma_E}}{4\pi}\right)^{-3\epsilon}\delta Z_i^{(3)} + \mathcal{O}\left(\alpha_s^4\right)\,,
\end{aligned}
\tag{2.20}
$$

where $i \in \{m, 2\}$. It is convenient to further decompose the three-loop contribution in terms of the different colour factors

$$\begin{aligned}\delta Z_i^{(3)} &= C_F^3\, Z_i^{FFF} + C_F^2 C_A\, Z_i^{FFA} + C_F C_A^2\, Z_i^{FAA} \\ &\quad + C_F T_F n_l \left(C_F\, Z_i^{FFL} + C_A\, Z_i^{FAL} + T_F n_l\, Z_i^{FLL} + T_F\, Z_i^{FHL}\right) \\ &\quad + C_F T_F \left(C_F\, Z_i^{FFH} + C_A\, Z_i^{FAH} + T_F\, Z_i^{FHH}\right) . \end{aligned} \tag{2.21}$$

In the case of DRED we present the results for $N_c = 3$ only, since our implementation of the $\eta_i$ couplings is only valid for SU(3). We cast the results in the following form

$$Z_i^{\text{OS,DRED}} = 1 + \left(\frac{e^{\gamma_E}}{4\pi}\right)^{-\epsilon} \delta\tilde{Z}_i^{(1)} + \left(\frac{e^{\gamma_E}}{4\pi}\right)^{-2\epsilon} \delta\tilde{Z}_i^{(2)} + \left(\frac{e^{\gamma_E}}{4\pi}\right)^{-3\epsilon} \delta\tilde{Z}_i^{(3)} + \dots , \tag{2.22}$$

where the ellipses denote higher order corrections. Furthermore, we decompose the two- and three-loop results in terms of the different couplings as

$$\tilde{Z}_i^{(2)} = \left(\frac{\alpha_s^{\overline{\text{DR}}}}{\pi}\right)^2 X_i^{ss} + \frac{\alpha_s^{\overline{\text{DR}}}}{\pi}\frac{\alpha_e}{\pi}\, X_i^{se} + \left(\frac{\alpha_e}{\pi}\right)^2 X_i^{ee} , \tag{2.23}$$

$$\begin{aligned}\tilde{Z}_i^{(3)} &= \left(\frac{\alpha_s^{\overline{\text{DR}}}}{\pi}\right)^3 Y_i^{sss} + \left(\frac{\alpha_s^{\overline{\text{DR}}}}{\pi}\right)^2 \frac{\alpha_e}{\pi}\, Y_i^{sse} + \frac{\alpha_s^{\overline{\text{DR}}}}{\pi}\left(\frac{\alpha_e}{\pi}\right)^2 Y_i^{see} + \left(\frac{\alpha_e}{\pi}\right)^3 Y_i^{eee} \\ &\quad + \sum_{j=1}^{3}\left[\frac{\alpha_e}{\pi}\frac{\eta_j}{\pi}\left(\frac{\alpha_e}{\pi}\, Y_i^{eej} + \frac{\eta_j}{\pi}\, Y_i^{ejj}\right)\right] + \frac{\alpha_e}{\pi}\frac{\eta_1}{\pi}\frac{\eta_3}{\pi}\, Y_i^{e13} , \end{aligned} \tag{2.24}$$

where we suppressed the $\mu$ dependence for brevity.

### 2.1.4 Renormalisation in DRED

The main complication of the DRED calculation is the more involved renormalisation. In addition to the strong coupling $\alpha_s$ also the evanescent coupling $\alpha_e$ has to be renormalised to two-loop order. The evanescent couplings $\eta_i$ appear for the first time at three-loop order and thus no renormalisation is necessary. For both the heavy quark mass, $m_Q$, and the $\varepsilon$-scalar mass, $m_\varepsilon$, two-loop counterterms are necessary. Whereas the couplings are renormalised using minimal subtraction the masses are renormalised on-shell. The corresponding renormalisation constants are defined through

$$\alpha_{s,0}^{\overline{\text{DR}}} = \mu^{2\epsilon}\left(Z_s^{\overline{\text{DR}}}\right)^2 \alpha_s^{\overline{\text{DR}}} , \tag{2.25}$$

$$\alpha_{e,0} = \mu^{2\epsilon}\left(Z_e\right)^2 \alpha_e , \tag{2.26}$$

$$m_{Q,0}^{\overline{\text{DR}}} = M_Q Z_m^{\text{OS,DRED}} , \tag{2.27}$$

$$\left(m_{\varepsilon,0}\right)^2 = m_\varepsilon^2 Z_{m_\varepsilon}^{\text{OS}} . \tag{2.28}$$

Recently, the quantities $Z_e$ and $Z_s^{\overline{\rm DR}}$ have been computed to three- [102] and four-loop order [98]. The results have been presented in terms of the corresponding $\beta$ functions. For completeness we present in the following the two-loop results for the renormalisation constants

$$\begin{aligned}
Z_s^{\overline{\rm DR}} &= 1+\frac{\alpha_s^{\overline{\rm DR}}}{\pi}\left(\frac{e^{\gamma_E}}{4\pi}\right)^{-\epsilon}\left(-\frac{11}{24}C_A+\frac{1}{6}T_F n_f\right)\frac{1}{\epsilon} \\
&\quad+\left(\frac{\alpha_s^{\overline{\rm DR}}}{\pi}\right)^2\left(\frac{e^{\gamma_E}}{4\pi}\right)^{-2\epsilon}\left[\left(\frac{121}{384}C_A^2-\frac{11}{48}C_A T_F n_f+\frac{1}{24}T_F^2 n_f^2\right)\frac{1}{\epsilon^2}\right. \\
&\quad\left.+\left(-\frac{17}{96}C_A^2+\frac{5}{48}C_A T_F n_f+\frac{1}{16}C_F T_F n_f\right)\frac{1}{\epsilon}\right], \qquad (2.29) \\
Z_e &= 1+\frac{\alpha_s^{\overline{\rm DR}}}{\pi}\left(\frac{e^{\gamma_E}}{4\pi}\right)^{-\epsilon}\left(-\frac{3}{4}C_F\right)\frac{1}{\epsilon} \\
&\quad+\frac{\alpha_e}{\pi}\left(\frac{e^{\gamma_E}}{4\pi}\right)^{-\epsilon}\left(-\frac{1}{4}C_A+\frac{1}{2}C_F+\frac{1}{4}T_F n_f\right)\frac{1}{\epsilon} \\
&\quad+\left(\frac{\alpha_s^{\overline{\rm DR}}}{\pi}\right)^2\left(\frac{e^{\gamma_E}}{4\pi}\right)^{-2\epsilon}\left\{\left(\frac{11}{32}C_A C_F+\frac{9}{32}C_F^2-\frac{1}{8}C_F T_F n_f\right)\frac{1}{\epsilon^2}\right. \\
&\quad\left.+\left[\frac{7}{256}C_A^2-\frac{55}{192}C_A C_F-\frac{3}{64}C_F^2-\left(\frac{1}{32}C_A-\frac{5}{48}C_F\right)T_F n_f\right]\frac{1}{\epsilon}\right\} \\
&\quad+\frac{\alpha_s^{\overline{\rm DR}}}{\pi}\frac{\alpha_e}{\pi}\left(\frac{e^{\gamma_E}}{4\pi}\right)^{-2\epsilon}\left[\left(\frac{3}{8}C_A C_F-\frac{3}{4}C_F^2-\frac{3}{8}C_F T_F n_f\right)\frac{1}{\epsilon^2}\right. \\
&\quad\left.+\left(\frac{3}{32}C_A^2-\frac{5}{8}C_A C_F+\frac{11}{16}C_F^2+\frac{5}{32}C_F T_F n_f\right)\frac{1}{\epsilon}\right] \\
&\quad+\left(\frac{\alpha_e}{\pi}\right)^2\left(\frac{e^{\gamma_E}}{4\pi}\right)^{-2\epsilon} \\
&\quad\times\left\{\left[\frac{3}{32}C_A^2-\frac{3}{8}C_A C_F+\frac{3}{8}C_F^2-\left(\frac{3}{16}C_A-\frac{3}{8}C_F-\frac{3}{32}T_F n_f\right)T_F n_f\right]\frac{1}{\epsilon^2}\right. \\
&\quad\left.+\left[-\frac{3}{32}C_A^2+\frac{5}{16}C_A C_F-\frac{1}{4}C_F^2+\left(\frac{3}{32}C_A-\frac{3}{16}C_F\right)T_F n_f\right]\frac{1}{\epsilon}\right\} \\
&\quad+\frac{\alpha_e}{\pi}\left(\frac{e^{\gamma_E}}{4\pi}\right)^{-2\epsilon}\left(\frac{\eta_1}{\pi}\frac{9}{32}-\frac{\eta_2}{\pi}\frac{5}{16}-\frac{\eta_3}{\pi}\frac{3}{16}\right)\frac{1}{\epsilon}-\left(\frac{\eta_1}{\pi}\right)^2\left(\frac{e^{\gamma_E}}{4\pi}\right)^{-2\epsilon}\frac{27}{256}\frac{1}{\epsilon} \\
&\quad+\left(\frac{\eta_2}{\pi}\right)^2\left(\frac{e^{\gamma_E}}{4\pi}\right)^{-2\epsilon}\frac{15}{16}\frac{1}{\epsilon}-\left(\frac{\eta_3}{\pi}\right)^2\left(\frac{e^{\gamma_E}}{4\pi}\right)^{-2\epsilon}\frac{21}{128}\frac{1}{\epsilon}+\frac{\eta_1}{\pi}\frac{\eta_3}{\pi}\left(\frac{e^{\gamma_E}}{4\pi}\right)^{-2\epsilon}\frac{9}{64}\frac{1}{\epsilon}. \qquad (2.30)
\end{aligned}$$

Here and in the following, we include factors $(e^{\gamma_E}/(4\pi))^{-\epsilon}$, where $\gamma_E$ is Euler's constant, in the $\overline{\rm MS}$ and $\overline{\rm DR}$ renormalisation constants to be consistent with the on-shell

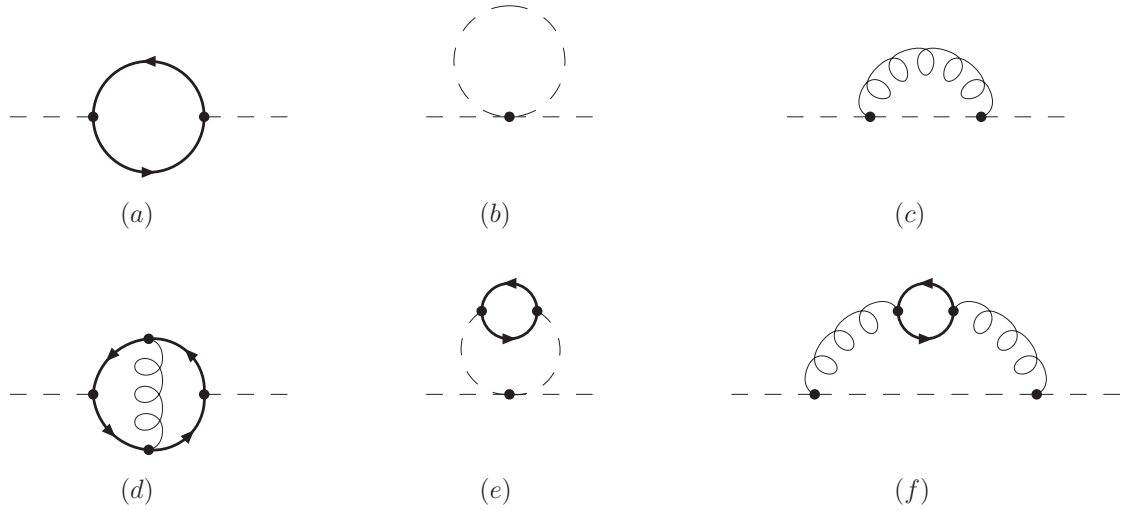


Figure 2.2: One- and two-loop Feynman diagrams contributing to the $\varepsilon$-scalar propagator. Dashed lines denote $\varepsilon$ scalars, curly lines denote gluons and solid lines denote massive quarks with mass $m_Q$.

quantities. Since a $\overline{\text{MS}}$ or $\overline{\text{DR}}$ renormalisation constant does not have $\mathcal{O}(\epsilon)$ terms, it is implied that these terms are dropped when the pre-factors are expanded in $\epsilon$. We also set $N_c = 3$ in all terms containing the couplings $\eta_i$ since our implementation of these couplings is only valid for SU(3).

We already pointed out above that we have to renormalise the $\varepsilon$-scalar mass as well, even though there is no tree-level term in the Lagrangian. The relevant Feynman diagrams contributing to the $\varepsilon$-scalar propagator show quadratic divergences and therefore we only need to consider contributions from massive particles. Thus, only diagrams involving a massive quark have to be taken into account. Some sample diagrams are shown in Fig. 2.2.

At one-loop order there is only one relevant diagram (cf. Fig. 2.2($a$)) which has to be evaluated for vanishing external momentum. A closer look to the two-loop diagrams shows that they develop infrared divergences in the limit $m_\varepsilon \to 0$ (cf., e.g., Fig. 2.2($e$)). They can be regulated by introducing a small but non-vanishing mass for the $\varepsilon$ scalars. After the subsequent application of an asymptotic expansion [23] in the limit $q^2 = m_\varepsilon^2 \ll M_Q^2$ the infrared divergences manifest themselves as $\ln(m_\varepsilon)$ terms. Furthermore, one-loop diagrams like the ones in Fig. 2.2($b$) and ($c$) do not vanish anymore and have to be taken into account as well. Although they are proportional to $m_\varepsilon^2$, after renormalisation they induce two-loop contributions which are proportional to $M_Q^2$, partly multiplied by $\ln(m_\varepsilon)$ terms. We want to stress that in the sum of the genuine two-loop diagrams and the counterterm contributions the limit $m_\varepsilon \to 0$ can be taken which demonstrates the infrared finiteness of the on-shell mass of the $\varepsilon$ scalar.

Taking the infrared finiteness for granted, it is also possible to choose $q^2 = m_\varepsilon^2 =$

0 from the very beginning. Then the individual diagrams are infrared divergent, however, the sum is not. We have performed the calculation both ways and checked that the final result is the same. It is given by

$$
\begin{aligned}
&\frac{M_Q^2}{m_\varepsilon^2} Z_{m_\varepsilon}^{\mathrm{OS}} = \\
&\quad 1 - \frac{\alpha_e}{\pi}\left(\frac{e^{\gamma_E}}{4\pi}\right)^{-\epsilon} n_h T_F \left[\frac{2}{\epsilon} + 2 + 2L_\mu + \epsilon\left(2 + \frac{1}{6}\pi^2 + 2L_\mu + L_\mu^2\right)\right] \\
&\quad - \left(\frac{\alpha_s^{\overline{\mathrm{DR}}}}{\pi}\right)^2 \left(\frac{e^{\gamma_E}}{4\pi}\right)^{-2\epsilon} n_h T_F \left(\frac{3}{4}\frac{1}{\epsilon} + \frac{1}{4} + \frac{3}{2}L_\mu\right) C_A \\
&\quad + \frac{\alpha_s^{\overline{\mathrm{DR}}}}{\pi}\frac{\alpha_e}{\pi}\left(\frac{e^{\gamma_E}}{4\pi}\right)^{-2\epsilon} n_h T_F \Bigg\{ \left(\frac{3}{8}C_A + \frac{3}{2}C_F\right)\frac{1}{\epsilon^2} \\
&\quad + \left[\frac{7}{8}C_A + \frac{3}{2}C_F + \left(\frac{3}{4}C_A + \frac{3}{2}C_F\right)L_\mu\right]\frac{1}{\epsilon} + \left(\frac{15}{8} + \frac{1}{16}\pi^2\right)C_A \\
&\quad + \left(\frac{3}{2} + \frac{1}{8}\pi^2\right)C_F + \left(\frac{7}{4}C_A + \frac{3}{2}C_F\right)L_\mu + \left(\frac{3}{4}C_A + \frac{3}{4}C_F\right)L_\mu^2 \Bigg\} \\
&\quad + \left(\frac{\alpha_e}{\pi}\right)^2 \left(\frac{e^{\gamma_E}}{4\pi}\right)^{-2\epsilon} n_h T_F \Bigg\{ \left(\frac{1}{4}C_A - \frac{1}{2}C_F - \frac{1}{2}T_F n_f\right)\frac{1}{\epsilon^2} \\
&\quad + \left[\frac{1}{2}C_F - \frac{1}{2}(1 + L_\mu)T_F n_f\right]\frac{1}{\epsilon} - \frac{1}{2}C_A + \frac{5}{2}C_F - \left(\frac{1}{2} + \frac{1}{24}\pi^2\right)T_F n_f \\
&\quad - \left(\frac{1}{2}C_A - 2C_F + \frac{1}{2}T_F n_f\right)L_\mu - \left(\frac{1}{4}C_A - \frac{1}{2}C_F + \frac{1}{4}T_F n_f\right)L_\mu^2 \Bigg\} \\
&\quad + \frac{\alpha_e}{\pi}\frac{\eta_1}{\pi}\left(\frac{e^{\gamma_E}}{4\pi}\right)^{-2\epsilon} n_h \left[\frac{3}{16}\frac{1}{\epsilon^2} + \left(\frac{3}{16} + \frac{3}{8}L_\mu\right)\frac{1}{\epsilon} + \frac{3}{16} + \frac{1}{32}\pi^2 + \frac{3}{8}L_\mu + \frac{3}{8}L_\mu^2\right] \\
&\quad - \frac{\alpha_e}{\pi}\frac{\eta_2}{\pi}\left(\frac{e^{\gamma_E}}{4\pi}\right)^{-2\epsilon} n_h \left[\frac{5}{4}\frac{1}{\epsilon^2} + \left(5 + \frac{5}{2}L_\mu\right)\frac{1}{\epsilon} + \frac{25}{2} + \frac{5}{24}\pi^2 + 10L_\mu + \frac{5}{2}L_\mu^2\right] \\
&\quad - \frac{\alpha_e}{\pi}\frac{\eta_3}{\pi}\left(\frac{e^{\gamma_E}}{4\pi}\right)^{-2\epsilon} n_h \left[\frac{7}{16}\frac{1}{\epsilon^2} + \left(\frac{7}{16} + \frac{7}{8}L_\mu\right)\frac{1}{\epsilon} + \frac{7}{16} + \frac{7}{96}\pi^2 + \frac{7}{8}L_\mu + \frac{7}{8}L_\mu^2\right].
\end{aligned}
\tag{2.31}
$$

The overall factor $n_h$ in front of the one- and two-loop corrections shows that the renormalisation of $m_\varepsilon$ only influences those terms which contain a closed heavy quark loop.

The counterterm diagrams for the $\varepsilon$ scalars are generated just like the ones for the heavy quarks by considering one- and two-loop diagrams with zero momentum insertions in $\varepsilon$-scalar lines. Sample diagrams are shown in Fig. 2.3($a$)–($c$). Their evaluation is straightforward. However, the diagram depicted in Fig. 2.3($d$) poses a technical problem. Since we take the $\varepsilon$ scalars to be massless during the calculation,

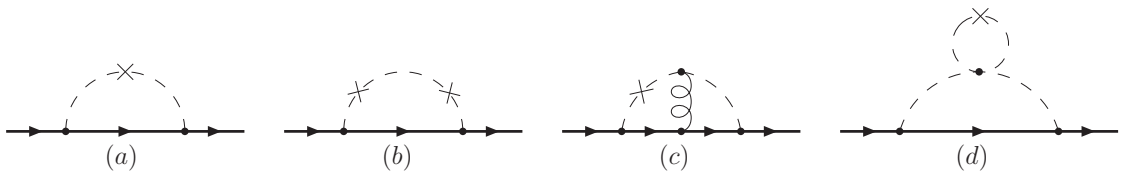


Figure 2.3: Sample counterterm diagrams for the $\varepsilon$-scalar mass. The same coding as in Fig. 2.2 is adopted.

this diagram vanishes since it contains a massless tadpole. On the other hand, at first glance it appears that we need the counterterm for the diagram shown in Fig. 2.4($f$). Let us analyse the situation in more detail in the following.

If we consider the diagrams of Fig. 2.3($d$) and Fig. 2.4($f$) for massive $\varepsilon$ scalars, we can perform an asymptotic expansion in the limit $m_Q \gg m_\varepsilon$. Since the diagrams factorise into a vacuum bubble and an on-shell propagator-type diagram, we can consider these parts separately. The expansion for the latter is exactly the same for both diagrams. It is given by the on-shell diagram evaluated for $m_\varepsilon = 0$ plus terms which are suppressed by powers of the $\varepsilon$-scalar mass.

The expansion of the vacuum bubble is different for the two diagrams. For the counterterm diagram there is only one contribution, namely a massive tadpole integral with a counterterm insertion. From Eq. (2.31) we know that the latter is proportional to $m_Q^2$. In the case of the genuine three-loop diagram we have again the massive tadpole, but now with an insertion of the $\varepsilon$-scalar self-energy diagram depicted in Fig. 2.2($a$) for non-zero $\varepsilon$-scalar momentum. The expansion of this part produces again a contribution proportional to $m_Q^2$, which is exactly the same as the corresponding contribution of the counterterm diagram. The sub-leading terms in the expansion are suppressed by powers of the $\varepsilon$-scalar mass.

So far, we have found the same contributions for the counterterm and the genuine three-loop diagram up to terms with positive powers of $m_\varepsilon$. In the case of the latter diagram there is however one more contribution, namely from the "naive" expansion where $m_\varepsilon$ is simply set to zero. Obviously, the counterterm diagram does not have a contribution from this term. Thus, the sum of the genuine three-loop diagram with non-zero $\varepsilon$-scalar mass and the counterterm diagram is given by the "naive" expansion of the three-loop diagram up to terms of $\mathcal{O}(m_\varepsilon)$. Since we set $m_\varepsilon$ to zero in the end, we can neglect the counterterm diagram and simply calculate the three-loop diagram for $m_\varepsilon = 0$, which is what we want to do anyway.

## 2.2 Mass Renormalisation

In this section we provide the results for the mass renormalisation constants in the framework DREG and DRED.

### 2.2.1 DREG Result

The one- and two-loop contributions to the mass renormalisation constant are

$$\begin{aligned}\delta Z_m^{(1)} &= -C_F\left[\frac{3}{4\epsilon}+1+\frac{3}{4}L_\mu+\left(2+\frac{1}{16}\pi^2+L_\mu+\frac{3}{8}L_\mu^2\right)\epsilon\right.\\ &\left.\quad+\left(4+\frac{1}{12}\pi^2-\frac{1}{4}\zeta_3+\left(2+\frac{1}{16}\pi^2\right)L_\mu+\frac{1}{2}L_\mu^2+\frac{1}{8}L_\mu^3\right)\epsilon^2\right]\end{aligned} \tag{2.32}$$

and

$$\begin{aligned}\delta Z_m^{(2)} =&\\ &\left[\frac{9}{32\epsilon^2}+\left(\frac{45}{64}+\frac{9}{16}L_\mu\right)\frac{1}{\epsilon}+\frac{199}{128}-\frac{17}{64}\pi^2+\frac{1}{2}\pi^2\ln 2-\frac{3}{4}\zeta_3+\frac{45}{32}L_\mu+\frac{9}{16}L_\mu^2\right.\\ &+\left(\frac{677}{256}-\frac{205}{128}\pi^2+3\pi^2\ln 2-\pi^2\ln^2 2-\frac{135}{16}\zeta_3+\frac{7}{40}\pi^4-\frac{1}{2}\ln^4 2-12a_4\right.\\ &\left.\left.+\left(\frac{199}{64}-\frac{17}{32}\pi^2+\pi^2\ln 2-\frac{3}{2}\zeta_3\right)L_\mu+\frac{45}{32}L_\mu^2+\frac{3}{8}L_\mu^3\right)\epsilon\right]C_F^2\\ &+\left[\frac{11}{32\epsilon^2}-\frac{97}{192\epsilon}-\frac{1111}{384}+\frac{1}{12}\pi^2-\frac{1}{4}\pi^2\ln 2+\frac{3}{8}\zeta_3-\frac{185}{96}L_\mu-\frac{11}{32}L_\mu^2\right.\\ &+\left(-\frac{8581}{768}+\frac{271}{1152}\pi^2-\frac{3}{2}\pi^2\ln 2+\frac{1}{2}\pi^2\ln^2 2+\frac{13}{4}\zeta_3-\frac{7}{80}\pi^4+\frac{1}{4}\ln^4 2+6a_4\right.\\ &\left.\left.+\left(-\frac{1463}{192}+\frac{7}{64}\pi^2-\frac{1}{2}\pi^2\ln 2+\frac{3}{4}\zeta_3\right)L_\mu-\frac{229}{96}L_\mu^2-\frac{11}{32}L_\mu^3\right)\epsilon\right]C_AC_F\\ &+\left[-\frac{1}{8\epsilon^2}+\frac{5}{48\epsilon}+\frac{71}{96}+\frac{1}{12}\pi^2+\frac{13}{24}L_\mu+\frac{1}{8}L_\mu^2\right.\\ &\left.+\left(\frac{581}{192}+\frac{97}{288}\pi^2+\zeta_3+\left(\frac{103}{48}+\frac{3}{16}\pi^2\right)L_\mu+\frac{17}{24}L_\mu^2+\frac{1}{8}L_\mu^3\right)\epsilon\right]C_FT_Fn_l\\ &+\left[-\frac{1}{8\epsilon^2}+\frac{5}{48\epsilon}+\frac{143}{96}-\frac{1}{6}\pi^2+\frac{13}{24}L_\mu+\frac{1}{8}L_\mu^2+\left(\frac{1133}{192}-\frac{227}{288}\pi^2\right.\right.\\ &\left.\left.+\pi^2\ln 2-\frac{7}{2}\zeta_3+\left(\frac{175}{48}-\frac{5}{16}\pi^2\right)L_\mu+\frac{17}{24}L_\mu^2+\frac{1}{8}L_\mu^3\right)\epsilon\right]C_FT_F\,,\end{aligned} \tag{2.33}$$

where $a_4=\mathrm{Li}_4\left(\frac{1}{2}\right)=\sum_{n=1}^{\infty}(2^n\,n^4)^{-1}$. We give the one- and two-loop results to $\mathcal{O}(\epsilon^2)$ and $\mathcal{O}(\epsilon)$, respectively. This is necessary for any three-loop calculation.

The individual three-loop terms read

$$
\begin{aligned}
Z_m^{FFF} &= -\frac{9}{128\epsilon^3} - \left(\frac{63}{256} + \frac{27}{128}L_\mu\right)\frac{1}{\epsilon^2} + \left(-\frac{457}{512} + \frac{111}{512}\pi^2 - \frac{3}{8}\pi^2\ln 2\right.\\
&\left. + \frac{9}{16}\zeta_3 - \frac{189}{256}L_\mu - \frac{81}{256}L_\mu^2\right)\frac{1}{\epsilon} - \frac{14225}{3072} - \frac{6037}{3072}\pi^2 + 5\pi^2\ln 2\\
&+ \frac{5}{4}\pi^2\ln^2 2 + \frac{153}{128}\zeta_3 - \frac{73}{480}\pi^4 - \frac{1}{16}\pi^2\zeta_3 + \frac{5}{8}\zeta_5 - \frac{1}{8}\ln^4 2 - 3a_4\\
&+ \left(-\frac{1371}{512} + \frac{333}{512}\pi^2 - \frac{9}{8}\pi^2\ln 2 + \frac{27}{16}\zeta_3\right)L_\mu - \frac{567}{512}L_\mu^2 - \frac{81}{256}L_\mu^3\,, \qquad (2.34)
\end{aligned}
$$

$$
\begin{aligned}
Z_m^{FFA} &= -\frac{33}{128\epsilon^3} + \left(\frac{49}{768} - \frac{33}{128}L_\mu\right)\frac{1}{\epsilon^2} + \left(\frac{3311}{1536} - \frac{43}{512}\pi^2 + \frac{3}{16}\pi^2\ln 2\right.\\
&\left. - \frac{9}{32}\zeta_3 + \frac{379}{256}L_\mu + \frac{33}{256}L_\mu^2\right)\frac{1}{\epsilon} + \frac{100247}{9216} + \frac{6545}{9216}\pi^2 + \frac{25}{36}\pi^2\ln 2\\
&- \frac{89}{72}\pi^2\ln^2 2 - \frac{3995}{384}\zeta_3 + \frac{1867}{8640}\pi^4 - \frac{19}{16}\pi^2\zeta_3 + \frac{45}{16}\zeta_5 - \frac{35}{144}\ln^4 2 - \frac{35}{6}a_4\\
&+ \left(\frac{14311}{1536} - \frac{1135}{1536}\pi^2 + \frac{71}{48}\pi^2\ln 2 - \frac{71}{32}\zeta_3\right)L_\mu + \frac{1797}{512}L_\mu^2 + \frac{121}{256}L_\mu^3\,, \qquad (2.35)
\end{aligned}
$$

$$
\begin{aligned}
Z_m^{FAA} &= -\frac{121}{576\epsilon^3} + \frac{1679}{3456\epsilon^2} - \frac{11413}{20736\epsilon} - \frac{1322545}{124416} - \frac{1955}{3456}\pi^2 - \frac{115}{72}\pi^2\ln 2\\
&+ \frac{11}{36}\pi^2\ln^2 2 + \frac{1343}{288}\zeta_3 - \frac{179}{3456}\pi^4 + \frac{51}{64}\pi^2\zeta_3 - \frac{65}{32}\zeta_5 + \frac{11}{72}\ln^4 2 + \frac{11}{3}a_4\\
&+ \left(-\frac{13243}{1728} + \frac{11}{72}\pi^2 - \frac{11}{24}\pi^2\ln 2 + \frac{11}{16}\zeta_3\right)L_\mu - \frac{2341}{1152}L_\mu^2 - \frac{121}{576}L_\mu^3\,, \qquad (2.36)
\end{aligned}
$$

$$
\begin{aligned}
Z_m^{FFL} &= \frac{3}{32\epsilon^3} + \left(-\frac{5}{192} + \frac{3}{32}L_\mu\right)\frac{1}{\epsilon^2} - \left(\frac{65}{384} + \frac{7}{128}\pi^2 + \frac{1}{4}\zeta_3 + \frac{23}{64}L_\mu + \frac{3}{64}L_\mu^2\right)\frac{1}{\epsilon}\\
&+ \frac{575}{2304} + \frac{1091}{2304}\pi^2 - \frac{11}{9}\pi^2\ln 2 + \frac{2}{9}\pi^2\ln^2 2 + \frac{145}{96}\zeta_3 - \frac{119}{2160}\pi^4 + \frac{1}{9}\ln^4 2\\
&+ \frac{8}{3}a_4 - \left(\frac{497}{384} - \frac{5}{384}\pi^2 + \frac{1}{3}\pi^2\ln 2 + \frac{1}{4}\zeta_3\right)L_\mu - \frac{117}{128}L_\mu^2 - \frac{11}{64}L_\mu^3\,, \qquad (2.37)
\end{aligned}
$$

$$
\begin{aligned}
Z_m^{FAL} &= \frac{11}{72\epsilon^3} - \frac{121}{432\epsilon^2} + \left(\frac{139}{1296} + \frac{1}{4}\zeta_3\right)\frac{1}{\epsilon} + \frac{70763}{15552} + \frac{175}{432}\pi^2 + \frac{11}{18}\pi^2\ln 2 \\
&\quad -\frac{1}{9}\pi^2\ln^2 2 + \frac{89}{144}\zeta_3 + \frac{19}{2160}\pi^4 - \frac{1}{18}\ln^4 2 - \frac{4}{3}a_4 \\
&\quad + \left(\frac{869}{216} + \frac{7}{72}\pi^2 + \frac{1}{6}\pi^2\ln 2 + \frac{1}{2}\zeta_3\right)L_\mu + \frac{373}{288}L_\mu^2 + \frac{11}{72}L_\mu^3\,, \qquad (2.38)
\end{aligned}
$$

$$
\begin{aligned}
Z_m^{FLL} &= -\frac{1}{36\epsilon^3} + \frac{5}{216\epsilon^2} + \frac{35}{1296\epsilon} - \frac{2353}{7776} - \frac{13}{108}\pi^2 - \frac{7}{18}\zeta_3 \\
&\quad - \left(\frac{89}{216} + \frac{1}{18}\pi^2\right)L_\mu - \frac{13}{72}L_\mu^2 - \frac{1}{36}L_\mu^3\,, \qquad (2.39)
\end{aligned}
$$

$$
\begin{aligned}
Z_m^{FHL} &= -\frac{1}{18\epsilon^3} + \frac{5}{108\epsilon^2} + \frac{35}{648\epsilon} - \frac{5917}{3888} + \frac{13}{108}\pi^2 + \frac{2}{9}\zeta_3 \\
&\quad - \left(\frac{143}{108} - \frac{1}{18}\pi^2\right)L_\mu - \frac{13}{36}L_\mu^2 - \frac{1}{18}L_\mu^3\,, \qquad (2.40)
\end{aligned}
$$

$$
\begin{aligned}
Z_m^{FFH} &= \frac{3}{32\epsilon^3} + \left(-\frac{5}{192} + \frac{3}{32}L_\mu\right)\frac{1}{\epsilon^2} - \left(\frac{281}{384} - \frac{17}{128}\pi^2 + \frac{1}{4}\zeta_3 + \frac{23}{64}L_\mu + \frac{3}{64}L_\mu^2\right)\frac{1}{\epsilon} \\
&\quad -\frac{5257}{2304} - \frac{1327}{6912}\pi^2 + \frac{5}{36}\pi^2\ln 2 - \frac{1}{9}\pi^2\ln^2 2 + \frac{37}{96}\zeta_3 + \frac{91}{2160}\pi^4 + \frac{1}{9}\ln^4 2 \\
&\quad +\frac{8}{3}a_4 - \left(\frac{1145}{384} - \frac{221}{384}\pi^2 + \frac{1}{3}\pi^2\ln 2 + \frac{1}{4}\zeta_3\right)L_\mu - \frac{117}{128}L_\mu^2 - \frac{11}{64}L_\mu^3\,, \qquad (2.41)
\end{aligned}
$$

$$
\begin{aligned}
Z_m^{FAH} &= \frac{11}{72\epsilon^3} - \frac{121}{432\epsilon^2} + \left(\frac{139}{1296} + \frac{1}{4}\zeta_3\right)\frac{1}{\epsilon} + \frac{144959}{15552} - \frac{449}{144}\pi^2 + \frac{32}{9}\pi^2\ln 2 \\
&\quad +\frac{1}{18}\pi^2\ln^2 2 - \frac{109}{144}\zeta_3 - \frac{43}{1080}\pi^4 + \frac{1}{8}\pi^2\zeta_3 - \frac{5}{8}\zeta_5 - \frac{1}{18}\ln^4 2 - \frac{4}{3}a_4 \\
&\quad + \left(\frac{583}{108} - \frac{13}{36}\pi^2 + \frac{1}{6}\pi^2\ln 2 + \frac{1}{2}\zeta_3\right)L_\mu + \frac{373}{288}L_\mu^2 + \frac{11}{72}L_\mu^3\,, \qquad (2.42)
\end{aligned}
$$

$$
\begin{aligned}
Z_m^{FHH} &= -\frac{1}{36\epsilon^3} + \frac{5}{216\epsilon^2} + \frac{35}{1296\epsilon} - \frac{9481}{7776} + \frac{4}{135}\pi^2 + \frac{11}{18}\zeta_3 \\
&\quad - \left(\frac{197}{216} - \frac{1}{9}\pi^2\right)L_\mu - \frac{13}{72}L_\mu^2 - \frac{1}{36}L_\mu^3\,. \qquad (2.43)
\end{aligned}
$$

Another important quantity is the relation between the mass renormalisation constants defined in the $\overline{\rm MS}$ and on-shell schemes. At $\mathcal{O}\left(\alpha_s^3\right)$, this relation was first found in a semi-numerical way in Refs. [8, 9]. It was confirmed by the analytical

calculation in Ref. [10]. To calculate this relation, we have to divide the renormalisation constant in the on-shell scheme by the renormalisation constant in the $\overline{\rm MS}$ scheme. The latter can be obtained by taking just the pole part of the quark self-energy diagrams. Since this does not depend on the masses and momenta, the calculation is significantly simpler. Thus, the mass renormalisation constant in the $\overline{\rm MS}$ scheme is even known at the four-loop level [103].

Another possibility is to make an ansatz and determine the coefficients by requiring the relation between the two renormalisation constants to be finite. Using this method we obtain

$$\begin{aligned}
Z_m^{\overline{\rm MS}} &= 1 - \frac{\alpha_s(\mu)}{\pi}\left(\frac{e^{\gamma_E}}{4\pi}\right)^{-\epsilon} C_F \frac{3}{4\epsilon} \\
&\quad + \left(\frac{\alpha_s(\mu)}{\pi}\right)^2 \left(\frac{e^{\gamma_E}}{4\pi}\right)^{-2\epsilon} C_F \\
&\quad \times \left[\left(\frac{9}{32} C_F + \frac{11}{32} C_A - \frac{1}{8} T_F n_f\right)\frac{1}{\epsilon^2} \right. \\
&\quad \left. + \left(-\frac{3}{64} C_F - \frac{97}{192} C_A + \frac{5}{48} T_F n_f\right)\frac{1}{\epsilon}\right] \\
&\quad + \left(\frac{\alpha_s(\mu)}{\pi}\right)^3 \left(\frac{e^{\gamma_E}}{4\pi}\right)^{-3\epsilon} C_F \\
&\quad \times \left\{\left[-\frac{9}{128} C_F^2 - \frac{33}{128} C_F C_A - \frac{121}{576} C_A^2 \right.\right. \\
&\quad \left. + \left(\frac{3}{32} C_F + \frac{11}{72} C_A - \frac{1}{36} T_F n_f\right) T_F n_f\right]\frac{1}{\epsilon^3} \\
&\quad + \left[\frac{9}{256} C_F^2 + \frac{313}{768} C_F C_A + \frac{1679}{3456} C_A^2 \right. \\
&\quad \left. - \left(\frac{29}{192} C_F + \frac{121}{432} C_A - \frac{5}{216} T_F n_f\right) T_F n_f\right]\frac{1}{\epsilon^2} \\
&\quad + \left[-\frac{43}{128} C_F^2 + \frac{43}{256} C_F C_A - \frac{11413}{20736} C_A^2 \right. \\
&\quad \left.\left. + \left(\left(\frac{23}{96} - \frac{1}{4}\zeta_3\right) C_F + \left(\frac{139}{1296} + \frac{1}{4}\zeta_3\right) C_A + \frac{35}{1296} T_F n_f\right) T_F n_f\right]\frac{1}{\epsilon}\right\} .
\end{aligned} \tag{2.44}$$

Since the one- and two-loop results for the on-shell renormalisation constant are given to the needed order in $\epsilon$, it is now possible to derive the relation between the $\overline{\rm MS}$ and on-shell renormalisation constants. However, since the result is quite lengthy, we refrain from listing it here.

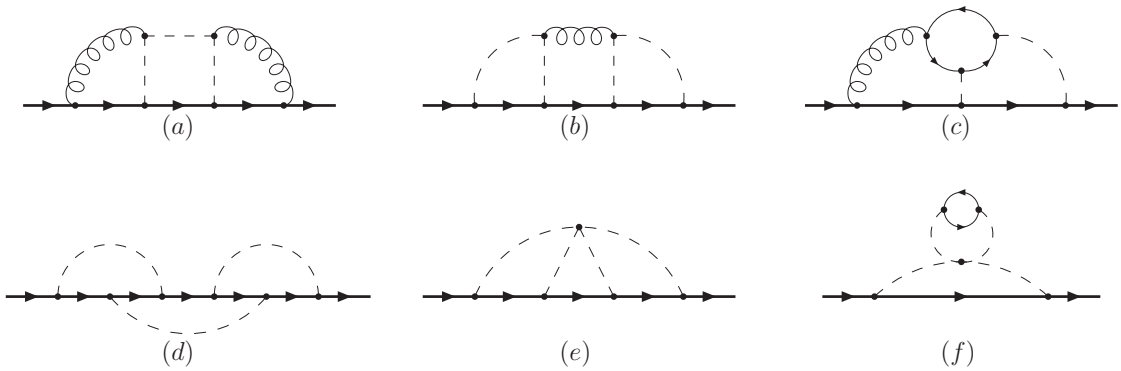


Figure 2.4: Sample three-loop diagrams contributing to the quark propagator which have to be considered additionally in case DRED is used for the regularisation. The same coding as in Figs. 2.1 and 2.2 is adopted.

### 2.2.2 DRED Result

If DREG is used for the regularisation, we have to calculate about 130 diagrams. Due to the additional couplings involving the $\varepsilon$ scalars, there are about 1100 diagrams in the case of DRED. Some sample diagrams are depicted in Fig. 2.4.

We give the result for $N_c = 3$ only, since our implementation of the $\eta_i$ couplings is only valid for SU(3). Even though $n_h = 1$, we keep the label in our formulae so that it is possible to discern the contributions from diagrams with closed massive quark loops.

Our result for the one-loop contribution to the on-shell mass renormalisation constant in DRED reads

$$\begin{aligned}\delta\tilde{Z}_m^{(1)} &= \frac{\alpha_s^{\overline{\mathrm{DR}}}}{\pi}\Bigg\{-\frac{1}{\epsilon}-\frac{4}{3}-L_\mu-\left(\frac{8}{3}+\frac{1}{12}\pi^2+\frac{4}{3}L_\mu+\frac{1}{2}L_\mu^2\right)\epsilon \\ &\qquad -\left[\frac{16}{3}+\frac{1}{9}\pi^2-\frac{1}{3}\zeta_3+\left(\frac{8}{3}+\frac{1}{12}\pi^2\right)L_\mu+\frac{2}{3}L_\mu^2+\frac{1}{6}L_\mu^3\right]\epsilon^2\Bigg\} \\ &\quad -\frac{\alpha_e}{\pi}\left[\frac{1}{3}+\left(\frac{1}{3}+\frac{1}{3}L_\mu\right)\epsilon+\left(\frac{1}{3}+\frac{1}{36}\pi^2+\frac{1}{3}L_\mu+\frac{1}{6}L_\mu^2\right)\epsilon^2\right]. \qquad (2.45)\end{aligned}$$

The individual two- and three-loop contributions read

$$
\begin{aligned}
X_m^{ss} &= \left(\frac{15}{8}-\frac{1}{12}n_f\right)\frac{1}{\epsilon^2}+\left(-\frac{31}{48}+L_\mu+\frac{5}{72}n_f\right)\frac{1}{\epsilon}-\frac{2375}{288}-\frac{5}{36}\pi^2-\frac{1}{9}\pi^2\ln 2 \\
&+\frac{1}{6}\zeta_3-\frac{119}{24}L_\mu-\frac{3}{8}L_\mu^2+\left(\frac{71}{144}+\frac{1}{18}\pi^2+\frac{13}{36}L_\mu+\frac{1}{12}L_\mu^2\right)n_l+\left(\frac{143}{144}\right. \\
&\left.-\frac{1}{9}\pi^2+\frac{13}{36}L_\mu+\frac{1}{12}L_\mu^2\right)n_h+\left\{-\frac{21901}{576}-\frac{173}{96}\pi^2-\frac{2}{3}\pi^2\ln 2+\frac{2}{9}\pi^2\ln^2 2\right. \\
&-2\zeta_3-\frac{7}{180}\pi^4+\frac{1}{9}\ln^4 2+\frac{8}{3}a_4-\left(\frac{3431}{144}+\frac{73}{144}\pi^2+\frac{2}{9}\pi^2\ln 2-\frac{1}{3}\zeta_3\right)L_\mu \\
&-\frac{163}{24}L_\mu^2-\frac{17}{24}L_\mu^3+\left[\frac{581}{288}+\frac{97}{432}\pi^2+\frac{2}{3}\zeta_3+\left(\frac{103}{72}+\frac{1}{8}\pi^2\right)L_\mu+\frac{17}{36}L_\mu^2\right. \\
&\left.+\frac{1}{12}L_\mu^3\right]n_l+\left[\frac{1133}{288}-\frac{227}{432}\pi^2+\frac{2}{3}\pi^2\ln 2-\frac{7}{3}\zeta_3+\left(\frac{175}{72}-\frac{5}{24}\pi^2\right)L_\mu\right. \\
&\left.\left.+\frac{17}{36}L_\mu^2+\frac{1}{12}L_\mu^3\right]n_h\right\}\epsilon\,, \qquad (2.46)
\end{aligned}
$$

$$
X_m^{se} = \frac{2}{3}\frac{1}{\epsilon}-\frac{1}{24}+\frac{2}{3}L_\mu-\left(\frac{187}{144}-\frac{1}{36}\pi^2+\frac{3}{4}L_\mu-\frac{1}{3}L_\mu^2\right)\epsilon\,, \qquad (2.47)
$$

$$
\begin{aligned}
X_m^{ee} &= \left(\frac{1}{36}-\frac{1}{24}n_f\right)\frac{1}{\epsilon}+\frac{1}{6}+\frac{1}{48}n_f+\left[\frac{5}{18}+\frac{1}{108}\pi^2+\frac{5}{18}L_\mu-\frac{1}{36}L_\mu^2\right. \\
&\left.+\left(\frac{1}{32}+\frac{1}{36}\pi^2+\frac{1}{8}L_\mu+\frac{1}{24}L_\mu^2\right)n_l-\left(\frac{5}{96}-\frac{1}{8}L_\mu-\frac{1}{24}L_\mu^2\right)n_h\right]\epsilon\,, \qquad (2.48)
\end{aligned}
$$

$$
\begin{aligned}
Y_m^{sss} &= -\left(\frac{65}{16}-\frac{7}{18}n_f+\frac{1}{108}n_f^2\right)\frac{1}{\epsilon^3}+\left[\frac{1507}{288}-\frac{15}{8}L_\mu-\left(\frac{41}{72}-\frac{1}{12}L_\mu\right)n_f\right.\\
&\left.+\frac{5}{648}n_f^2\right]\frac{1}{\epsilon^2}+\left[\frac{527}{192}+\frac{19}{288}\pi^2+\frac{1}{9}\pi^2\ln 2-\frac{1}{6}\zeta_3+\frac{277}{48}L_\mu-\frac{1}{16}L_\mu^2\right.\\
&+\left(\frac{43}{648}-\frac{7}{144}\pi^2+\frac{5}{18}\zeta_3-\frac{23}{72}L_\mu-\frac{1}{24}L_\mu^2\right)n_l-\left(\frac{281}{648}-\frac{17}{144}\pi^2-\frac{5}{18}\zeta_3\right.\\
&\left.\left.+\frac{23}{72}L_\mu+\frac{1}{24}L_\mu^2\right)n_h+\frac{35}{3888}n_f^2\right]\frac{1}{\epsilon}-\frac{759833}{10368}-\frac{39721}{5184}\pi^2-\frac{32}{9}\pi^2\ln 2\\
&+\frac{1}{27}\pi^2\ln^2 2+\frac{29}{9}\zeta_3+\frac{2209}{12960}\pi^4+\frac{1331}{432}\pi^2\zeta_3-\frac{1705}{216}\zeta_5+\frac{13}{54}\ln^4 2+\frac{52}{9}a_4\\
&-\left(\frac{13139}{288}+\frac{163}{288}\pi^2+\frac{5}{18}\pi^2\ln 2-\frac{5}{12}\zeta_3\right)L_\mu-\frac{49}{6}L_\mu^2-\frac{3}{4}L_\mu^3+\left[\frac{70799}{7776}\right.\\
&+\frac{3119}{2592}\pi^2+\frac{11}{81}\pi^2\ln 2-\frac{2}{81}\pi^2\ln^2 2+\frac{557}{216}\zeta_3-\frac{61}{1944}\pi^4-\frac{1}{81}\ln^4 2-\frac{8}{27}a_4\\
&+\left(\frac{967}{144}+\frac{89}{432}\pi^2+\frac{1}{27}\pi^2\ln 2+\frac{7}{9}\zeta_3\right)L_\mu+\frac{125}{72}L_\mu^2+\frac{11}{72}L_\mu^3\Big]n_l-\left[\frac{2353}{23328}\right.\\
&\left.+\frac{13}{324}\pi^2+\frac{7}{54}\zeta_3+\left(\frac{89}{648}+\frac{1}{54}\pi^2\right)L_\mu+\frac{13}{216}L_\mu^2+\frac{1}{108}L_\mu^3\right]n_l^2-\left[\frac{5917}{11664}\right.\\
&\left.-\frac{13}{324}\pi^2-\frac{2}{27}\zeta_3+\left(\frac{143}{324}-\frac{1}{54}\pi^2\right)L_\mu+\frac{13}{108}L_\mu^2+\frac{1}{54}L_\mu^3\right]n_ln_h+\left[\frac{125555}{7776}\right.\\
&-\frac{49387}{7776}\pi^2+\frac{586}{81}\pi^2\ln 2+\frac{1}{81}\pi^2\ln^2 2-\frac{253}{216}\zeta_3-\frac{41}{972}\pi^4+\frac{1}{4}\pi^2\zeta_3-\frac{5}{4}\zeta_5\\
&-\frac{1}{81}\ln^4 2-\frac{8}{27}a_4+\left(\frac{1147}{144}-\frac{91}{432}\pi^2+\frac{1}{27}\pi^2\ln 2+\frac{7}{9}\zeta_3\right)L_\mu+\frac{125}{72}L_\mu^2\\
&\left.+\frac{11}{72}L_\mu^3\right]n_h-\left[\frac{9481}{23328}-\frac{4}{405}\pi^2-\frac{11}{54}\zeta_3+\left(\frac{197}{648}-\frac{1}{27}\pi^2\right)L_\mu+\frac{13}{216}L_\mu^2\right.\\
&\left.+\frac{1}{108}L_\mu^3\right]n_h^2\,, \qquad (2.49)
\end{aligned}
$$

$$
\begin{aligned}
Y_m^{sse} &= -\left(\frac{107}{72}-\frac{5}{108}n_f\right)\frac{1}{\epsilon^2}+\left[\frac{979}{576}-\frac{31}{24}L_\mu-\left(\frac{17}{216}-\frac{1}{36}L_\mu\right)n_f\right]\frac{1}{\epsilon}\\
&+\frac{57233}{20736}-\frac{5}{864}\pi^2+\frac{1}{27}\pi^2\ln 2+\frac{7}{24}\zeta_3+\frac{517}{144}L_\mu-\frac{17}{48}L_\mu^2-\left(\frac{721}{1728}+\frac{7}{432}\pi^2\right.\\
&\left.+\frac{43}{216}L_\mu+\frac{1}{72}L_\mu^2\right)n_l-\left(\frac{1009}{1728}-\frac{17}{432}\pi^2+\frac{43}{216}L_\mu+\frac{1}{72}L_\mu^2\right)n_h\,, \qquad (2.50)
\end{aligned}
$$

$$
\begin{aligned}
Y_m^{see} &= -\left(\frac{1}{12}-\frac{1}{8}n_f\right)\frac{1}{\epsilon^2}-\left[\frac{97}{432}+\frac{1}{36}L_\mu+\left(\frac{31}{288}-\frac{1}{24}L_\mu\right)n_f\right]\frac{1}{\epsilon}\\
&\quad+\frac{197}{2592}-\frac{5}{432}\pi^2-\frac{5}{36}\zeta_3-\frac{16}{27}L_\mu+\frac{1}{72}L_\mu^2+\left(\frac{193}{1728}-\frac{7}{288}\pi^2+\frac{5}{36}\zeta_3\right.\\
&\quad\left.-\frac{13}{144}L_\mu-\frac{1}{48}L_\mu^2\right)n_l+\left(\frac{337}{1728}+\frac{1}{288}\pi^2+\frac{5}{36}\zeta_3-\frac{13}{144}L_\mu-\frac{1}{48}L_\mu^2\right)n_h\,,
\end{aligned}
\tag{2.51}
$$

$$
\begin{aligned}
Y_m^{eee} &= -\left(\frac{1}{324}-\frac{1}{108}n_f+\frac{1}{144}n_f^2\right)\frac{1}{\epsilon^2}-\left(\frac{1}{216}-\frac{5}{216}n_f-\frac{1}{288}n_f^2\right)\frac{1}{\epsilon}\\
&\quad-\frac{25}{432}-\frac{5}{216}\zeta_3-\frac{1}{108}L_\mu-\left(\frac{23}{576}-\frac{1}{72}L_\mu\right)n_f+\frac{5}{576}n_f^2\,,
\end{aligned}
\tag{2.52}
$$

$$
Y_m^{ee1} = -\frac{1}{8}\frac{1}{\epsilon}\,, \tag{2.53}
$$

$$
Y_m^{ee2} = \frac{5}{36}\frac{1}{\epsilon}-\frac{5}{24}\,, \tag{2.54}
$$

$$
Y_m^{ee3} = \frac{1}{12}\frac{1}{\epsilon}\,, \tag{2.55}
$$

$$
Y_m^{e11} = \frac{3}{64}\frac{1}{\epsilon}-\frac{9}{256}\,, \tag{2.56}
$$

$$
Y_m^{e22} = -\frac{5}{12}\frac{1}{\epsilon}+\frac{15}{16}\,, \tag{2.57}
$$

$$
Y_m^{e33} = \frac{7}{96}\frac{1}{\epsilon}-\frac{7}{128}\,, \tag{2.58}
$$

$$
Y_m^{e13} = -\frac{1}{16}\frac{1}{\epsilon}+\frac{3}{64}\,. \tag{2.59}
$$

The one-loop corrections to $Z_m^{\mathrm{OS,DRED}}$ can be found in Ref. [12] and the two-loop terms have been computed in Ref. [13], albeit for $\alpha_e = \alpha_s^{\overline{\mathrm{DR}}}$.

Just as in the DREG case, one can also consider the finite ratio $Z_m^{\mathrm{OS,DRED}}/Z_m^{\overline{\mathrm{DR}}}$. $Z_m^{\overline{\mathrm{DR}}}$ has been computed in Ref. [102] to three and in Ref. [98] even to four-loop order. There, it is given in terms of the corresponding anomalous dimension. For completeness, we provide the result for the renormalisation constant in Appendix E. Dividing $Z_m^{\mathrm{OS,DRED}}$ by $Z_m^{\overline{\mathrm{DR}}}$ we obtain indeed a finite result. Again, we do not list the result for brevity. It can be found in Ref. [14].

## 2.3 Wave Function Renormalisation

In this section we provide the results for the mass renormalisation constants in the framework DREG and DRED.

### 2.3.1 DREG Result

At the one-loop level we have $\delta Z_2^{(1)} = \delta Z_m^{(1)}$. The two-loop contribution to the wave function renormalisation constant reads

$$
\begin{aligned}
\delta Z_2^{(2)} = \\
&\left[\frac{9}{32\epsilon^2} + \left(\frac{51}{64} + \frac{9}{16}L_\mu\right)\frac{1}{\epsilon} + \frac{433}{128} - \frac{49}{64}\pi^2 + \pi^2\ln 2 - \frac{3}{2}\zeta_3 + \frac{51}{32}L_\mu + \frac{9}{16}L_\mu^2\right.\\
&+\left(\frac{211}{256} - \frac{339}{128}\pi^2 + \frac{23}{4}\pi^2\ln 2 - 2\pi^2\ln^2 2 - \frac{297}{16}\zeta_3 + \frac{7}{20}\pi^4 - \ln^4 2 - 24a_4\right.\\
&\left.\left.+\left(\frac{433}{64} - \frac{49}{32}\pi^2 + 2\pi^2\ln 2 - 3\zeta_3\right)L_\mu + \frac{51}{32}L_\mu^2 + \frac{3}{8}L_\mu^3\right)\epsilon\right] C_F^2\\
&+\left[\frac{11}{32\epsilon^2} - \frac{127}{192\epsilon} - \frac{1705}{384} + \frac{5}{16}\pi^2 - \frac{1}{2}\pi^2\ln 2 + \frac{3}{4}\zeta_3 - \frac{215}{96}L_\mu - \frac{11}{32}L_\mu^2\right.\\
&+\left(-\frac{9907}{768} + \frac{769}{1152}\pi^2 - \frac{23}{8}\pi^2\ln 2 + \pi^2\ln^2 2 + \frac{129}{16}\zeta_3 - \frac{7}{40}\pi^4 + \frac{1}{2}\ln^4 2 + 12a_4\right.\\
&\left.\left.+\left(-\frac{2057}{192} + \frac{109}{192}\pi^2 - \pi^2\ln 2 + \frac{3}{2}\zeta_3\right)L_\mu - \frac{259}{96}L_\mu^2 - \frac{11}{32}L_\mu^3\right)\epsilon\right] C_A C_F\\
&+\left[-\frac{1}{8\epsilon^2} + \frac{11}{48\epsilon} + \frac{113}{96} + \frac{1}{12}\pi^2 + \frac{19}{24}L_\mu + \frac{1}{8}L_\mu^2\right.\\
&\left.+\left(\frac{851}{192} + \frac{127}{288}\pi^2 + \zeta_3 + \left(\frac{145}{48} + \frac{3}{16}\pi^2\right)L_\mu + \frac{23}{24}L_\mu^2 + \frac{1}{8}L_\mu^3\right)\epsilon\right] C_F T_F n_l\\
&+\left[\left(\frac{1}{16} + \frac{1}{4}L_\mu\right)\frac{1}{\epsilon} + \frac{947}{288} - \frac{5}{16}\pi^2 + \frac{11}{24}L_\mu + \frac{3}{8}L_\mu^2 + \left(\frac{17971}{1728} - \frac{445}{288}\pi^2\right.\right.\\
&\left.\left.+2\pi^2\ln 2 - \frac{85}{12}\zeta_3 + \left(\frac{1043}{144} - \frac{29}{48}\pi^2\right)L_\mu + \frac{5}{8}L_\mu^2 + \frac{7}{24}L_\mu^3\right)\epsilon\right] C_F T_F\,. \qquad (2.60)
\end{aligned}
$$

Again, we give the result to $\mathcal{O}(\epsilon)$, which is necessary for three-loop calculations.

The individual three-loop terms are given in the following

$$
\begin{aligned}
Z_2^{FFF} &= -\frac{9}{128\epsilon^3} - \left(\frac{81}{256} + \frac{27}{128}L_\mu\right)\frac{1}{\epsilon^2} + \left(-\frac{1039}{512} + \frac{303}{512}\pi^2 - \frac{3}{4}\pi^2\ln 2\right.\\
&\left. +\frac{9}{8}\zeta_3 - \frac{243}{256}L_\mu - \frac{81}{256}L_\mu^2\right)\frac{1}{\epsilon} - \frac{10823}{3072} - \frac{58321}{9216}\pi^2 + \frac{685}{48}\pi^2\ln 2\\
&+3\pi^2\ln^2 2 - \frac{739}{128}\zeta_3 - \frac{41}{120}\pi^4 + \frac{1}{8}\pi^2\zeta_3 - \frac{5}{16}\zeta_5 - \frac{5}{12}\ln^4 2 - 10a_4\\
&+\left(-\frac{3117}{512} + \frac{909}{512}\pi^2 - \frac{9}{4}\pi^2\ln 2 + \frac{27}{8}\zeta_3\right)L_\mu - \frac{729}{512}L_\mu^2 - \frac{81}{256}L_\mu^3\,, \qquad (2.61)
\end{aligned}
$$

$$
\begin{aligned}
Z_2^{FFA} &= -\frac{33}{128\epsilon^3} + \left(\frac{95}{768} - \frac{33}{128}L_\mu\right)\frac{1}{\epsilon^2} + \left(\frac{1787}{512} - \frac{131}{512}\pi^2 + \frac{3}{8}\pi^2\ln 2\right.\\
&\left. -\frac{5}{8}\zeta_3 + \frac{469}{256}L_\mu + \frac{33}{256}L_\mu^2\right)\frac{1}{\epsilon} + \frac{136945}{9216} + \frac{29695}{9216}\pi^2 - \frac{755}{288}\pi^2\ln 2\\
&-\frac{235}{72}\pi^2\ln^2 2 - \frac{6913}{384}\zeta_3 + \frac{1793}{3456}\pi^4 - \frac{45}{16}\pi^2\zeta_3 + \frac{145}{16}\zeta_5 - \frac{55}{144}\ln^4 2 - \frac{55}{6}a_4\\
&+\left(\frac{25609}{1536} - \frac{3335}{1536}\pi^2 + \frac{71}{24}\pi^2\ln 2 - \frac{37}{8}\zeta_3\right)L_\mu + \frac{2155}{512}L_\mu^2 + \frac{121}{256}L_\mu^3\,, \qquad (2.62)
\end{aligned}
$$

$$
\begin{aligned}
Z_2^{FAA} &= -\frac{121}{576\epsilon^3} + \frac{2009}{3456\epsilon^2} - \left[\frac{12793}{20736} + \frac{3}{128}\zeta_3 + \frac{1}{1080}\pi^4 + \left(\frac{1}{768} + \frac{3}{256}\zeta_3\right.\right.\\
&\left.\left. -\frac{1}{4320}\pi^4\right)\xi\right]\frac{1}{\epsilon} - \frac{1654711}{124416} - \frac{4339}{3456}\pi^2 - \frac{325}{144}\pi^2\ln 2 + \frac{127}{144}\pi^2\ln^2 2\\
&+\frac{5857}{576}\zeta_3 - \frac{3419}{23040}\pi^4 + \frac{127}{72}\pi^2\zeta_3 - \frac{37}{6}\zeta_5 + \frac{85}{288}\ln^4 2 + \frac{85}{12}a_4\\
&+\left(-\frac{13}{768} - \frac{1}{256}\pi^2 - \frac{13}{256}\zeta_3 + \frac{17}{27648}\pi^4 + \frac{1}{144}\pi^2\zeta_3 + \frac{7}{384}\zeta_5\right)\xi\\
&+\left[-\frac{36977}{3456} + \frac{55}{96}\pi^2 - \frac{11}{12}\pi^2\ln 2 + \frac{167}{128}\zeta_3 - \frac{1}{360}\pi^4\right.\\
&\left. +\left(-\frac{1}{256} - \frac{9}{256}\zeta_3 + \frac{1}{1440}\pi^4\right)\xi\right]L_\mu - \frac{2671}{1152}L_\mu^2 - \frac{121}{576}L_\mu^3\,, \qquad (2.63)
\end{aligned}
$$

$$
\begin{aligned}
Z_2^{FFL} &= \frac{3}{32\epsilon^3} + \left(-\frac{19}{192} + \frac{3}{32}L_\mu\right)\frac{1}{\epsilon^2} - \left(\frac{235}{384} + \frac{7}{128}\pi^2 + \frac{1}{4}\zeta_3 + \frac{41}{64}L_\mu + \frac{3}{64}L_\mu^2\right)\frac{1}{\epsilon}\\
&-\frac{3083}{2304} + \frac{2845}{2304}\pi^2 - \frac{47}{18}\pi^2\ln 2 + \frac{4}{9}\pi^2\ln^2 2 + \frac{473}{96}\zeta_3 - \frac{229}{2160}\pi^4 + \frac{2}{9}\ln^4 2\\
&+\frac{16}{3}a_4 + \left(-\frac{1475}{384} + \frac{133}{384}\pi^2 - \frac{2}{3}\pi^2\ln 2 + \frac{1}{4}\zeta_3\right)L_\mu - \frac{179}{128}L_\mu^2 - \frac{11}{64}L_\mu^3\,,
\end{aligned}
\qquad (2.64)
$$

$$
\begin{aligned}
Z_2^{FAL} &= \frac{11}{72\epsilon^3} - \frac{169}{432\epsilon^2} + \left(\frac{313}{1296} + \frac{1}{4}\zeta_3\right)\frac{1}{\epsilon} + \frac{111791}{15552} + \frac{13}{48}\pi^2 + \frac{47}{36}\pi^2\ln 2 \\
&\quad -\frac{2}{9}\pi^2\ln^2 2 - \frac{35}{72}\zeta_3 + \frac{19}{1080}\pi^4 - \frac{1}{9}\ln^4 2 - \frac{8}{3}a_4 \\
&\quad + \left(\frac{169}{27} - \frac{1}{18}\pi^2 + \frac{1}{3}\pi^2\ln 2 + \frac{1}{4}\zeta_3\right)L_\mu + \frac{469}{288}L_\mu^2 + \frac{11}{72}L_\mu^3\,, \qquad (2.65)
\end{aligned}
$$

$$
\begin{aligned}
Z_2^{FLL} &= -\frac{1}{36\epsilon^3} + \frac{11}{216\epsilon^2} + \frac{5}{1296\epsilon} - \frac{5767}{7776} - \frac{19}{108}\pi^2 - \frac{7}{18}\zeta_3 \\
&\quad - \left(\frac{167}{216} + \frac{1}{18}\pi^2\right)L_\mu - \frac{19}{72}L_\mu^2 - \frac{1}{36}L_\mu^3\,, \qquad (2.66)
\end{aligned}
$$

$$
\begin{aligned}
Z_2^{FHL} &= \left(\frac{1}{36} + \frac{1}{12}L_\mu\right)\frac{1}{\epsilon^2} + \left(-\frac{5}{216} + \frac{1}{144}\pi^2 - \frac{1}{9}L_\mu + \frac{1}{24}L_\mu^2\right)\frac{1}{\epsilon} \\
&\quad -\frac{4721}{1296} + \frac{19}{54}\pi^2 - \frac{1}{36}\zeta_3 + \left(-\frac{329}{108} + \frac{25}{144}\pi^2\right)L_\mu - \frac{7}{12}L_\mu^2 - \frac{5}{72}L_\mu^3\,, \qquad (2.67)
\end{aligned}
$$

$$
\begin{aligned}
Z_2^{FFH} &= -\left(\frac{7}{192} + \frac{3}{16}L_\mu\right)\frac{1}{\epsilon^2} - \left(\frac{707}{384} - \frac{15}{64}\pi^2 + \frac{29}{64}L_\mu + \frac{15}{32}L_\mu^2\right)\frac{1}{\epsilon} \\
&\quad -\frac{76897}{6912} - \frac{11551}{20736}\pi^2 + \frac{7}{18}\pi^2\ln 2 - \frac{1}{2}\pi^2\ln^2 2 + \frac{1763}{288}\zeta_3 + \frac{31}{720}\pi^4 + \frac{1}{2}\ln^4 2 \\
&\quad +12a_4 + \left(-\frac{2891}{384} + \frac{233}{192}\pi^2 - \frac{2}{3}\pi^2\ln 2 + \zeta_3\right)L_\mu - \frac{143}{128}L_\mu^2 - \frac{19}{32}L_\mu^3\,, \qquad (2.68)
\end{aligned}
$$

$$
\begin{aligned}
Z_2^{FAH} &= \frac{1-\xi}{192\epsilon^3} - \left[\frac{7}{72} - \frac{1}{64}\xi + \left(\frac{41}{192} + \frac{1}{64}\xi\right)L_\mu\right]\frac{1}{\epsilon^2} + \left[\frac{13}{216} - \frac{41}{2304}\pi^2\right. \\
&\quad \left. - \left(\frac{35}{576} + \frac{1}{768}\pi^2\right)\xi + \left(\frac{83}{144} + \frac{3}{64}\xi\right)L_\mu - \left(\frac{35}{384} + \frac{3}{128}\xi\right)L_\mu^2\right]\frac{1}{\epsilon} \\
&\quad +\frac{49901}{2592} - \frac{36019}{5184}\pi^2 + \frac{80}{9}\pi^2\ln 2 + \frac{1}{3}\pi^2\ln^2 2 - \frac{77}{16}\zeta_3 - \frac{17}{360}\pi^4 + \frac{11}{48}\pi^2\zeta_3 \\
&\quad -\frac{15}{16}\zeta_5 - \frac{1}{3}\ln^4 2 - 8a_4 + \left(\frac{407}{1728} + \frac{1}{256}\pi^2 - \frac{7}{192}\zeta_3\right)\xi \\
&\quad + \left[\frac{4141}{432} - \frac{641}{768}\pi^2 + \frac{1}{3}\pi^2\ln 2 - \frac{1}{2}\zeta_3 - \left(\frac{35}{192} + \frac{1}{256}\pi^2\right)\xi\right]L_\mu \\
&\quad + \left(\frac{35}{16} + \frac{9}{128}\xi\right)L_\mu^2 + \left(\frac{247}{1152} - \frac{3}{128}\xi\right)L_\mu^3\,, \qquad (2.69)
\end{aligned}
$$

$$
\begin{aligned}
Z_2^{FHH} &= \frac{1}{72\epsilon^2} - \left(\frac{5}{432} + \frac{1}{12}L_\mu^2\right)\frac{1}{\epsilon} - \frac{8425}{2592} + \frac{2}{45}\pi^2 + \frac{7}{3}\zeta_3 \\
&\quad - \left(\frac{481}{216} - \frac{5}{24}\pi^2\right)L_\mu - \frac{11}{72}L_\mu^2 - \frac{1}{6}L_\mu^3\,. \qquad (2.70)
\end{aligned}
$$

Starting from the three-loop level, the wave function renormalisation constant depends on the gauge parameter, $\xi$. The parameter in the above equations is defined through the gluon propagator as

$$
D_{\mu\nu}^{ab}(k) = -\frac{i}{k^2}\left(g_{\mu\nu} - \xi\,\frac{k_\mu k_\nu}{k^2}\right)\delta^{ab}\,, \qquad (2.71)
$$

where $a$ and $b$ are colour indices.

### 2.3.2 DRED Result

Just as in DREG, we have $\delta\tilde{Z}_2^{(1)} = \delta\tilde{Z}_m^{(1)}$. The individual two and three-loop contributions to the wave function renormalisation constant in DRED are given by

$$
\begin{aligned}
X_2^{ss} &= \left(\frac{15}{8} - \frac{1}{12}n_l\right)\frac{1}{\epsilon^2} - \left[\frac{53}{48} - L_\mu - \frac{11}{72}n_l - \left(\frac{1}{24} + \frac{1}{6}L_\mu\right)n_h\right]\frac{1}{\epsilon} - \frac{3185}{288} - \frac{1}{9}\pi^2 \\
&\quad - \frac{2}{9}\pi^2\ln 2 + \frac{1}{3}\zeta_3 - \frac{47}{8}L_\mu - \frac{3}{8}L_\mu^2 + \left(\frac{113}{144} + \frac{1}{18}\pi^2 + \frac{19}{36}L_\mu + \frac{1}{12}L_\mu^2\right)n_l \\
&\quad + \left(\frac{947}{432} - \frac{5}{24}\pi^2 + \frac{11}{36}L_\mu + \frac{1}{4}L_\mu^2\right)n_h + \Bigg\{ - \frac{27419}{576} - \frac{557}{288}\pi^2 - \frac{23}{18}\pi^2\ln 2 \\
&\quad + \frac{4}{9}\pi^2\ln^2 2 - \frac{3}{4}\zeta_3 - \frac{7}{90}\pi^4 + \frac{2}{9}\ln^4 2 + \frac{16}{3}a_4 - \left(\frac{4241}{144} + \frac{65}{144}\pi^2 + \frac{4}{9}\pi^2\ln 2\right. \\
&\quad \left. - \frac{2}{3}\zeta_3\right)L_\mu - \frac{185}{24}L_\mu^2 - \frac{17}{24}L_\mu^3 + \left[\frac{851}{288} + \frac{127}{432}\pi^2 + \frac{2}{3}\zeta_3 + \left(\frac{145}{72} + \frac{1}{8}\pi^2\right)L_\mu\right. \\
&\quad \left. + \frac{23}{36}L_\mu^2 + \frac{1}{12}L_\mu^3\right]n_l + \left[\frac{17971}{2592} - \frac{445}{432}\pi^2 + \frac{4}{3}\pi^2\ln 2 - \frac{85}{18}\zeta_3\right. \\
&\quad \left. + \left(\frac{1043}{216} - \frac{29}{72}\pi^2\right)L_\mu + \frac{5}{12}L_\mu^2 + \frac{7}{36}L_\mu^3\right]n_h\Bigg\}\epsilon\,, \qquad (2.72)
\end{aligned}
$$

$$
X_2^{se} = \frac{2}{3}\frac{1}{\epsilon} - \frac{1}{8} + \frac{2}{3}L_\mu - \left(\frac{221}{144} + \frac{1}{12}\pi^2 + \frac{11}{12}L_\mu - \frac{1}{3}L_\mu^2\right)\epsilon\,, \qquad (2.73)
$$

$$
\begin{aligned}
X_2^{ee} &= \left(\frac{1}{36} - \frac{1}{24}n_f\right)\frac{1}{\epsilon} + \frac{7}{36} + \frac{1}{16}n_f + \left[\frac{5}{9} - \frac{1}{108}\pi^2 + \frac{1}{3}L_\mu - \frac{1}{36}L_\mu^2\right. \\
&\quad \left. + \left(\frac{13}{96} + \frac{1}{36}\pi^2 + \frac{5}{24}L_\mu + \frac{1}{24}L_\mu^2\right)n_l - \left(\frac{11}{96} - \frac{5}{24}L_\mu - \frac{1}{24}L_\mu^2\right)n_h\right]\epsilon\,, \qquad (2.74)
\end{aligned}
$$

$$
\begin{aligned}
Y_2^{sss} = \\
&-\left(\frac{65}{16}-\frac{7}{18}n_l+\frac{1}{108}n_l^2+\frac{\xi-1}{96}n_h\right)\frac{1}{\epsilon^3}+\left\{\frac{209}{32}-\frac{15}{8}L_\mu-\left(\frac{185}{216}-\frac{1}{12}L_\mu\right)n_l\right.\\
&+\frac{11}{648}n_l^2+\left(\frac{1}{108}+\frac{1}{36}L_\mu\right)n_l n_h-\left[\frac{49}{216}-\frac{1}{32}\xi+\left(\frac{19}{32}+\frac{1}{32}\xi\right)L_\mu\right]n_h\\
&\left.+\frac{1}{216}n_h^2\right\}\frac{1}{\epsilon^2}+\left\{\frac{3553}{576}+\frac{11}{288}\pi^2+\frac{2}{9}\pi^2\ln 2-\frac{91}{96}\zeta_3-\frac{1}{90}\pi^4+\frac{343}{48}L_\mu-\frac{1}{16}L_\mu^2\right.\\
&-\left(\frac{1}{64}+\frac{9}{64}\zeta_3-\frac{1}{360}\pi^4\right)\xi-\left(\frac{47}{648}+\frac{7}{144}\pi^2-\frac{5}{18}\zeta_3+\frac{41}{72}L_\mu+\frac{1}{24}L_\mu^2\right)n_l\\
&+\frac{5}{3888}n_l^2-\left(\frac{5}{648}-\frac{1}{432}\pi^2+\frac{1}{27}L_\mu-\frac{1}{72}L_\mu^2\right)n_l n_h-\left[\frac{329}{216}+\frac{35}{288}\xi\right.\\
&\left.-\left(\frac{199}{1152}-\frac{1}{384}\xi\right)\pi^2-\left(\frac{17}{24}+\frac{3}{32}\xi\right)L_\mu+\left(\frac{115}{192}+\frac{3}{64}\xi\right)L_\mu^2\right]n_h\\
&\left.-\left(\frac{5}{1296}+\frac{1}{36}L_\mu^2\right)n_h^2\right\}\frac{1}{\epsilon}-\frac{826919}{10368}-\frac{200605}{15552}\pi^2-\frac{2309}{324}\pi^2\ln 2+\frac{31}{108}\pi^2\ln^2 2\\
&+\frac{5251}{432}\zeta_3+\frac{9143}{51840}\pi^4+\frac{349}{54}\pi^2\zeta_3-\frac{713}{27}\zeta_5+\frac{335}{648}\ln^4 2+\frac{335}{27}a_4-\left(\frac{13}{64}+\frac{3}{64}\pi^2\right.\\
&\left.+\frac{39}{64}\zeta_3-\frac{17}{2304}\pi^4-\frac{1}{12}\pi^2\zeta_3-\frac{7}{32}\zeta_5\right)\xi-\left[\frac{3659}{72}+\frac{143}{288}\pi^2+\frac{5}{9}\pi^2\ln 2+\frac{97}{96}\zeta_3\right.\\
&\left.+\frac{1}{30}\pi^4+\left(\frac{3}{64}+\frac{27}{64}\zeta_3-\frac{1}{120}\pi^4\right)\xi\right]L_\mu-\frac{69}{8}L_\mu^2-\frac{3}{4}L_\mu^3+\left[\frac{99431}{7776}+\frac{4177}{2592}\pi^2\right.\\
&+\frac{47}{162}\pi^2\ln 2-\frac{4}{81}\pi^2\ln^2 2+\frac{92}{27}\zeta_3-\frac{287}{4860}\pi^4-\frac{2}{81}\ln^4 2-\frac{16}{27}a_4+\left(\frac{1273}{144}+\frac{85}{432}\pi^2\right.\\
&\left.\left.+\frac{2}{27}\pi^2\ln 2+\frac{13}{18}\zeta_3\right)L_\mu+\frac{71}{36}L_\mu^2+\frac{11}{72}L_\mu^3\right]n_l-\left[\frac{5767}{23328}+\frac{19}{324}\pi^2+\frac{7}{54}\zeta_3\right.\\
&\left.+\left(\frac{167}{648}+\frac{1}{54}\pi^2\right)L_\mu+\frac{19}{216}L_\mu^2+\frac{1}{108}L_\mu^3\right]n_l^2-\left[\frac{4721}{3888}-\frac{19}{162}\pi^2+\frac{1}{108}\zeta_3\right.\\
&\left.+\left(\frac{329}{324}-\frac{25}{432}\pi^2\right)L_\mu+\frac{7}{36}L_\mu^2+\frac{5}{216}L_\mu^3\right]n_l n_h+\left\{\frac{106921}{3888}-\frac{333211}{23328}\pi^2\right.\\
&+\frac{1468}{81}\pi^2\ln 2+\frac{2}{9}\pi^2\ln^2 2-\frac{2711}{648}\zeta_3-\frac{91}{1620}\pi^4+\frac{11}{24}\pi^2\zeta_3-\frac{15}{8}\zeta_5-\frac{2}{9}\ln^4 2-\frac{16}{3}a_4\\
&+\left(\frac{407}{864}+\frac{1}{128}\pi^2-\frac{7}{96}\zeta_3\right)\xi+\left[\frac{587}{48}-\frac{2041}{3456}\pi^2+\frac{2}{27}\pi^2\ln 2-\frac{1}{9}\zeta_3\right.\\
&\left.\left.-\left(\frac{35}{96}+\frac{1}{128}\pi^2\right)\xi\right]L_\mu+\left(\frac{59}{18}+\frac{9}{64}\xi\right)L_\mu^2-\left(\frac{19}{192}+\frac{3}{64}\xi\right)L_\mu^3\right\}n_h\\
&-\left[\frac{8425}{7776}-\frac{2}{135}\pi^2-\frac{7}{9}\zeta_3+\left(\frac{481}{648}-\frac{5}{72}\pi^2\right)L_\mu+\frac{11}{216}L_\mu^2+\frac{1}{18}L_\mu^3\right]n_h^2\,, \qquad (2.75)
\end{aligned}
$$

$$
\begin{aligned}
Y_2^{sse} &= -\left(\frac{107}{72}-\frac{5}{108}n_l-\frac{1}{54}n_h\right)\frac{1}{\epsilon^2}+\left[\frac{397}{192}-\frac{31}{24}L_\mu-\left(\frac{1}{9}-\frac{1}{36}L_\mu\right)n_l\right.\\
&\quad\left.-\left(\frac{17}{108}+\frac{1}{18}L_\mu\right)n_h\right]\frac{1}{\epsilon}+\frac{29311}{6912}+\frac{83}{864}\pi^2+\frac{2}{27}\pi^2\ln 2-\frac{161}{864}\zeta_3\\
&\quad+\frac{619}{144}L_\mu-\frac{17}{48}L_\mu^2-\left(\frac{913}{1728}+\frac{7}{432}\pi^2+\frac{61}{216}L_\mu+\frac{1}{72}L_\mu^2\right)n_l\\
&\quad-\left(\frac{2699}{5184}-\frac{5}{72}\pi^2+\frac{91}{216}L_\mu+\frac{5}{36}L_\mu^2\right)n_h\,, \qquad (2.76)\\
Y_2^{see} &= -\left(\frac{1}{12}-\frac{1}{8}n_f\right)\frac{1}{\epsilon^2}-\left[\frac{41}{144}+\frac{1}{36}L_\mu+\left(\frac{61}{288}-\frac{1}{24}L_\mu\right)n_f\right]\frac{1}{\epsilon}-\frac{25}{2592}\\
&\quad+\frac{1}{144}\pi^2-\frac{5}{108}\zeta_3-\frac{73}{108}L_\mu+\frac{1}{72}L_\mu^2+\left(\frac{55}{1728}-\frac{7}{288}\pi^2+\frac{5}{36}\zeta_3-\frac{31}{144}L_\mu\right.\\
&\quad\left.-\frac{1}{48}L_\mu^2\right)n_l+\left(\frac{487}{1728}+\frac{1}{288}\pi^2+\frac{5}{36}\zeta_3-\frac{31}{144}L_\mu-\frac{1}{48}L_\mu^2\right)n_h\,, \qquad (2.77)\\
Y_2^{eee} &= -\left(\frac{1}{324}-\frac{1}{108}n_f+\frac{1}{144}n_f^2\right)\frac{1}{\epsilon^2}-\left(\frac{5}{648}-\frac{5}{216}n_f-\frac{1}{96}n_f^2\right)\frac{1}{\epsilon}\\
&\quad-\frac{55}{432}+\frac{5}{216}\zeta_3-\frac{1}{108}L_\mu-\left(\frac{173}{1728}-\frac{1}{72}L_\mu\right)n_f+\frac{1}{192}n_f^2\,, \qquad (2.78)\\
Y_2^{ee1} &= Y_m^{ee1}\,, \qquad (2.79)\\
Y_2^{ee2} &= Y_m^{ee2}\,, \qquad (2.80)\\
Y_2^{ee3} &= Y_m^{ee3}\,, \qquad (2.81)\\
Y_2^{e11} &= \frac{3}{64}\frac{1}{\epsilon}-\frac{21}{256}\,, \qquad (2.82)\\
Y_2^{e22} &= -\frac{5}{12}\frac{1}{\epsilon}+\frac{65}{48}\,, \qquad (2.83)\\
Y_2^{e33} &= \frac{7}{96}\frac{1}{\epsilon}-\frac{49}{384}\,, \qquad (2.84)\\
Y_2^{e13} &= -\frac{1}{16}\frac{1}{\epsilon}+\frac{7}{64}\,. \qquad (2.85)
\end{aligned}
$$

Just like in DREG, the three-loop contribution to the wave function renormalisation constant depends on the gauge parameter, $\xi$. Note, however, that there are no $\xi$-dependent terms involving the evanescent couplings. In fact, the $\xi$-dependent terms are exactly the same as in the case of DREG.

# Chapter 3

# Chromomagnetic Interaction

In this chapter we discuss the calculation of the chromomagnetic moment at the three-loop level. As byproducts we obtain the analytical results for the anomalous magnetic moment of electrons and quarks at the same order. While the former is known, the latter result is new. The calculation is outlined in general in the following section. The results for the electron and quark anomalous magnetic moments are given in Section 3.2 and 3.3, respectively, while Section 3.4 contains the results for the chromomagnetic moment.

## 3.1 Calculation

Just as in the case of the matching coefficient we have to consider vertex corrections to the quark-anti-quark photon and gluon vertices to calculate the anomalous magnetic moment and the chromomagnetic moment, respectively. In this case, however, the momentum of the photon or gluon vanishes, while the momenta of the quarks are still on their mass shell. In the following, we will describe the calculation of the chromomagnetic moment. However, everything applies for the electron anomalous magnetic moment as well. In fact, the results for the latter can be determined from the former by setting the colour factors to their corresponding values in Quantum Electrodynamics (QED).

The tensor structure of the vertex is of course still given by Eq. (1.17). Let us repeat the definition of the relevant form factors,

$$\Gamma^\mu = \gamma^\mu \, F_1(q^2) + \frac{[\gamma^\mu, \not{q}\,]}{4m_Q} F_2(q^2)\,, \tag{3.1}$$

where $q = p_1 - p_2$ is the gluon momentum and $p_1$ and $p_2$ are the momenta of the quark and anti-quark, respectively. In colour space the vertex is proportional to $t^a$. However, since we can treat the colour structure separately from the Dirac structure, we do not include it in Eq. (3.1) and the following.

The chromomagnetic moment is given by $\mu_c = Z_2^{\rm OS} F_2(0)$, where we assume that the quark mass and $\alpha_s$ are already renormalised. The renormalised colour charge form factor is given by $\varepsilon_c = Z_2^{\rm OS} F_1(0) = 1$. Thus, $F_1(0)$ is the inverse of the on-shell wave function renormalisation constant, which was discussed in Chapter 2. Since we already know the result for $Z_2^{\rm OS}$, we can use the calculation of $F_1$ as a check of our implementation.

In order to extract the form factors, we use projection operators. To obtain these operators, it is convenient to introduce the momentum $p = (p_1 + p_2)/2$, since $p \cdot q = 0$. With this definition we obtain (see for example Ref. [104])

$$\begin{aligned} F_1(q^2) &= \frac{1}{2(d-2)(q^2-4m_Q^2)} \\ &\quad \times \mathrm{Tr}\left\{ (\not{p}_1 + m_Q) \left( \gamma_\mu + \frac{4m_Q(d-1)}{q^2-4m_Q^2}\, p_\mu \right) (\not{p}_2 + m_Q)\ \Gamma^\mu \right\}, \qquad (3.2) \\ F_2(q^2) &= -\frac{2m_Q^2}{(d-2)q^2(q^2-4m_Q^2)} \\ &\quad \times \mathrm{Tr}\left\{ (\not{p}_1 + m_Q) \left( \gamma_\mu + \frac{4m_Q^2 + (d-2)q^2}{m_Q(q^2-4m_Q^2)}\, p_\mu \right) (\not{p}_2 + m_Q)\ \Gamma^\mu \right\}. \qquad (3.3) \end{aligned}$$

Since the projector for $F_2$ develops a pole for $q^2 = 0$, we cannot set $q^2 = 0$ from the beginning. Instead, we expand in $q$ and keep all terms which are at most quadratic in $q$. In the final result the limit $q^2 = 0$ can be taken. Due to the expansion in $q$ all integrals are again the on-shell propagator-type integrals, which we encountered before.

For the calculation of the chromomagnetic moment it is useful to employ the background field method [105, 106] (see also reference therein). In this method the gauge field in the classical action is split into a background field and a quantum field. The former can only appear as an external field, while the latter appears only inside loops. By choosing the background field gauge it is ensured that the background field variable remains explicitly gauge invariant, even when radiative corrections are included.

The technical advantage is that the number of diagrams, which have to be calculated, is reduced. On the other hand, we now have additional vertices containing background fields (see for example Ref. [105]). The vertex of a background field with two gluons, for example, contains a term proportional to $1/(1-\xi)$, where $\xi$ is the gauge parameter defined by Eq. (2.71), which does not appear in the usual QCD Feynman rules. In some cases these terms can actually be used to simplify the occurring expressions. If one Lorentz index of a gluon propagator is contracted with $k^\mu/(1-\xi)$, where $k$ is the gluon's momentum, the $\xi$-dependent terms vanish,

$$\frac{k^\mu}{1-\xi}\, D^{ab}_{\mu\nu}(k) = -i\, \frac{k_\nu}{k^2}\, \delta^{ab}\,. \qquad (3.4)$$

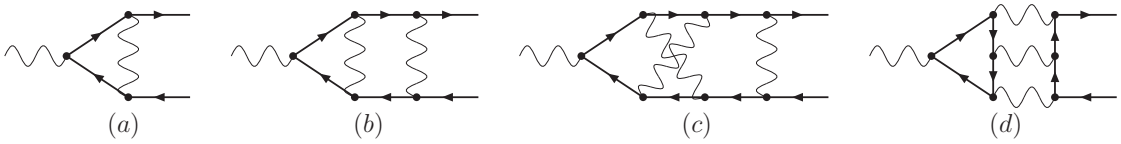


Figure 3.1: Sample diagrams contributing to the electron anomalous magnetic moment in QED. Solid lines denote electrons and wavy lines denote photons. In $(d)$ a diagram of the so-called light-by-light contribution is depicted.

$D^{ab}_{\mu\nu}$ is the gluon propagator defined in Eq. (2.71). Thus, the number of terms in the calculation is reduced.

The calculation is performed for an arbitrary gauge parameter in order to use the cancellation of the gauge parameter as a check. However, since the expressions for the individual diagrams are very large, we discard all terms with more than linear $\xi$ dependence at the three-loop level. In particular, this means that we also have to expand the remaining $1/(1-\xi)$ terms in the limit $\xi \to 0$ to order $\mathcal{O}(\xi^2)$. If this is done, our final result is gauge-parameter independent up to terms which are quadratic in $\xi$. Furthermore, our calculation of $F_1$ reproduces the gauge dependent terms of $Z_2^{\mathrm{OS}}$.

To calculate the colour factors, we have used the program described in Ref. [107][1].

## 3.2 Electron Magnetic Moment

The anomalous magnetic moment of the electron is one of the most precisely known observables. It is experimentally known to 0.76 parts per trillion [15], which leads to the most precise determination of the QED coupling $\alpha$ [17]. Naturally, this requires a theoretical knowledge of the anomalous magnetic moment, which is of equal precision. Currently, the QED three-loop contribution is known analytically [67], while the four-loop one is known numerically [108].

Here, we recalculate the three-loop term. Sample diagrams are shown in Fig. 3.1. This calculation provides a check on our computation of the quark electro- and chromomagnetic moments. In particular, we perform the renormalisation exactly in the same way. This means that we renormalise $\alpha$ in the $\overline{\mathrm{MS}}$ scheme and use the renormalisation group equation to switch to $\overline{\alpha}(M_e)$, where $M_e$ is the electron pole mass. For these two steps we can use the corresponding QCD formulae and set $C_F = T_F = n_f = 1$ and $C_A = 0$. At this point the result is finite and devoid of logarithms. However, in QED calculations $\alpha$ is renormalised on-shell. Therefore,

[1] We thank Philipp Kant for providing his interface between the setup described in Appendix C and the program of Ref. [107].

we have to switch from the $\overline{\text{MS}}$ scheme to the on-shell scheme by using [109]

$$\frac{\overline{\alpha}(M_e)}{\pi} = \frac{\alpha}{\pi} + \frac{15}{16}\left(\frac{\alpha}{\pi}\right)^3 + \mathcal{O}\left(\alpha^4\right) . \tag{3.5}$$

The result for the electron anomalous magnetic moment in QED reads

$$\begin{aligned} a_e &= \frac{\alpha}{2\pi} + \left(\frac{\alpha}{\pi}\right)^2 \left(\frac{197}{144} + \frac{1}{12}\pi^2 - \frac{1}{2}\pi^2 \ln 2 + \frac{3}{4}\zeta_3\right) \\ &\quad + \left(\frac{\alpha}{\pi}\right)^3 \left(\frac{28259}{5184} + \frac{17101}{810}\pi^2 - \frac{298}{9}\pi^2 \ln 2 - \frac{25}{18}\pi^2 \ln^2 2 + \frac{139}{18}\zeta_3 \right. \\ &\quad \left. - \frac{239}{2160}\pi^4 + \frac{83}{72}\pi^2\zeta_3 - \frac{215}{24}\zeta_5 + \frac{25}{18}\ln^4 2 + \frac{100}{3}a_4\right) + \mathcal{O}\left(\alpha^4\right) , \end{aligned} \tag{3.6}$$

where $\alpha$ is renormalised in the on-shell scheme. The one-loop term was obtained by Schwinger in Ref. [110]. The two-loop correction was found independently in Ref. [111] and [112]. The analytical three-loop result was found in Ref. [67] and confirmed in Ref. [11].

Using $\alpha = 1/137.0359911$ [113] we find

$$\begin{aligned} a_e &= \frac{1}{2}\frac{\alpha}{\pi} - 0.328479\left(\frac{\alpha}{\pi}\right)^2 + 1.18124\left(\frac{\alpha}{\pi}\right)^3 \\ &= 0.00116141 - 0.00000177231 + 0.0000000148042 \\ &= 0.00115965 . \end{aligned} \tag{3.7}$$

The series in $\alpha$ is alternating and converges very well. This behaviour is confirmed by the numerical calculation of the fourth order correction, which yields $-0.0000000000503131$ [108].

## 3.3 Quark Magnetic Moment

The magnetic moments of heavy quarks have not yet been determined experimentally. For the bottom and the lighter quarks there are upper bounds from LEP1 data [114]. For the bottom quark this bound was found to be saturated by the two-loop QCD correction in Ref. [115]. Thus, a more precise measurement at a future linear collider should be able to determine the bottom-quark magnetic moment or even find deviations from the standard model prediction.

The top-quark magnetic moment has not been measured so far. However, such a measurement would be very interesting since the top-quark couplings to photons or Z bosons are very sensitive to contributions from physics beyond the standard model.

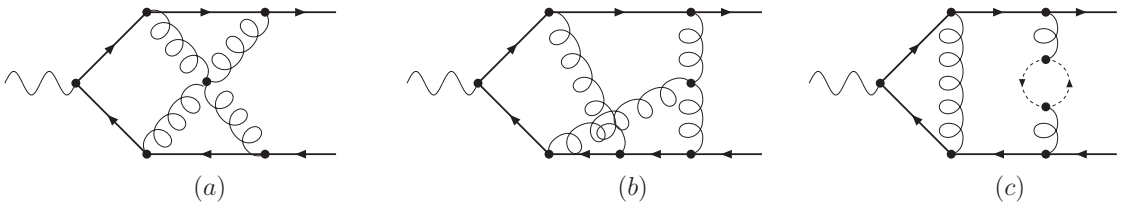


Figure 3.2: Examples of non-abelian diagrams contributing to the quark magnetic moment. Solid, curly and dotted lines denote quarks, gluons and gluon ghosts, respectively. The external wavy line denotes the photon.

Having this in mind, it is mandatory to have precise standard model predictions for these couplings.

The diagrams which we have to consider in order to compute the quark magnetic moment are essentially the same as the diagrams for the matching coefficient of the vector current. Sample diagrams for the part with closed massless quark loops are depicted in Figs. 1.3 and 1.4. However, due to the different kinematical situation, we are able to perform the full three-loop calculation for the magnetic moment. Therefore, we have to consider additional three-loop diagrams. On the one hand, we have the abelian diagrams, which are also present in the QED calculation, and on the other hand there are non-abelian diagrams with triple and quartic gluon couplings and gluons ghosts. Examples of the latter are shown in Fig. 3.2.

The anomalous magnetic moment of a heavy quark reads

$$\begin{aligned}\frac{a_Q}{Q_Q} &= \frac{\alpha_s(M_Q)}{2\pi}C_F \\ &\quad + \left(\frac{\alpha_s(M_Q)}{\pi}\right)^2 \left[\left(-\frac{31}{16} + \frac{5}{12}\pi^2 - \frac{1}{2}\pi^2\ln 2 + \frac{3}{4}\zeta_3\right)C_F^2\right. \\ &\qquad + \left(\frac{317}{144} - \frac{1}{8}\pi^2 + \frac{1}{4}\pi^2\ln 2 - \frac{3}{8}\zeta_3\right)C_F C_A \\ &\qquad \left. + \left(-\frac{25}{36}n_l + \frac{119}{36} - \frac{1}{3}\pi^2\right)C_F T_F\right] \\ &\quad + \left(\frac{\alpha_s(M_Q)}{\pi}\right)^3 a_Q^{(3)} + \mathcal{O}\left(\alpha_s^4\right) , \end{aligned} \tag{3.8}$$

where $Q_Q$ is the charge of the heavy quark in terms of the positron charge. The two-loop result was already obtained in Ref. [116]. We agree with their result up to an overall factor of four. Recently, $a_Q$ was also found to two-loops as the limit of the off-shell calculation of the corresponding form factor [115]. We are in full agreement with their result.

Our new three-loop term is given by

$$
\begin{aligned}
a_Q^{(3)} &= \left(-\frac{101}{64}+\frac{23}{6}\pi^2-\frac{22}{3}\pi^2\ln 2-\frac{5}{18}\pi^2\ln^2 2+\frac{241}{24}\zeta_3-\frac{139}{2160}\pi^4+\frac{103}{72}\pi^2\zeta_3\right.\\
&\left.-\frac{235}{24}\zeta_5+\frac{5}{18}\ln^4 2+\frac{20}{3}a_4\right)C_F^3-\left(\frac{955}{72}-\frac{1505}{432}\pi^2+\frac{31}{12}\pi^2\ln 2-\frac{49}{36}\pi^2\ln^2 2\right.\\
&\left.+\frac{113}{48}\zeta_3+\frac{35}{432}\pi^4+\frac{5}{12}\pi^2\zeta_3-\frac{185}{24}\zeta_5+\frac{5}{18}\ln^4 2+\frac{20}{3}a_4\right)C_F^2C_A\\
&+\left(\frac{31231}{2592}-\frac{463}{216}\pi^2+\frac{25}{8}\pi^2\ln 2-\frac{11}{18}\pi^2\ln^2 2-\frac{1}{2}\zeta_3+\frac{103}{2880}\pi^4+\frac{29}{288}\pi^2\zeta_3\right.\\
&\left.-\frac{65}{32}\zeta_5+\frac{5}{72}\ln^4 2+\frac{5}{3}a_4\right)C_FC_A^2+\left(\frac{125}{32}-\frac{79}{54}\pi^2+\frac{5}{3}\pi^2\ln 2-\frac{2}{9}\pi^2\ln^2 2\right.\\
&\left.-3\zeta_3+\frac{11}{216}\pi^4-\frac{1}{9}\ln^4 2-\frac{8}{3}a_4\right)C_F^2T_Fn_l-\left(\frac{2411}{324}-\frac{77}{216}\pi^2+\frac{5}{6}\pi^2\ln 2\right.\\
&\left.-\frac{1}{9}\pi^2\ln^2 2-\frac{19}{12}\zeta_3+\frac{11}{432}\pi^4-\frac{1}{18}\ln^4 2-\frac{4}{3}a_4\right)C_FC_AT_Fn_l\\
&+\left[\frac{317}{324}n_l-\frac{61}{162}+\frac{1}{27}\pi^2(n_l+1)\right]C_FT_F^2n_l+\left(\frac{7703}{864}+\frac{11}{162}\pi^2-\frac{16}{9}\pi^2\ln 2\right.\\
&\left.-\frac{4}{9}\pi^2\ln^2 2-\frac{263}{72}\zeta_3+\frac{4}{135}\pi^4+\frac{4}{9}\ln^4 2+\frac{32}{3}a_4\right)C_F^2T_F+\left(\frac{2117}{162}-\frac{1375}{648}\pi^2\right.\\
&\left.+\frac{32}{9}\pi^2\ln 2+\frac{5}{18}\pi^2\ln^2 2-\frac{241}{36}\zeta_3-\frac{143}{2160}\pi^4+\frac{1}{8}\pi^2\zeta_3-\frac{25}{24}\zeta_5-\frac{5}{18}\ln^4 2\right.\\
&\left.-\frac{20}{3}a_4\right)C_FC_AT_F-\left(\frac{943}{324}+\frac{4}{135}\pi^2-\frac{8}{3}\zeta_3\right)C_FT_F^2+\frac{d_{33}^{FF}}{N_F}X_{ll}\,, \qquad (3.9)
\end{aligned}
$$

where $N_F = N_c$ is the dimension of the fundamental representation of SU($N_c$) and $d_{33}^{FF} = (N_c^2-1)(N_c^2-4)/(16N_c)$ [107]. $X_{ll}$ denotes the contribution from singlet diagrams. It is given by

$$
\begin{aligned}
X_{ll} &= \frac{5}{9}+\frac{931}{54}\pi^2-24\pi^2\ln 2-\frac{2}{3}\pi^2\ln^2 2-\frac{4}{3}\zeta_3-\frac{41}{540}\pi^4\\
&\quad-\frac{5}{18}\pi^2\zeta_3+\frac{5}{6}\zeta_5+\frac{2}{3}\ln^4 2+16a_4\,, \qquad (3.10)
\end{aligned}
$$

where we only include the contribution from diagrams with closed heavy-quark loops. In principle there are contributions from diagrams with massless quarks as well. However, these are divergent and cannot be calculated in perturbation theory. This divergence can also be seen in the light-by-light contribution to the anomalous magnetic moment of the muon [117], which contains logarithms of the electron mass. In the case of quarks, however, we cannot introduce a mass to regulate the infrared divergence in these diagrams.

It is possible to obtain the electron result given in Eq. (3.6) from the expressions in Eqs. (3.8)–(3.10) by setting $C_F = T_F = 1$, $C_A = 0$, $N_F = 1$, $d_{33}^{FF} = 1$ and $n_l = 0$. For example, we can see immediately that the result in Eq. (3.10) is equal to the light-by-light contribution given in Ref. [118]. Furthermore, by taking the difference of Eq. (3.6) and Eq. (3.10) we find the universal QED contribution to the lepton magnetic moment.

Let us evaluate the quark magnetic moment numerically for charm, bottom and top quarks. Inserting the numerical values for the coefficients, we find

$$\begin{aligned}\frac{a_Q}{Q_Q} &= 0.212207\,\alpha_s(M_Q) + (0.841712 - 0.046908\,n_l)\,\alpha_s^2(M_Q) \\ &\quad + \left(4.5763 - 0.585553\,n_l + 0.014448\,n_l^2\right)\alpha_s^3(M_Q) + \mathcal{O}\left(\alpha_s^4\right) . \quad (3.11)\end{aligned}$$

In the following, we use the values $M_c = 1.6$ GeV, $M_b = 4.7$ GeV and $M_t = 175$ GeV. The number of light-quark flavours $n_l$ is three, four and five for the charm, bottom and top quark, respectively. To evaluate $\alpha_s(M_Q)$, defined with $n_l + 1$ active flavours, from $\alpha_s(M_Z) = 0.118$, defined with five active flavours, we use the program `RunDec` [74]. We obtain $\alpha_s(M_c) = 0.3378$, $\alpha_s(M_b) = 0.2169$ and $\alpha_s(M_t) = 0.1075$. This leads us to

$$a_c = 0.0478 + 0.0533 + 0.0758 = 0.1770\,, \quad (3.12)$$

$$a_b = -0.0153 - 0.0103 - 0.0084 = -0.0340\,, \quad (3.13)$$

$$a_t = 0.0152 + 0.0047 + 0.0017 = 0.0215\,. \quad (3.14)$$

In the case of the charm quark, we see that the perturbative series does not seem to converge at all. This is not unexpected since the charm quark is relatively light. Thus, there are potentially large non-perturbative corrections to quantities at the scale of the charm-quark mass. While the situation is better in the case of the bottom quark, the corrections are still very large. The three-loop correction amounts to more than 50% of the one-loop contribution. For the top quark, we find that our new term contributes about 10% of the one-loop correction.

We have mentioned above that the LEP1 bound for the bottom quark was found to be saturated by the two-loop correction. It is therefore interesting to see what happens if we include our three-loop term. For this purpose, we have to evaluate $a_b$ at $M_Z$. We find

$$a_b(M_Z) = -0.0084 - 0.0066 - 0.0056 = -0.0206\,. \quad (3.15)$$

Since the three-loop correction is almost as large as the two-loop one this overshoots the bound $a_b/Q_b < 0.045$ (68%C.L.) given in Ref. [114]. In this context we want to mention again that contributions from closed light-quark loops could not be included in our calculation. These contributions might decrease the three-loop correction. In any case, a more precise measurement of $a_b$ would certainly be interesting.

## 3.4 Quark Chromomagnetic Moment

The chromomagnetic moment of a quark is of particular interest in Heavy Quark Effective Theory (HQET) [24], where it appears in the matching coefficient of the chromomagnetic interaction. This matching coefficient and in particular its anomalous dimension play a role in non-perturbative tests of HQET on the lattice [119].

The relevant part of the HQET Lagrangian reads [120, 121]

$$\mathcal{L}_{\text{HQET}} = \ldots + \frac{C_m(\mu)}{4m_Q}\overline{Q}_v G_{\mu\nu}\sigma^{\mu\nu}Q_v + \ldots \,, \tag{3.16}$$

where $Q_v$ denotes a static quark field with velocity $v$, $G_{\mu\nu}$ is the gluon field strength tensor and $\sigma^{\mu\nu} = i\left[\gamma^\mu, \gamma^\nu\right]/2$. The matching coefficient of the chromomagnetic interaction is given by the chromomagnetic moment in QCD through

$$C_m(\mu) = Z_{cm}\left(1 + \mu_c\right), \tag{3.17}$$

where the HQET renormalisation constant $Z_{cm}$ is defined in the $\overline{\text{MS}}$ scheme with $n_l$ active flavours. This has to be taken into account in Eq. (3.17) since $\alpha_s$ in $\mu_c$ is defined in the full theory with $n_l + 1$ active flavours. The strong coupling $\alpha_s$ in $Z_{cm}$ has to be related to the coupling with one additional flavour through the use of the QCD decoupling relation. Since $Z_{cm}$ is divergent the order $\mathcal{O}(\epsilon)$ part of this relation is necessary as well. For the two-loop calculation the decoupling relation is given by [122]

$$\frac{\alpha_s^{(n_l)}}{\pi} = -\frac{\alpha_s^{(n_l+1)}}{\pi}\left[\frac{1}{3}L_\mu + \left(\frac{1}{36}\pi^2 + \frac{1}{6}L_\mu\right)\epsilon + \mathcal{O}\left(\epsilon^2\right)\right]T_F + \mathcal{O}\left(\alpha_s^2\right), \tag{3.18}$$

where the superscript denotes the number of active flavours.

The diagrams which we have to calculate in order to obtain the quark chromomagnetic moment consist of all diagrams which are needed for the electromagnetic moment (with the external photon replaced by the background gluon) plus additional diagrams where the background field couples to gluons or gluon ghosts. Some sample diagrams are depicted in Fig. 3.3. We want to stress that we include singlet diagrams with massless quark loops in the calculation of the chromomagnetic moment, even though these contributions are divergent. Contrary to the electromagnetic moment the chromomagnetic moment is not a physical quantity and thus it may be divergent. In the computation of the matching coefficient all divergences are absorbed into the renormalisation constant $Z_{cm}$.

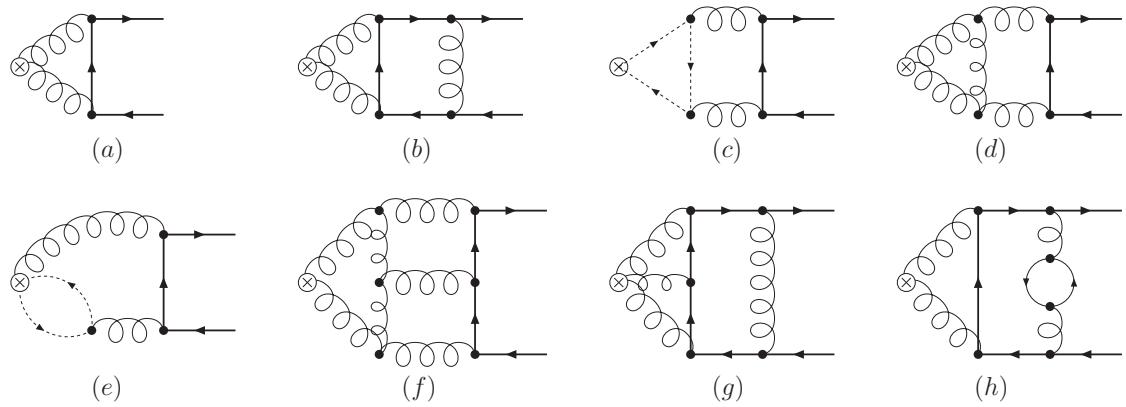


Figure 3.3: Sample diagrams contributing to the quark chromomagnetic moment. Solid, curly and dotted lines denote quarks, gluons and ghosts, respectively. $\otimes$ represents the coupling of the background field. In the closed quark loop all flavours have to be considered.

Our result for $C_m$ reads

$$\begin{aligned}
C_m(\mu) &= 1 + \frac{\alpha_s^{(n_l+1)}(M_Q)}{\pi}\left[\left(\frac{1}{2}+\frac{1}{4}L_\mu\right)C_A + \frac{1}{2}C_F\right] \\
&\quad + \left(\frac{\alpha_s^{(n_l+1)}(M_Q)}{\pi}\right)^2 \\
&\quad \times \left\{ \left(\frac{805}{432} - \frac{17}{144}\pi^2 + \frac{1}{12}\pi^2\ln 2 - \frac{1}{8}\zeta_3 + \frac{13}{36}L_\mu - \frac{1}{12}L_\mu^2\right)C_A^2 \right. \\
&\quad + \left(\frac{269}{144} + \frac{1}{12}\pi^2 + \frac{1}{12}\pi^2\ln 2 - \frac{1}{8}\zeta_3 + \frac{1}{8}L_\mu\right)C_F C_A \\
&\quad - \left(\frac{31}{16} - \frac{5}{12}\pi^2 + \frac{1}{2}\pi^2\ln 2 - \frac{3}{4}\zeta_3\right)C_F^2 \\
&\quad - \left[\left(\frac{299}{432} + \frac{1}{36}\pi^2 + \frac{13}{72}L_\mu - \frac{1}{24}L_\mu^2\right)C_A + \frac{25}{36}C_F\right]T_F n_l \\
&\quad \left. + \left[\left(-\frac{149}{216} + \frac{5}{72}\pi^2\right)C_A + \left(\frac{119}{36} - \frac{1}{3}\pi^2\right)C_F\right]T_F \right\} \\
&\quad + \left(\frac{\alpha_s^{(n_l+1)}(M_Q)}{\pi}\right)^3 c_m^{(3)} + \mathcal{O}\left(\alpha_s^4\right) . \qquad (3.19)
\end{aligned}$$

The two-loop result was already calculated in Ref. [123]. With the exception of the $\pi^2 C_A T_F$ term we agree with their result. The difference in this term is due to the inclusion of the order $\mathcal{O}(\epsilon)$ terms in the decoupling relation for $\alpha_s$, which was not done in Ref. [123].

Our new three-loop term is given by

$$
\begin{aligned}
c_m^{(3)} = {} & \\
& \left[\frac{1302797}{186624} + \frac{1585}{1296}\pi^2 - \frac{317}{864}\pi^2\ln 2 - \frac{1}{36}\pi^2\ln^2 2 - \frac{6079}{1728}\zeta_3 - \frac{17}{810}\pi^4 - \frac{653}{864}\pi^2\zeta_3\right. \\
& + \frac{925}{192}\zeta_5 - \frac{1}{9}\ln^4 2 - \frac{8}{3}a_4 + \left(\frac{2917}{3456} - \frac{17}{576}\pi^2 + \frac{1}{48}\pi^2\ln 2 + \frac{1}{32}\zeta_3\right)L_\mu - \frac{497}{1728}L_\mu^2 \\
& \left. + \frac{19}{432}L_\mu^3\right]C_A^3 + \left[\frac{122971}{10368} - \frac{17375}{3456}\pi^2 + \frac{1745}{432}\pi^2\ln 2 - \frac{169}{216}\pi^2\ln^2 2 + \frac{2951}{288}\zeta_3\right. \\
& + \frac{491}{10368}\pi^4 + \frac{161}{72}\pi^2\zeta_3 - \frac{265}{16}\zeta_5 + \frac{191}{432}\ln^4 2 + \frac{191}{18}a_4 + \left(\frac{337}{576} + \frac{1}{48}\pi^2 + \frac{1}{48}\pi^2\ln 2\right. \\
& \left.\left. - \frac{1}{32}\zeta_3\right)L_\mu - \frac{1}{24}L_\mu^2\right]C_A^2C_F - \left[\frac{2803}{288} - \frac{9767}{1728}\pi^2 + \frac{101}{24}\pi^2\ln 2 - \frac{13}{9}\pi^2\ln^2 2\right. \\
& + \frac{847}{96}\zeta_3 + \frac{209}{2880}\pi^4 + \frac{17}{9}\pi^2\zeta_3 - \frac{115}{6}\zeta_5 + \frac{35}{72}\ln^4 2 + \frac{35}{3}a_4 + \left(\frac{31}{64} - \frac{5}{48}\pi^2\right. \\
& \left.\left. + \frac{1}{8}\pi^2\ln 2 - \frac{3}{16}\zeta_3\right)L_\mu\right]C_AC_F^2 - \left(\frac{101}{64} - \frac{23}{6}\pi^2 + \frac{22}{3}\pi^2\ln 2 + \frac{5}{18}\pi^2\ln^2 2 - \frac{241}{24}\zeta_3\right. \\
& + \frac{139}{2160}\pi^4 - \frac{103}{72}\pi^2\zeta_3 + \frac{235}{24}\zeta_5 - \frac{5}{18}\ln^4 2 - \frac{20}{3}a_4\Big)C_F^3 - \left(\frac{5}{24} + \frac{151}{36}\pi^2\right. \\
& \left. - \frac{91}{16}\pi^2\ln 2 - \frac{5}{3}\pi^2\ln^2 2 + \frac{73}{32}\zeta_3 - \frac{7}{360}\pi^4 - \frac{97}{96}\pi^2\zeta_3 + \frac{15}{2}\zeta_5 + \frac{5}{12}\ln^4 2 + 10a_4\right. \\
& \left. - \frac{3}{16}\pi^2L_\mu\right)\frac{d_{44}^{FA}}{N_F} + \left\{\left[-\frac{236801}{46656} + \frac{35}{864}\pi^2 - \frac{89}{216}\pi^2\ln 2 + \frac{1}{27}\pi^2\ln^2 2 - \frac{101}{432}\zeta_3\right.\right. \\
& + \frac{1}{180}\pi^4 + \frac{1}{54}\ln^4 2 + \frac{4}{9}a_4 - \left(\frac{715}{1728} + \frac{1}{144}\pi^2 + \frac{1}{4}\zeta_3\right)L_\mu + \frac{235}{864}L_\mu^2 - \frac{35}{864}L_\mu^3\Big]C_A^2 \\
& - \left[\frac{88351}{10368} + \frac{23}{72}\pi^2 + \frac{1}{108}\pi^2\ln 2 - \frac{1}{27}\pi^2\ln^2 2 - \frac{2}{3}\zeta_3 + \frac{23}{3240}\pi^4 - \frac{1}{54}\ln^4 2 - \frac{4}{9}a_4\right. \\
& + \left(\frac{299}{576} - \frac{1}{4}\zeta_3\right)L_\mu - \frac{5}{96}L_\mu^2\Big]C_AC_F + \left(\frac{125}{32} - \frac{79}{54}\pi^2 + \frac{5}{3}\pi^2\ln 2 - \frac{2}{9}\pi^2\ln^2 2 - 3\zeta_3\right. \\
& \left.\left. + \frac{11}{216}\pi^4 - \frac{1}{9}\ln^4 2 - \frac{8}{3}a_4\right)C_F^2\right\}T_Fn_l + \left(\frac{1}{2} - \frac{11}{9}\pi^2 - \frac{9}{4}\zeta_3 + \frac{29}{360}\pi^4\right. \\
& \left. - \frac{1}{4}\pi^2L_\mu\right)\frac{d_{44}^{FF}}{N_F}n_l + \left[\left(\frac{3535}{5832} + \frac{25}{324}\pi^2 + \frac{7}{54}\zeta_3 - \frac{1}{72}L_\mu - \frac{13}{216}L_\mu^2 + \frac{1}{108}L_\mu^3\right)C_A\right. \\
& \left. + \left(\frac{317}{324} + \frac{1}{27}\pi^2\right)C_F\right]T_F^2n_l^2 + \ldots\,, \qquad (3.20)
\end{aligned}
$$

where the ellipses denote contributions from diagrams with closed heavy-quark loops, which we have not been computed so far. $d_{44}^{FF} = (N_c^2-1)(N_c^4-6N_c^2+18)/(96N_c)$ [107] and $d_{44}^{FA} = N_c(N_c^2-1)(N_c^2+6)/48$ [103]. The $n_l^2$ part agrees with the result obtained

in Ref. [124].

The anomalous dimension of the chromomagnetic interaction is found to be

$$\begin{aligned}
\gamma_{cm} &= \frac{\mathrm{d}\ln Z_{cm}}{\mathrm{d}\ln\mu} \\
&= \frac{\alpha_s^{(n_l)}}{\pi}\frac{1}{2}C_A + \left(\frac{\alpha_s^{(n_l)}}{\pi}\right)^2\left(\frac{17}{36}C_A^2 - \frac{13}{36}C_A T_F n_l\right) \\
&\quad + \left(\frac{\alpha_s^{(n_l)}}{\pi}\right)^3\left\{\left(\frac{899}{1728}+\frac{1}{8}\zeta_3\right)C_A^3 + \frac{3}{8}\pi^2\,\frac{d_{44}^{FA}}{N_F}\right. \\
&\qquad - \left[\left(\frac{65}{216}+\frac{1}{2}\zeta_3\right)C_A^2 + \left(\frac{49}{96}-\frac{1}{2}\zeta_3\right)C_A C_F\right. \\
&\qquad\quad \left.\left. + \frac{1}{36}C_A T_F n_l\right]T_F n_l - \frac{1}{2}\pi^2\,\frac{d_{44}^{FF}}{N_F}n_l\right\} + \mathcal{O}\left(\alpha_s^4\right) . \qquad (3.21)
\end{aligned}$$

The two-loop result agrees with the results of Refs. [123, 125].

For the numerical evaluation of $C_m(M_Q)$ and $\gamma_{cm}$, we choose the same setup as in the previous section. We find

$$\begin{aligned}
C_m(M_Q) &= 1 + 0.6897\,\alpha_s(M_Q) + (2.218 - 0.1938\,n_l + 0.0004\,n_h)\,\alpha_s^2(M_Q) \\
&\quad + \left(11.076 - 1.7495\,n_l + 0.0513\,n_l^2 + \ldots\right)\alpha_s^3(M_Q) + \mathcal{O}\left(\alpha_s^4\right) , \qquad (3.22)
\end{aligned}$$

where the ellipses denote contributions from diagrams with closed heavy-quark loops, which are not yet included at the three-loop level. At the two-loop level these contributions are labelled by $n_h$. Their numerical contribution is small. For the charm, bottom and top quark we find

$$\begin{aligned}
C_m(M_c) &= 1 + 0.2330 + 0.1869 + 0.2425 = 1.6624\,, \qquad (3.23) \\
C_m(M_b) &= 1 + 0.1496 + 0.0679 + 0.0500 = 1.2676\,, \qquad (3.24) \\
C_m(M_t) &= 1 + 0.0741 + 0.0144 + 0.0045 = 1.0931\,. \qquad (3.25)
\end{aligned}$$

The pattern is very similar to the quark electromagnetic moment. In the charm-quark case the series does not seem to converge, while the convergence is very slow at best in the bottom-quark case. Only for the top quark do we find an acceptable behaviour.

To numerically evaluate the anomalous dimension we need $\alpha_s(M_Q)$ with $n_l$ active flavours. Using `RunDec` we find $\alpha_s^{(3)}(M_c) = 0.3348$, $\alpha_s^{(4)}(M_b) = 0.2163$ and $\alpha_s^{(5)}(M_t) = 0.1074$. From Eq. (3.21) we have

$$\begin{aligned}
\gamma_{cm} &= 0.4775\,\alpha_s(M_Q) + (0.4306 - 0.0549\,n_l)\,\alpha_s^2(M_Q) \\
&\quad + \left(0.8823 - 0.1472\,n_l - 0.0007\,n_l^2\right)\alpha_s^3(M_Q) + \mathcal{O}\left(\alpha_s^4\right) . \qquad (3.26)
\end{aligned}$$

For the individual quark flavours this leads to

$$\gamma_{cm}(M_c) = 0.1599 + 0.0298 + 0.0163 = 0.2060\,, \tag{3.27}$$
$$\gamma_{cm}(M_b) = 0.1033 + 0.0099 + 0.0029 = 0.1160\,, \tag{3.28}$$
$$\gamma_{cm}(M_t) = 0.0513 + 0.0018 + 0.0002 = 0.0533\,. \tag{3.29}$$

Thus, as far as the anomalous dimension is concerned the convergence behaviour is acceptable even for the charm quark.

An interesting phenomenological application is the mass splitting between the ground-state vector and pseudo-scalar mesons containing a charm or a bottom quark,

$$R = \frac{m_{B^*}^2 - m_B^2}{m_{D^*}^2 - m_D^2} = \frac{C_m(M_b)}{C_m(M_c)} + \mathcal{O}\left(\frac{1}{m_Q}\right)\,, \tag{3.30}$$

which was also discussed in Ref. [125]. For this purpose we resum the logarithms in $C_m(\mu)$ to next-to-next-to leading logarithmic (NNLL) order. In this case, $R$ can be written as (see also Ref. [126])

$$\begin{aligned} R &= \left(\frac{\alpha_s(M_b)}{\alpha_s(M_c)}\right)^{\gamma_0/(2\beta_0)} \left\{1 + r_1\left(\frac{\alpha_s(M_c)}{\alpha_s(M_b)} - 1\right)\frac{\alpha_s(M_b)}{\pi}\right. \\ &\quad + \left[r_{20} + r_{21}\left(\left(\frac{\alpha_s(M_c)}{\alpha_s(M_b)}\right)^2 - 1\right) + \frac{r_1^2}{2}\left(\frac{\alpha_s(M_c)}{\alpha_s(M_b)} - 1\right)^2\right]\left(\frac{\alpha_s(M_b)}{\pi}\right)^2 \\ &\quad \left. + \mathcal{O}\left(\frac{\Lambda_{\rm QCD}}{M_{b,c}}\right)\right\}, \end{aligned} \tag{3.31}$$

where the coefficients are given by

$$r_1 = -c_m^{(1)} - \frac{\gamma_0}{2\beta_0}\left(\frac{\gamma_1}{\gamma_0} - \frac{\beta_1}{\beta_0}\right)\,, \tag{3.32}$$
$$r_{20} = c_m^{(2)}(n_l = 4) - c_m^{(2)}(n_l = 3) + \frac{z_2}{16}\,, \tag{3.33}$$
$$r_{21} = -c_m^{(2)} + \frac{(c_m^{(1)})^2}{2} + \frac{z_2}{16} + \frac{\gamma_0}{4\beta_0}\left[-\frac{\gamma_2}{\gamma_0} + \frac{\beta_2}{\beta_0} + \frac{\beta_1}{\beta_0}\frac{\gamma_1}{\gamma_0} - \left(\frac{\beta_1}{\beta_0}\right)^2\right]\,. \tag{3.34}$$

$c_m^{(i)}$ denotes the $i$-loop contribution to $C_m$ considered for $n_l = 3$. In $r_{20}$ the number of flavours for the two-loop coefficient is given explicitly. The term $z_2 = -71/(27)C_A T_F$ stems from decoupling in HQET [127, 128]. $\gamma_i$ and $\beta_i$ denote the coefficients of $(\alpha_s/\pi)^{i+1}$ of the anomalous dimension and the $\beta$ function, respectively. The latter can be found in Appendix E. $\gamma_i$, $\beta_i$, $\alpha_s(M_c)$ and $\alpha_s(M_b)$ are considered with four active flavours. The values for the latter are given above. Inserting them we find

$$R = 0.8517 - 0.0739 - 0.0931 + \cdots = 0.6848 + \ldots\,, \tag{3.35}$$

where the ellipses denote terms of higher order and non-perturbative contributions. The NNLL correction is larger than the NLL one, which means that the value for $R$ is decreased even further. Taking the experimental values for the meson masses from Ref. [113] we find $R_{exp} = 0.88$. An explanation for the large difference may be the behaviour of the perturbative series for $C_m(M_c)$. The corrections are very large, which makes the application of perturbation theory questionable. Since $R$ is determined up to non-perturbative corrections only, it is conceivable that the difference between the experimental and theoretical values are due to non-perturbative effects.

# Chapter 4

# Conclusions and Outlook

In this work we have calculated the fermionic non-singlet contributions to the matching coefficients of the vector, axial-vector, scalar and pseudo-scalar current in NRQCD at the three-loop level. The matching coefficient of the vector and axial-vector current are of particular interest, since they are building blocks of the top-anti-top production cross section at threshold. For the N$^3$LO evaluation of this cross section the former is needed to $\mathcal{O}(\alpha_s^3)$, while the latter is needed to $\mathcal{O}(\alpha_s)$. Thus, our calculation is a first step towards the full three-loop computation. Nevertheless, there is still quite some work to be done to calculate the singlet and the non-fermionic contributions.

A further step in this direction is the calculation of the three-loop on-shell propagator-type integrals. Moreover, this has allowed us to compute the three-loop quark mass and wave function renormalisation constants in QCD in the framework of dimensional regularisation and dimensional reduction. While the former constitutes a check on the analytical results in the literature, the latter results are new. They are of particular interest in the context of supersymmetry, where DREG cannot be applied. Since almost all QCD calculations have been performed in DREG, it is important to know how to related these quantities to their counterparts in DRED. Furthermore, our calculation can be a starting point for further calculations in supersymmetric theories.

Finally, we have calculated the third order strong corrections to the matching coefficient and the anomalous dimension of the chromomagnetic interaction in HQET. In the course of this calculation we could correct an error in the previous two-loop calculation of the matching coefficient. So far, we have not computed the three-loop contribution from diagrams with closed heavy-quark loops. This will of course be done in the future. As byproducts of this calculation we have obtained the three-loop QCD corrections to the quark magnetic moment and recalculated the three-loop QED corrections to the electron magnetic moment. As an extension of this work it would be possible to compute the weak magnetic moment of heavy quarks to three loops in QCD. This is especially interesting for top quarks since their couplings are

very sensitive to contribution from physics beyond the standard model.

# Appendix A

# Integration-by-Parts

The integration-by-parts (IBP) algorithm was developed in Ref. [63]. It is the method of choice in most multi-loop calculations today. For the calculations in this work, two approaches were used which are based on the IBP relations, but offer a systematic way to find a solution of the recurrence relations. In the following section a brief general introduction to IBP relations is given. Baikov's method [64,65] in the approach of Ref. [66] is explained in Section A.2 and Laporta's algorithm [67,68] in Section A.3. In Section A.4, we introduce additional recurrence relations which can be used to perform the partial fractioning mentioned in Section 1.2.2.

## A.1 Basics

The method of calculating Feynman integrals by means of IBP relations is based on the fact that the integral over a total derivative is zero in dimensional regularisation,

$$\int \mathrm{d}^d k \, \frac{\partial}{\partial k_\mu} \, p_\mu f(k, q_i, m_i) = 0 \,, \tag{A.1}$$

where the function $f$ depends on the external momenta $q_i$ and masses $m_i$ as well as on the loop momentum $k$. $p$ can be either a loop or an external momentum. This identity can be used to construct recurrence relations for the integral with arbitrary powers of the propagators in the following way. One writes down the above relations for all combinations of loop and external momenta, performs the derivatives and expresses the resulting scalar products in the numerator in terms of the propagators. Taking the derivative of a propagator results in the power of that propagator to be raised by one. If a propagator appears in the numerator due to some scalar product, its power is lowered by one. For an $h$-loop Feynman integral $F$ with $n$ external momenta and $N$ propagators, this procedure results in $h(h+n)$ relations of the form

$$\sum_{i,j=0}^{N} c_{ij}^k \, \mathbf{i}^+ \mathbf{j}^- F(a_1, \ldots, a_N) = 0 \,, \tag{A.2}$$

where the $a_i$ denote the powers of the propagators (also called indices) and $k = 1, \ldots, h(h+n)$. The dependence of $F$ on masses and momenta is suppressed in Eq. (A.2) and in the following. The operators $\mathbf{i}^+$ and $\mathbf{j}^-$ raise and lower the indices of the integral, respectively,

$$\begin{aligned} \mathbf{i}^+ F(a_1, \ldots, a_{i-1}, a_i, a_{i+1}, \ldots, a_N) &= F(a_1, \ldots, a_{i-1}, a_i + 1, a_{i+1}, \ldots, a_N)\,, \\ \mathbf{j}^- F(a_1, \ldots, a_{j-1}, a_j, a_{j+1}, \ldots, a_N) &= F(a_1, \ldots, a_{j-1}, a_j - 1, a_{j+1}, \ldots, a_N)\,, \\ \mathbf{0}^\pm &= 1\,. \end{aligned} \tag{A.3}$$

The coefficients $c_{ij}^k$ depend on the indices and the kinematical invariants of the integral. The coefficient $c_{00}^k$ can also depend on the dimension $d$. In general, there can also be higher powers of the raising and lowering operators. However, this does not change the algorithm described in this section.

The relations of Eq. (A.2) can be used to express any integral of a given class as a linear combination of a subset of integrals of that class, the so-called master integrals. The latter are the only integrals which have to be calculated explicitly.

As an example of this method, we consider the one-loop on-shell integral

$$J(a_1, a_2) = \int \frac{\mathrm{d}^d k}{(k^2)^{a_1}\,(k^2 + 2q \cdot k)^{a_2}}\,, \tag{A.4}$$

with $q^2 = m^2$. The first relation is derived by taking the derivative with respect to $k_\mu$ contracted with $k_\mu$, resulting in

$$\begin{aligned} 0 &= \left[\frac{\partial}{\partial k_\mu} k_\mu\right] J(a_1, a_2) \\ &= \left[d - 2a_1\,\mathbf{1}^+ k^2 - 2a_2\,\mathbf{2}^+\left(k^2 + q \cdot k\right)\right] J(a_1, a_2) \\ &= \left[d - 2a_1 - a_2\,\mathbf{2}^+\left(\mathbf{1}^- + \mathbf{2}^-\right)\right] J(a_1, a_2) \\ &= \left[(d - 2a_1 - a_2) - a_2\,\mathbf{1}^-\mathbf{2}^+\right] J(a_1, a_2)\,, \end{aligned} \tag{A.5}$$

where it is understood, that the operators in the square brackets are applied under the integral sign. The dimension $d$ appears due to the derivative of $k$ with respect to itself. Thus one arrives at an identity which can be used to reduce the first index to zero, e.g. for $a_1 > 0$ one has

$$J(a_1, a_2) = \frac{a_2}{d - 2a_1 - a_2} J(a_1 - 1, a_2 + 1)\,. \tag{A.6}$$

The second relation is derived by contracting the derivative with the external momentum $q_\mu$, resulting in

$$\begin{aligned} 0 &= \left[\frac{\partial}{\partial k_\mu} q_\mu\right] J(a_1, a_2) \\ &= \left[(a_1 - a_2) - a_1\,\mathbf{1}^+\mathbf{2}^- + a_2\,\mathbf{1}^-\mathbf{2}^+ - 2a_2 m^2\,\mathbf{2}^+\right] J(a_1, a_2) \end{aligned} \tag{A.7}$$

This can be further simplified by inserting Eq. (A.5) to obtain

$$0 = \left[(d - a_1 - 2a_2) - a_1\, \mathbf{1}^+\mathbf{2}^- - 2a_2 m^2\, \mathbf{2}^+\right] J(a_1, a_2) \tag{A.8}$$

Since $a_1 = 0$ can always be achieved by using the first relation, it is sufficient to consider only this case. Thus the second term in Eq. (A.8) vanishes and we arrive at the final relation

$$J(0, a_2) = \frac{d - 2(a_2 - 1)}{2(a_2 - 1)m^2}\, J(0, a_2 - 1)\,, \tag{A.9}$$

where the commutation relation

$$\left[\mathbf{i}^\pm, a_j\right] = \pm\, \delta_{ij}\, \mathbf{i}^\pm \tag{A.10}$$

has been used. The second relation allows to lower the second index. Since the integral vanishes if $a_2 \leq 0$, it can be used to reduce $a_2$ to one. Therefore, all integrals of the type $J(a_1, a_2)$ of Eq. (A.4) can be reduced to $J(0, 1)$, the master integral of this class. The coefficient of this integral is always a rational function of the dimension, the indices and $q^2$, the only kinematical invariant of this integral class.

Since in any multi-loop calculation the number of integrals of a given class can easily be of the order of a thousand, the reduction to master integrals is a huge simplification. However, for more complicated integrals, the recurrence relations themselves become more complicated so that a solution by hand is not easily achieved. In these cases a systematic approach to the solution of the recurrence relations is crucial. In the present work, two methods were applied which are discussed in the following sections.

## A.2 Baikov's Method

Baikov's method was developed in Refs. [64, 65]. In the present work, the approach of Ref. [66] was used. This method along with the implementation for the present calculations is explained in the following.

### A.2.1 General Considerations

We consider a general scalar $h$-loop Feynman integral $F$ with $N$ internal lines and $n$ external momenta $q_i$

$$F(a_1, \ldots, a_N) = \int \frac{\mathrm{d}^d k_i \ldots \mathrm{d}^d k_h}{D_1^{a_1} \ldots D_N^{a_N}}\,. \tag{A.11}$$

The propagators $D_i$ can be written as

$$D_i = \sum_{\substack{j=1 \\ k \geq j}}^{h+n} A_i^{jk}\, p_j \cdot p_k - m_i^2 \,, \tag{A.12}$$

with $p_i = k_i$ for $i \leq h$ and $p_i = q_{i-h}$ for $i > h$. A solution to the recurrence relations is found, if any integral can be expressed in terms of a set of master integrals,

$$F(a_1, \ldots, a_N) = \sum_i c_i(a_1, \ldots, a_N)\, I_i \,, \tag{A.13}$$

where the $I_i$ denote the master integrals and the $c_i$ are the corresponding coefficient functions. The master integrals correspond to the integral $F$ where all indices are either zero or one, i.e.

$$I_i = F(a_{i_1}, \ldots, a_{i_N}) \,, \text{ with } \; a_{i_j} \in \{0, 1\} \,. \tag{A.14}$$

There are special cases where an index can be equal to minus one instead of zero or, equivalently, equal to two instead of one. This is discussed below. From Eq. (A.14) one can immediately see the normalisation condition for the coefficient functions

$$c_i(a_{j_1}, \ldots, a_{j_N}) = \delta_{ij} \,. \tag{A.15}$$

It was shown by Baikov that the coefficient functions can be constructed as integrals over some auxiliary parameters $x_i$ as

$$c_i(a_1, \ldots, a_N) = \mathcal{N} \int \frac{\mathrm{d}x_1 \ldots \mathrm{d}x_N}{x_1^{a_1} \ldots x_N^{a_N}} \left(P(x_1, \ldots, x_N)\right)^{(d-h-1)/2} \,, \tag{A.16}$$

where the normalisation factor $\mathcal{N}$ is determined using Eq. (A.15). The so-called basic polynomial $P$ is a polynomial of degree $h$ in the parameters $x_i$ and the kinematical invariants. According to Refs. [64, 65] it is given by

$$P(x_1, \ldots, x_N) = \det\left( \sum_{i=1}^{N} \tilde{A}_i^{jk} (x_i + m_i) \right) \,, \tag{A.17}$$

where the determinant is taken with respect to $j$ and $k$. The matrices $\tilde{A}_i$ are constructed as follows. The coefficients $A_i^{jk}$ of Eq. (A.12) are defined for $j \geq k \geq 1$. If a pair of $j$ and $k$ is considered as one index and $i$ as the other, one has a $N \times N$-matrix whose inverse fulfils

$$\sum_{i=1}^{N} A_i^{(jk)} (A^{-1})_i^{(lm)} = \delta_{jl}\delta_{km} \,. \tag{A.18}$$

$\tilde{A}_i$ is the symmetric extension of $(A^{-1})_i^{jk}$ to all values of $j$ and $k$. A more practical recipe to construct the basic polynomial is given in the example in Section A.2.2.

Strictly speaking, Eqs. (A.16)–(A.18) only hold if $N = h(h+1)/2$, which is only true for vacuum integrals. However, it has been shown in Ref. [129] that every Feynman integral can be converted to a vacuum integral by introducing additional propagators for the missing kinematical invariants. Since this also means that the number of loops is changed to $h_{eff} > h$, $h_{eff}$ instead of $h$ has to be used in all of the above equations.

So far we have not specified the boundaries for the integrals in Eq. (A.16). According to Refs. [64,65], the integration contours have to be chosen in such a way that surface terms vanish, i.e. that the integrand vanishes on the integral's boundaries. This means that the boundaries are typically the roots of a quadratic polynomial. A special case is the case where the index corresponding to the integration variable is equal to one in the master integral. In this case the integration contour has to be chosen as a closed circle around the origin in the complex plane. Using Cauchy's theorem one has in this case

$$\oint \frac{\mathrm{d}x_i}{x_i^{a_i}} \left(P(x_1,\ldots,x_i,\ldots,x_N)\right)^z = \left[\frac{\mathrm{d}^{a_i-1}}{\mathrm{d}x_i^{a_i-1}} \left(P(x_1,\ldots,x_i,\ldots,x_N)\right)^z\right]_{x_i=0} . \quad \text{(A.19)}$$

### A.2.2 One-loop Example

Let us again consider the one-loop on-shell integral of Eq. (A.4) as an example. To convert this integral to the vacuum case, the external line has to be closed. This is achieved by introducing a third propagator,

$$J(a_1,a_2) \;\rightarrow\; J'(a_1,a_2,a_3) = \int \frac{\mathrm{d}^d k}{(k^2)^{a_1}\left[(k+q)^2-m^2\right]^{a_2}\left(q^2-m^2\right)^{a_3}} . \quad \text{(A.20)}$$

The original integral is recovered by setting the third index equal to zero. The number of loops is now effectively equal to two.

To find the basic polynomial, we set the parameters $x_i$ equal to the corresponding propagators $D_i$, neglecting the masses for the moment. Thus we arrive at a system of linear equations,

$$\begin{aligned} x_1 &= k^2 , \\ x_2 &= k^2 + 2q\cdot k + q^2 , \\ x_3 &= q^2 , \end{aligned} \quad \text{(A.21)}$$

which can be solved for the scalar products of the momenta. The basic polynomial

is then

$$\begin{aligned} P(x_1,x_2,x_3) &= \det\begin{pmatrix} k^2 & q\cdot k \\ q\cdot k & q^2 \end{pmatrix}_{x_i\to x_i+m_i} \\ &= \det\begin{pmatrix} x_1 & \frac{1}{2}(x_2-x_1-x_3) \\ \frac{1}{2}(x_2-x_1-x_3) & x_3 \end{pmatrix}_{x_i\to x_i+m_i} \\ &= \frac{1}{4}\left(4m^2x_1 - x_1^2 - (x_2-x_3)^2 + 2x_1(x_2+x_3)\right), \end{aligned} \tag{A.22}$$

where the masses have been restored by shifting the $x_i$ appropriately. It should be noted that an overall factor of the basic polynomial can always be dropped since the coefficient functions are normalised according to Eq. (A.15) in the end. The parameter $x_3$ can be set to zero immediately since we are only interested in integrals of the form $J'(a_1,a_2,0)$.

The next step is to determine the possible master integrals. To do this, we consider all combinations of zeros and ones for the indices. Here, we have three possibilities, namely $J'(1,1,0)$, $J'(1,0,0)$ and $J'(0,1,0)$. The second one can be discarded immediately since the integral is a massless vacuum integral and thus vanishes in dimensional regularisation. To determine whether the first one can be a master integral, we have to look at the corresponding coefficient function. The rule for choosing the integration contour for an index equal to one is to integrate over a circle around the origin. Thus, according to Cauchy's theorem, we only have to take derivatives with respect to the corresponding parameter and set it to zero afterwards. Since $P(0,0,0)=0$, $J'(1,1,0)$ cannot be a master integral.

The only master integral is therefore $J'(0,1,0) = J(0,1)$ as we already know from Section A.1. Now we are left with the task of constructing the coefficient function of this master integral. So far we have

$$\begin{aligned} c(a_1,a_2,0) &= \mathcal{N}\int \frac{\mathrm{d}x_1\mathrm{d}x_2}{x_1^{a_1}x_2^{a_2}}\left(P(x_1,x_2,0)\right)^{(d-3)/2} \\ &= \mathcal{N}\int \frac{\mathrm{d}x_1}{x_1^{a_1}}\left[\frac{\mathrm{d}^{a_2-1}}{\mathrm{d}x_2^{a_2-1}}\left(P(x_1,x_2,0)\right)^{(d-3)/2}\right]_{x_2=0}, \end{aligned} \tag{A.23}$$

since the second index of the master integral is equal to 1. After the derivatives have been performed the integrand takes the form $x_1^\alpha\,(4m^2-x_1)^\beta$, where both $\alpha$ and $\beta$ depend on the dimension $d$. In this case, the integration contour has to be chosen as a contour from zero to $4m^2$, yielding

$$\int_0^{4m^2} \mathrm{d}x\, x_1^\alpha\,(4m^2-x_1)^\beta = \left(4m^2\right)^{\alpha+\beta+1}\frac{\Gamma(\alpha+1)\,\Gamma(\beta+1)}{\Gamma(\alpha+\beta+2)}. \tag{A.24}$$

The choice of zero as one of the integration boundaries is only possible because the dimension appears in the exponent $\alpha$. Otherwise there would be singularities for negative integer values, which would not be regularised.

Since we expect the coefficient function to be a rational function of $d$ and $m^2$, the $\Gamma$-functions and all non-integer powers have to drop out in the normalisation. This is indeed the case and we now have an algorithm for the construction of the coefficient function for arbitrary integer indices.

### A.2.3 More Complicated Cases

The example in the last section is quite easy in the sense that there is only one master integral. If there are more, one has to define a certain hierarchy between them. The reason is that the coefficient functions of the master integrals are now linear combinations of the coefficient function for the integral itself and the coefficient functions of the integrals which are higher in the hierarchy. In the calculation of the original coefficient function, this means that the integration over some parameters can only be performed for non-positive integer values of the corresponding indices.

The hierarchy between the integrals is the following. Suppose we have two master integrals $I_1$ and $I_2$ with indices $a_{1_i}$ and $a_{2_i}$, respectively. Let $J_j$ be the set of integers with $a_{j_i} = 1$ for $i \in J_j$. The integral $I_1$ is higher in the hierarchy than $I_2$ if $J_2$ is a subset of $J_1$.

To see how we can now construct the coefficient functions, let us assume that we have only those two master integrals. Let us further assume that the set $J_1$ has only one more element than $J_2$, and let us denote this element by $k$. The construction of the coefficient function $c_1$ of the highest master integral, $I_1$, proceeds just as described above. It is in the case of $I_2$ that we encounter a difficulty. The integral over $x_k$ can now only be performed if $a_k \leq 0$. Usually, one has an integral of the type

$$\int_A^B \mathrm{d}x_k \, x^a \, (x_k - A)^\alpha \, (B - x_k)^\beta \,, \tag{A.25}$$

where $a$ is integral and $\alpha$ and $\beta$ are complex. In general, this integral is a hypergeometric function ${}_2F_1$. Since this is an infinite series, the coefficient function would not be a rational function. However, if $a \geq 0$ the infinite sum turns into a finite one and we can use the result.

The problem is now to find a way to turn positive values of $a_k$ into zero or negative values. The solution is to use once again IBP recurrence relations, but now for the parametric integral. After the integrations over some parameters have been performed using Cauchy's theorem, we are left with an integral of the form

$$f(n_1, \ldots, n_{N'}, n_d) = \int \frac{\mathrm{d}x_1}{x_1^{n_1}} \ldots \frac{\mathrm{d}x_{N'}}{x_{N'}^{n_{N'}}} P(x_1, \ldots, x_{N'})^{z - n_d} \,, \tag{A.26}$$

where $z = (d - h - 1)/2$. For this integral, we can write down $N'$ relations of the type

$$0 = \frac{\mathrm{d}}{\mathrm{d}x_i} \, f(n_1, \ldots, n_{N'}, n_d) \,. \tag{A.27}$$

One more relation can be constructed by writing $P^{z-n_d}$ as $P \cdot P^{z-(n_d+1)}$. The latter can in some cases be used to reduce $n_d$ to zero. Another relation can be derived from the fact that the integral of Eq. (A.26) is a homogeneous function of the kinematical invariants of the corresponding Feynman integral. According to Euler's theorem we have

$$\left( N' - \sum_{i=1}^{N'} n_i + m(z - n_d) \right) f(n_1, \ldots, n_{N'}, n_d) = \sum_j m_j \frac{\mathrm{d}}{\mathrm{d}m_j} f(n_1, \ldots, n_{N'}, n_d) \,, \tag{A.28}$$

where $m$ is the mass dimension of $P$ and $m_j$ denotes the kinematical invariants of the integral. This relation is just a special combination of the IBP relations. However, it turned out to be very useful in the present work.

Using these relations, it is possible to reduce the index $a_k$ to non-positive values and, since there is an integral which is higher in the hierarchy, to one. Thus, we find a so-called auxiliary master integral corresponding to $c_2^0(a_{1_1}, \ldots, a_{1_N})$, where $c_2^0$ is the coefficient function of $I_2$ constructed according to the usual procedure. However, in this case we have to consider the coefficient function as a linear combination of $c_2^0$ and $c_1$,

$$c_2(a_1, \ldots, a_N) = c_2^0(a_1, \ldots, a_N) + A \cdot c_1(a_1, \ldots, a_N) \,. \tag{A.29}$$

The coefficient $A$ can be determined from the normalisation condition of Eq. (A.15). We get

$$A = -c_2^0(a_{1_1}, \ldots, a_{1_N}) \,. \tag{A.30}$$

$c_2^0(a_{1_1}, \ldots, a_{1_N})$ has to drop out for any set of indices if the combination of Eq. (A.29) is used as coefficient function. This is a very powerful check on the consistency of the implementation.

Even if one considers the highest integral of a certain hierarchy, it can happen that it is not possible to perform some of the integrations. One possibility of this was mentioned in the example in the previous section. If the exponent $\alpha$ in Eq. (A.24) is a negative integer, singularities occur which are not regularised. Another example is a basic polynomial which is cubic in some integration parameter. If these problems cannot be circumvented by choosing a different order of integrations, it is necessary to calculate the coefficient function algebraically, i.e. using only IBP relations.

In Section A.2.1, we mentioned the possibility that a master integral has an index which is not equal to zero or one. Since we do not consider this case when we list the possible master integrals of the problem, this has to come out of the calculation. Indeed, this is the case. Suppose that we have a master integral $I = F(1, 1, 0)$, but that the problem has also a different master integral $I' = F(1, 1, -1)$. If this is the case, we will again encounter similar difficulties as in the above cases in the calculation of the coefficient function corresponding to $I$. The solution of the corresponding recurrence relations will again yield an auxiliary master integral. In this case, however, it will not vanish if a linear combination with other coefficient

functions is considered. Instead, we now have to construct the coefficient function for $I'$. This is done exactly as for $I$. The only difference is the normalisation condition. In this way we have introduced an additional master integral into the problem.

The IBP relations for the parametric integrals have a structure very similar to the relations for the Feynman integral itself. However, since some integrations can always be performed using Cauchy's theorem, one has to deal with a smaller number of indices. Even though the values of these indices are usually higher, this can be a significant simplification. Furthermore, if the integrations are possible for certain values of the indices, the solution to the recurrence relations has to be constructed for some special cases only, which again simplifies the problem. Still, the solution by hand is tedious at best. Thus, it is desirable to let a computer do this work. As it turns out, this is possible. One can apply Laporta's algorithm also to these relations. In the present work, the program `AIR` [79] was used for this task.

### A.2.4 Implementation

All calculations in this work were carried out using the computer algebra system `FORM` [130]. However, it turned out to be convenient to first implement the algorithms for the integrals in `Mathematica`. The reason is that almost all needed `Mathematica`-code can be generated automatically. This is very useful when one tries to determine the best order of integration. Afterwards everything can be translated to `FORM` and the `Mathematica` version can be used for debugging.

As an example, we give the `FORM` code for the calculation of one-loop on-shell integrals with one massive and one massless line, which is also discussed in Section A.2.2.

```
*********************************************
*                                           *
*     integration procedure for topVAtt1l     *
*                                           *
*********************************************

** jpint1l(a,b) = 1 / (k^2 + k.q)^a / (k^2)^b
** q^2 = 4*m^2
** z = (d - 3)/2 = 1/2 - ep

** basic polynomial is P(x1,x2) = x1^2 - 2 x1 x2 + x2 ( x2 - 4 m^2 )


* express integral through coefficient function
```

```
id jpint1l(jpa?,jpb?) = [jp_dx1]^(jpa-1)*[jp_polly](0)*
                        invfac_(jpa-1)/jpx2^jpb*[jp_check]^(jpa-1);
.sort

* differentiate basic polynomial

#do i = 1,1
 id [jp_dx1]*[jp_x1] = 1 + [jp_x1]*[jp_dx1];
 id [jp_dx1]*[jp_polly](jpa?) = jpznum(jpa,1)*(2*[jp_x1] - 2*jpx2)*
                                [jp_polly](jpa-1)
                              + [jp_polly](jpa)*[jp_dx1];
 id [jp_dx1]*[jp_check] = 0;
 if (count([jp_dx1],1)!=0) redefine i "0";
 .sort
#enddo

id [jp_check] = 1;
id [jp_x1] = 0;
.sort

* perform parameter integration

id jpx2^jpa?*[jp_polly](jpb?) =
   (-1)^jpb*[jp_-1^z]*4^(jpa+2*jpb+1)*[jp_4^2z]*
   (M1^2)^(jpa+2*jpb+1)*[jp_mm^2z]*jpGamma(jpa+jpb+1,1)*
   jpGamma(jpb+1,1)*jpiGamma(jpa+2*jpb+2,2);
.sort

* normalisation

multiply, 1/4*jpiGz(1,1)^2*jpGz(1,2)*jpznum(1,2)/
          [jp_-1^z]/[jp_mm^2z]/[jp_4^2z]/M1^2;
.sort

* reduce Gamma functions

#include Gamma
.sort

* express z through ep

id jpznum(jpa?,jpb?) = nom(jpa+jpb/2,-jpb);
id jpzden(jpa?,jpb?) = deno(jpa+jpb/2,-jpb);
```

```
id [jp_z] = nom(1/2,-1);

* insert master integral

multiply, -Gam(-1,1)*M1^2*eM1;
.sort
```

The derivative with respect to $x_1$ (`[jp_x1]`) is implemented as a commutation relation with the differential operator `[jp_dx1]`. The object `[jp_check]` is used to check whether there are still derivatives to be taken. In this way it is possible to use the more efficient `#do-#enddo` loop instead of `repeat-endrepeat`. `jpGamma`$(a, b)$ denotes $\Gamma(a + bz)$ and `jpiGamma` is its inverse. Both functions are reduced to `jpGz`$(1, b) = \Gamma(1 + bz)$ and its inverse by repeated use of the identity $\Gamma(x + 1) = x\,\Gamma(x)$. This is done in the file `Gamma`. `jpznum`$(a, b)$ denotes $a + bz$ and `jpzden` is its inverse. `nom` and `deno` are the corresponding `MATAD` functions for polynomials in $\epsilon$. Since there is only one master integral for this integral class, the insertion of this master integral is simply done by multiplying the coefficient functions with the result of Eq. (D.1).

## A.3 Laporta's Algorithm

Laporta's algorithm [67, 68] uses the fact that in practical applications it is usually enough to know the reduction for a finite number of integrals. If one plugs in values for the indices, the IBP equations form a linear system of equations. The unknowns are the integrals themselves and the coefficients are rational functions of the dimension and the kinematical invariants. This system can be solved in terms of the simplest integrals using Gauss' algorithm. A solution is found if all needed integrals can be expressed in terms of these simplest integrals. These are defined to be the master integrals of the integral class under consideration.

An essential ingredient for this method is the definition of an ordering between integrals with different values of the indices. This is needed to define which integrals are easier and which are more complicated. From experience it is obvious that integrals with less lines, i.e. more indices smaller or equal to zero, are less complicated than integrals with more lines. Furthermore, an integral with less dots on the lines or with less scalar products in the numerator is considered to be easier as well. Using these rules, each integral is assigned a weight which determines its complexity. The equations are solved in such a way that more complex integrals are expressed in terms of less complex ones.

Many different programs which implement this method are mentioned in the literature. However, to date there is only one program which is publicly available, `AIR` [79]. This program was used for two-loop calculations in the present work, both for Feynman integrals and for parametric integrals occurring in Baikov's method. It is, however, not able to perform the full reduction at the three-loop level. Here,

we used the program `Crusher` [69], which is written in `C++` and uses `GiNaC` [131] for simple manipulations like taking derivatives of polynomials. The rational functions, which appear as coefficients of the integrals, are handled with the help of `Fermat` [132], where the interface described in Ref. [133] has been used. The main features of the program are the automatic generation of IBP relations, the full symmetrisation of the occurring integrals and the possibility to expand the integral coefficients in $\epsilon$ during the calculation. In the latter case, the master integrals are chosen to be $\epsilon$-finite [134].

## A.4 Partial Fractions

In Section 1.2.2 we mentioned that it is possible to implement the partial fractioning, which is used to simplify the vertex integrals, via recurrence relations. Here we explain how this is done. For this purpose, let us consider the one-loop vertex diagram depicted in Fig. 1.3($a$) as an example. The corresponding scalar integral is given by

$$V_1(a_1, a_2, a_3) = \int \frac{\mathrm{d}^d k}{(k^2 + 2q_1 \cdot k)^{a_1} (k^2 - 2q_2 \cdot k)^{a_2} (k^2)^{a_3}} \,. \tag{A.31}$$

The partial fractioning for this integral is derived in Eq. (1.19) of Section 1.2.2. With this knowledge, we can immediately write down a recurrence relation which accomplishes the same thing. The integral itself is replaced by one half times the sum of two integrals where the power of one of the massive propagators is lowered by one and the power of the massless propagator is raised by one. Thus, we arrive at the following relation

$$0 = 1 - \frac{1}{2} \left( \mathbf{1}^- \mathbf{3}^+ + \mathbf{2}^- \mathbf{1}^+ \right) \,. \tag{A.32}$$

However, if we do not know how the partial fractioning works for some integral, we have to find an alternative way to find the corresponding recurrence relation. This is indeed possible for the integrals considered in this work [57]. Even though we distinguish $q_1$ and $q_2$ when we write down the integral, we know already that we can set $q_1 = q_2 = q/2$. This fact can be used to derive the desired relation. Starting from $0 = q_1 \cdot k - q_2 \cdot k$, we derive the recurrence relation in the usual way by expressing the scalar products through the propagators.

$$\begin{aligned} 0 &= q_1 \cdot k - q_2 \cdot k \\ &= \frac{1}{2} \left( (k^2 + 2q_1 \cdot k) - k^2 \right) + \frac{1}{2} \left( (k^2 - 2q_2 \cdot k) - k^2 \right) \\ &= \frac{1}{2} \left( \mathbf{1}^- + \mathbf{2}^- \right) - \mathbf{3}^- \,. \end{aligned} \tag{A.33}$$

Multiplying Eq. (A.33) with $-\mathbf{3}^+$, we arrive at Eq. (A.32).

The advantage of the above derivation is that it works for any integral. If we are dealing with a multi-loop integral, we can write down one relation for each loop momentum. These relations can be used in addition to the IBP relations in the Laporta reduction of the integral. As a result, we will in general find less master integrals than without these relations. We have verified this through an explicit calculation, using the program `AIR`, of the two-loop singlet integrals of Eq. (1.42) and the non-singlet integrals corresponding to Figs. 1.3($b$) and ($c$). In the latter cases, we found only the master integrals of $J_{\pm}^{(2)}$ and $L_{\pm}^{(2)}$. This shows again that the relations are equivalent to the partial fractioning.

# Appendix B

# Mellin-Barnes Integrals

In this chapter we describe the evaluation of Feynman integrals using Mellin-Barnes integrations [135, 136]. Most of the master integrals needed for the present work were calculated using this method. It turned out to be convenient to choose the Feynman parameter representation [137] of the integrals as a starting point. This representation is explained in the next section. The actual Mellin-Barnes method is described in Section B.2. For a more detailed introduction to both topics see e.g. Ref. [138].

## B.1 Feynman Parameters

Feynman parameters [137] can be used to rewrite a product, where the individual factors are raised to different powers, as a sum of the two factors raised to some power. The basic formula is[1]

$$\frac{1}{A^{\alpha_1} B^{\alpha_2}} = \frac{\Gamma(\alpha_1+\alpha_2)}{\Gamma(\alpha_1)\Gamma(\alpha_2)} \int\limits_0^\infty \mathrm{d}x\, \mathrm{d}y\, \delta(x+y-1) \frac{x^{\alpha_1-1}\, y^{\alpha_2-1}}{(Ax+By)^{\alpha_1+\alpha_2}}\,. \tag{B.1}$$

If $A$ and $B$ are propagators of a Feynman integral, the terms in the denominator can always the rewritten in the form $1/(k^2-C^2)$ by completing the square. Here, $k$ is a loop momentum and $C$ depends on the Feynman parameters. Thus, the integration over the loop momentum can be performed.

For a general $h$-loop Feynman integral with $N$ internal lines, the Feynman pa-

[1] The usual form follows if the integration over $y$ is performed using the properties of the $\delta$ function.

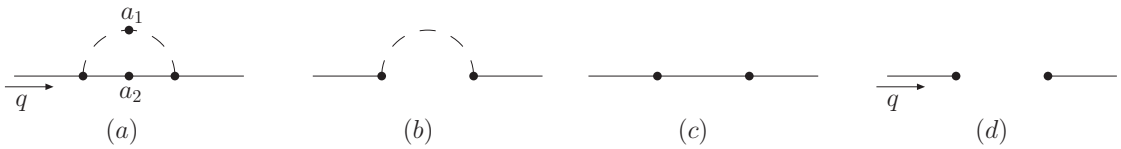


Figure B.1: One-loop on-shell integral with arbitrary powers of the propagators. Solid lines are massive with mass $m$ and dashed lines are massless. In $(a)$ the integral itself is depicted. $(b)$ and $(c)$ show the summands of the $U$ function. $(d)$ is the only contribution to the $V$ function.

rameters can be introduced using the formula

$$\begin{aligned} F(a_1,\ldots,a_N) &= (-1)^a \left(i\pi^{d/2}\right)^h \frac{\Gamma(a-dh/2)}{\prod_i \Gamma(a_i)} \\ &\quad \times \int_0^\infty \prod_i \mathrm{d}x_i\, \delta\left(\sum_i x_i - 1\right) \frac{\left(\prod_i x_i^{a_i-1}\right)\, U^{a-(h+1)d/2}}{\left(U(\sum_i x_i m_i^2) - V\right)^{a-dh/2}}\,, \end{aligned} \tag{B.2}$$

where $a = \sum_i a_i$ and the integration over the loop momenta has already been performed. The functions $U$ and $V$ encode the topology of the integral. They are defined as

$$U = \sum_{T\in \mathrm{T}_1} \prod_{i\notin T} x_i\,, \tag{B.3}$$

$$V = \sum_{T\in \mathrm{T}_2} \prod_{i\notin T} x_i (q_T)^2\,. \tag{B.4}$$

$\mathrm{T}_1$ denotes the set of all trees of the corresponding diagram, i.e. the maximally connected subgraphs without loops. $\mathrm{T}_2$ denotes the so-called two-trees, i.e. the set of trees with two connectivity components. $\pm q_T$ is the momentum flowing into one of these connectivity components. Due to momentum conservation it is not important into which of the two components $q_T$ flows.

An important tool is the Cheng-Wu theorem [139], which states that one can choose any subset of Feynman parameters in the argument of the $\delta$ function in Eq. (B.2). This can lead to significant simplifications for the evaluation of the integrals.

Let us again consider the one-loop on-shell integral of Eq. (A.4) as an example. From Fig. B.1 we know that we have $U = x_1 + x_2$ and $V = q^2 x_1 x_2$. Using Eq. (B.2)

and $q^2 = m^2$ we can now write down the Feynman parameter representation of $J$,

$$\begin{aligned} J(a_1, a_2) &= (-1)^a \, i\pi^{d/2} \, \frac{\Gamma(a-2+\epsilon)}{\Gamma(a_1)\,\Gamma(a_2)} \\ &\quad \times \int\limits_0^\infty \mathrm{d}x_1 \, \mathrm{d}x_2 \, \delta(x_1+x_2-1) \frac{x_1^{a_1-1} \, x_2^{a_2-1} \, (x_1+x_2)^{a-4+2\epsilon}}{((x_1+x_2)x_2 m^2 - m^2 x_1 x_2)^{a-2+\epsilon}} \, . \end{aligned} \tag{B.5}$$

Performing the integration over $x_2$ with the help of the $\delta$ function, we find that the integral over $x_1$ is just Euler's Beta function,

$$\begin{aligned} J(a_1, a_2) &= (-1)^a \, i\pi^{d/2} \, \frac{\Gamma(a-2+\epsilon)}{\Gamma(a_1)\,\Gamma(a_2)} \int\limits_0^1 \mathrm{d}x_1 \frac{x_1^{a_1-1} \, (1-x_1)^{a_2-1}}{(m^2(1-x_1)^2)^{a-2+\epsilon}} \\ &= (-1)^a \, i\pi^{d/2} \, \frac{\Gamma(a-2+\epsilon)}{\Gamma(a_1)\,\Gamma(a_2)} (m^2)^{2-a-\epsilon} \int\limits_0^1 \mathrm{d}x_1 \, x_1^{a_1-1} \, (1-x_1)^{3-2a_1-a_2-2\epsilon} \\ &= (-1)^a \, i\pi^{d/2} \, \frac{\Gamma(4-2a_1-a_2-2\epsilon)}{\Gamma(a_2)\,\Gamma(4-a-2\epsilon)} \, \frac{\Gamma(a-2+\epsilon)}{(m^2)^{a-2+\epsilon}} \, . \end{aligned} \tag{B.6}$$

Thus, we find an analytical result for the integral with arbitrary powers of the propagators. Whereas the algorithm of Appendix A only works for integer powers of the propagators, the result of Eq. (B.6) also holds for complex values.

The above example is, of course, an easy one. For more complicated integrals it is not possible to find analytical results to all orders in $\epsilon$. However, for the master integrals of the present work, it turned out that the Feynman parameter representation is a very convenient starting point for the evaluation. In particular, this means that we introduce an additional Mellin-Barnes integration if an integration over the Feynman parameters cannot be performed immediately. This method is explained in detail in the following section.

## B.2 Mellin-Barnes Representation

Using the Mellin-Barnes [135, 136] method one can rewrite a sum as a product by introducing an additional complex integration. The basic formula is

$$\frac{1}{(A+B)^\lambda} = \frac{1}{2\pi i} \frac{1}{\Gamma(\lambda)} \int\limits_{-i\infty}^{+i\infty} \mathrm{d}z \, \Gamma(\lambda+z) \, \Gamma(-z) \frac{A^z}{B^{\lambda+z}} \, . \tag{B.7}$$

The integration contour has to be chosen in such a way that poles of $\Gamma$ functions with a $\Gamma(\ldots - z)$ dependence are separated from poles of $\Gamma$ functions with a $\Gamma(\ldots + z)$

dependence. Afterwards the contour can be closed to the left or right and the integral can be evaluated using Cauchy's theorem, i.e. by summing up the residuals.

If one is dealing with a Mellin-Barnes representation of a Feynman integral, the crucial point is the treatment of the poles in $\epsilon$. In the case of a finite integral, the choice of the integration contour is straightforward. It is then possible to expand the integrand in $\epsilon$ and evaluate the Mellin-Barnes integral using Barnes lemmas or by summing up the residuals. However, if there are poles in $\epsilon$, they manifest themselves by the so-called glueing together of poles in the complex plain. Due to this, it is not possible to find a contour which separates the poles with a "$-z$" dependences from poles with a "$+z$". In this case, one has to successively change the "nature" of one or more poles until a contour is found. This is done by replacing the integral over the original contour by the sum of the integral over a shifted contour and the residual at the point where the glueing occurred.

Recently, two algorithms [140, 141] have been proposed, which automatise the whole procedure in the formulation of Ref. [136]. The program described in the latter reference, `MB`, is publicly available and has been used for the numerical evaluation of the master integrals in this work.

Let us consider the master integral $I_3^{(2)} = J_-^{(2)}(0,0,1,1,1)$ (cf. Appendix D) as an example. Starting from the Feynman parameter representation given in Eq. (3.50) of Ref. [138], we introduce one additional Mellin-Barnes integration

$$\begin{aligned} I_3^{(2)} &= -m_Q^2 \left(\frac{\mu^2}{m_Q^2}\right)^{2\epsilon} \Gamma(2\epsilon-1) \int_0^1 \mathrm{d}\xi \int_0^\infty \mathrm{d}t \, \frac{[t+\xi(1-\xi)]^{3\epsilon-3}}{[t(1-2\xi)^2+\xi(1-\xi)]^{2\epsilon-1}} \\ &= -m_Q^2 \left(\frac{\mu^2}{m_Q^2}\right)^{2\epsilon} \frac{1}{2\pi i} \int_{-i\infty}^{+i\infty} \mathrm{d}z \, \Gamma(2\epsilon-1+z)\,\Gamma(-z) \\ &\quad \times \int_0^1 \mathrm{d}\xi \, (1-2\xi)^{2z} [\xi(1-\xi)]^{1-2\epsilon-z} \int_0^\infty \mathrm{d}t \, t^z [t+\xi(1-\xi)]^{3\epsilon-3} \,. \end{aligned} \tag{B.8}$$

The integral over $t$ can now be performed. Writing the integral over $\xi$ as two times the integral from 0 to 1/2 and using the substitution $\xi \to (1-\sqrt{1-x})/2$, just as

in Ref. [138], we obtain

$$\begin{aligned} I_3^{(2)} &= -m_Q^2 \left(\frac{\mu^2}{m_Q^2}\right)^{2\epsilon} \frac{2}{4^\epsilon\,\Gamma(3-3\epsilon)} \\ &\quad \times \frac{1}{2\pi i} \int\limits_{-i\infty}^{+i\infty} \mathrm{d}z\, \Gamma(2\epsilon-1+z)\,\Gamma(-z)\,\Gamma(1+z)\,\Gamma(2-3\epsilon-z) \\ &\quad \times \int\limits_0^1 \mathrm{d}x\, x^{\epsilon-1}\,(1-x)^{z-1/2}\,. \end{aligned} \tag{B.9}$$

Now we can also perform the integration over $x$. The result is the following one-fold Mellin-Barnes representation for the master integral

$$\begin{aligned} I_3^{(2)} &= -m_Q^2 \left(\frac{\mu^2}{m_Q^2}\right)^{2\epsilon} \frac{2\,\Gamma(\epsilon)}{4^\epsilon\,\Gamma(3-3\epsilon)} \\ &\quad \times \frac{1}{2\pi i} \int\limits_{-i\infty}^{+i\infty} \mathrm{d}z\, \frac{\Gamma(2\epsilon-1+z)\,\Gamma(-z)\,\Gamma(1+z)\,\Gamma(2-3\epsilon-z)\,\Gamma(z+1/2)}{\Gamma(\epsilon+1/2+z)}\,. \end{aligned} \tag{B.10}$$

The evaluation can now, for example, be done with the program `MB`. Using the following `Mathematica` program, we have numerically checked the known analytical result.

```
(* 2-loop sunset with one massless and two massive lines   *)
(* at threshold                                            *)
(* prefactor of the integral is (i Pi^(d/2))^2 mm^(1-2*ep) *)

<<~/mathematica/MB/MB.m;

(* define prefactor and integrand *)

MBprefactor = -Exp[2*ep*EulerGamma]*2*Gamma[ep]/4^ep/Gamma[3-3*ep];
(MBex = Gamma[2*ep-1+z]*Gamma[-z]*Gamma[1+z]*Gamma[2-3*ep-z]*
 Gamma[z+1/2]/Gamma[ep+1/2+z]);

(* choose integration contour *)

rules = MBoptimizedRules[MBex,ep->0,{},{ep}];
cont = MBcontinue[MBex,ep->0,rules];
```

```
(* expand in ep to order n; prefactor is included in this step *)

expr[n_] := MBmerge[MBexpand[cont,MBprefactor,{ep,0,n}]];

(* perform numerical integration *)

sun[n_] := MBintegrate[expr[n],{},Complex->True];

(* calculate poles analytically *)

(poles = FullSimplify[MBmerge[{expr[-1][[1]],
                               Barnes1[expr[-1][[2]],z]}]]);
```

The poles can even be evaluated analytically with the help of the first Barnes lemma. The results we get are

```
poles[[1,1]] = 1/ep^2 + 2/ep
sun[2] = ep^(-2)
       + (1.9999999999994615 + 5.551115123125783*^-16*I)/ep
       + (8.547137367590192 + 7.867187803989317*^-15*I)
       + (14.133627433378415 + 1.737259225365051*^-9*I)*ep
       + (44.10934076701088 - 2.2737367544323206*^-13*I)*ep^2
```

Using the analytical result of Eq. (D.4), we get

$$I_3^{(2)} = m_Q^2 \left(\frac{\mu^2}{m_Q^2} e^{-\gamma_E}\right)^{2\epsilon} \left\{\frac{1}{\epsilon^2} + \frac{2}{\epsilon} + 8.547137367665245 + 14.13362743588118\,\epsilon + 44.10934076704626\,\epsilon^2 + \mathcal{O}\left(\epsilon^3\right)\right\}, \quad \text{(B.11)}$$

which is in excellent agreement.

# Appendix C

# Program Packages

Calculations like the ones of this work are only possible due to the use of computers. We used a collection of existing program packages, which are described in this chapter. The successive use of these packages allows an almost complete automatisation of the calculations, starting with the generation of the Feynman diagrams and ending with the evaluation of the corresponding integrals.

## C.1 QGRAF

QGRAF [58] is a very fast Feynman graph generator written in Fortran. The output format can be manipulated by providing a style file. Apart from this, the program requires two files to specify which diagrams should be generated. One file, "qgraf.dat", contains general information about the considered process like the incoming and outgoing particles and the number of loops. For the calculation of the matching coefficient of the vector current, the following file was used:

```
 output = 'qlist.' ;         * name of output file
 style = 'q2e.sty' ;         * name of style file
 model = 'gammatt.lag' ;     * name of model file

 in = ft,fT ;                * incoming particles
 out = a ;                   * outgoing particles

 loops = 3 ;                 * number of loops
 loop_momentum = k ;         * name of loop momenta

 options = onepi;            * additional options, here: graphs
                             * should be one-particle irreducible
* only nl part
 false = iprop[fq,0,0];      * require the presence of light quarks
```

In the other file, one has to specify the model to be used. This means that one has to state all occurring propagators and vertices. The model file for the calculation of the matching coefficients is the following:

```
* propagators

  [ft,fT,-]                 * top quark

  [fq,fQ,-]                 * light quarks

  [g,g,+t]                  * gluon (no tadpoles)

  [a,a,+p]                  * photon (only external)

  [ug,uG,-]                 * gluon ghost

  [s,s,+]                   * dummy scalar for four gluon vertex

* vertices

  [fT,ft,g]
  [fQ,fq,g]

  [fT,ft,a]

  [uG,ug,g]

  [g,g,g]

  [g,g,s]

* for 3-loop only (n_l singlet diagrams)

  [fQ,fq,a]
```

The program's output is a list of all diagrams in the specified format. The diagrams' symmetry factors are given as well.

## C.2 q2e and exp

`q2e` [59] and `exp` [60,61] are used to further process `QGRAF`'s output. `exp` is capable of performing an asymptotic expansion for large or small masses and external momenta

in the euclidean region. This is done in a diagrammatic way where the resulting diagrams are mapped onto previously specified topologies. With the exception of the singlet contribution for bottom quarks, we did not perform an asymptotic expansion in the present work, but used `exp` only for the mapping. The output is given in a `FORM` readable way. The Feynman rules corresponding to the different particles are also inserted at this step. Furthermore, labels for diagrams with massive and massless quark loops are inserted by `q2e`.

## C.3 MATAD

`MATAD` [62] is a `FORM` [130] program designed for the calculation of massive tadpole diagrams up to three loops. Here, we use a version which has been modified to be used within the automatic setup described in this chapter. This makes the use of the program very convenient even though we do not want to calculate massive tadpoles. The program takes care of the whole Dirac algebra and computes the colour factors of the diagrams. The only things which have to be supplied are topology files for the calculation of the integrals. As an example, we give the `FORM` code for the calculation of one-loop vertex integrals at threshold (cf. Section A.2.4 for the file `VAtt1l`).

```
*************************************************************************
* topology file for 1-loop vertex diagram at threshold                  *
*                                                                       *
* {topVAtt1l;3;1;2;1;;(q1:1,3)(q2:2,3)(p1:1,3)(p2:3,2)(p3:2,1);110} *
*************************************************************************


** p3 = k,
** s1m1 = 1/(k^2 + k.q),
** s2m1 = 1/(k^2 - k.q),
** q^2 = 4*m^2


* express p1 and p2 through p3 and Q

id p1 = p3 + Q/2;
id p2 = p3 - Q/2;
.sort

* express remaining scalar products through denominators

id p3.Q = 1/s1m1 - p3.p3;
```

```
* apply on-shell condition (euclidean)

id Q.Q = -4*M1^2;
id 1/Q.Q = -1/4/M1^2;
.sort

* use partial fractions to reduce the integrals to propagator type

if ( (count(s1m1,1)!=0) && (count(s2m1,1)!=0) );
 id s1m1 =  1/[jp_den1];
 id s2m1 = -1/[jp_den2];
 id 1/s1m1 = [jp_den1];
 id 1/s2m1 = -[jp_den2];
endif;
.sort

ratio [jp_den2],[jp_den1],[jp_diff];

id [jp_den1] = 1/s1m1;
id [jp_den2] = -1/s2m1;
id 1/[jp_den1] = s1m1;
id 1/[jp_den2] = -s2m1;
id [jp_diff] = 2*p3.p3;
id 1/[jp_diff] = 1/2/p3.p3;
.sort

* sign of external momentum does not matter
* for propagator-type on-shell integral

multiply,replace_(s2m1,s1m1);
.sort

* discard massless tadpoles

if (count(s1m1,1)<=0) discard;
.sort

* identify the integrals

** jpint1l(a,b) = 1/(k^2+k.q)^a/(k^2)^b = 1/(k^2-k.q)^a/(k^2)^b

id s1m1^jpa?*p3.p3^jpb? = (-1)^(jpa+jpb)*jpint1l(jpa,-jpb);
.sort
```

```
* calculate integral with analytical formula

* id jpint1l(jpa?,jpb?) = (-1)^(jpa+jpb)*Gam(jpa+jpb-2,1)*
*                         Gam(-2*jpb-jpa+4,-2)*iGam(jpa,0)*
*                         iGam(-jpa-jpb+4,-2)/(M1^2)^(jpa+jpb-2)*eM1;

* ... or with Baikov's method

#include VAtt1l
.sort

* expand in epsilon

#include redcut
#include expepgam
.sort
```

# Appendix D

# Master Integrals

In this chapter the results for all master integrals, which occur in the present work, are provided and some details of their evaluation are presented. The integrals are evaluated in dimensional regularisation with $d = 4 - 2\epsilon$. The integral names correspond to the ones given in Chapters 1 and 2. All results are given in Minkowski space.

## D.1 One-loop integrals

At one-loop level, there is only one master integral. It is shown in Fig. D.1. The integral can be easily evaluated to all orders in $\epsilon$ using Feynman parameters (cf. Appendix B). In fact, this can also be done for arbitrary complex powers of the propagator. The result for the master integral reads

$$I_1^{(1)} = J^{(1)}(0,1) = -m_Q^2 \left(\frac{\mu^2}{m_Q^2}\right)^\epsilon \Gamma(\epsilon - 1) \,. \tag{D.1}$$

## D.2 Two-loop integrals

There are four master integrals which are needed for the calculation of the non-singlet contribution at the two-loop level. They are depicted in Fig. D.2. The

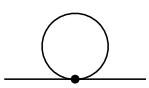

Figure D.1: One-loop master integral $I_1^{(1)}$.

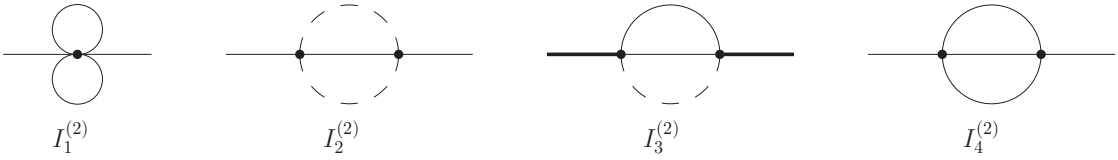


Figure D.2: Two-loop master integrals for non-singlet the contribution. Bold lines denote massive lines with mass $2m_Q$, thin lines denote massive lines with mass $m_Q$ and dashed lines denote massless lines. All external lines are on-shell.

results read

$$I_1^{(2)} = J_+^{(2)}(0,0,0,1,1) = m_Q^4 \left(\frac{\mu^2}{m_Q^2}\right)^{2\epsilon} \Gamma^2(\epsilon-1)\,, \tag{D.2}$$

$$\begin{aligned} I_2^{(2)} &= J_+^{(2)}(1,0,1,0,1) \\ &= -m_Q^2 \left(\frac{\mu^2}{m_Q^2}\right)^{2\epsilon} \frac{\Gamma^2(1-\epsilon)\,\Gamma(\epsilon)}{\Gamma(2-2\epsilon)} \frac{\Gamma(2\epsilon-1)\,\Gamma(3-4\epsilon)}{\Gamma(3-3\epsilon)}\,, \end{aligned} \tag{D.3}$$

$$\begin{aligned} I_3^{(2)} &= J_-^{(2)}(0,0,1,1,1) \\ &= m_Q^2 \left(\frac{\mu^2}{m_Q^2} e^{-\gamma_E}\right)^{2\epsilon} \left\{ \frac{1}{\epsilon^2} + \frac{2}{\epsilon} - \frac{1}{2} + \frac{11}{12}\pi^2 \right. \\ &\quad + \left(-\frac{85}{4} + \frac{17}{24}\pi^2 + \frac{3}{2}\pi^2 \ln 2 + \frac{181}{12}\zeta_3\right)\epsilon + \left(-\frac{907}{8} - \frac{373}{48}\pi^2 + \frac{3}{4}\pi^2 \ln 2 \right. \\ &\quad \left. \left. + 3\pi^2 \ln^2 2 + \frac{157}{24}\zeta_3 + \frac{167}{72}\pi^4 - \frac{3}{2}\ln^4 2 - 36 a_4\right)\epsilon^2 + \mathcal{O}\left(\epsilon^3\right) \right\}\,, \end{aligned} \tag{D.4}$$

$$\begin{aligned} I_4^{(2)} &= L_+(0,0,1,1,1) \\ &= m_Q^2 \left(\frac{\mu^2}{m_Q^2} e^{-\gamma_E}\right)^{2\epsilon} \left\{ \frac{3}{2\epsilon^2} + \frac{17}{4\epsilon} + \frac{59}{8} + \frac{\pi^2}{4} + \left(\frac{65}{16} + \frac{49}{24}\pi^2 - \zeta_3\right)\epsilon \right. \\ &\quad + \left(-\frac{1117}{32} + \frac{475}{48}\pi^2 - 8\pi^2 \ln 2 + \frac{151}{6}\zeta_3 + \frac{7}{240}\pi^4\right)\epsilon^2 \\ &\quad + \left(-\frac{13783}{64} + \frac{3745}{96}\pi^2 - 52\pi^2 \ln 2 + 16\pi^2 \ln^2 2 + \frac{2125}{12}\zeta_3 - \frac{103}{96}\pi^4 - \frac{1}{6}\pi^2\zeta_3 \right. \\ &\quad \left. \left. - \frac{3}{5}\zeta_5 + 8\ln^4 2 + 192 a_4\right)\epsilon^3 + \mathcal{O}\left(\epsilon^4\right) \right\}\,, \end{aligned} \tag{D.5}$$

where $\gamma_E$ is Euler's constant, $\zeta_n$ denotes Riemann's zeta-function with integer argument $n$ and $a_4 = \mathrm{Li}_4\left(\frac{1}{2}\right) = \sum_{n=1}^{\infty} (2^n\, n^4)^{-1}$.

$I_2^{(2)}$ can be calculated for arbitrary complex powers of the propagators by means

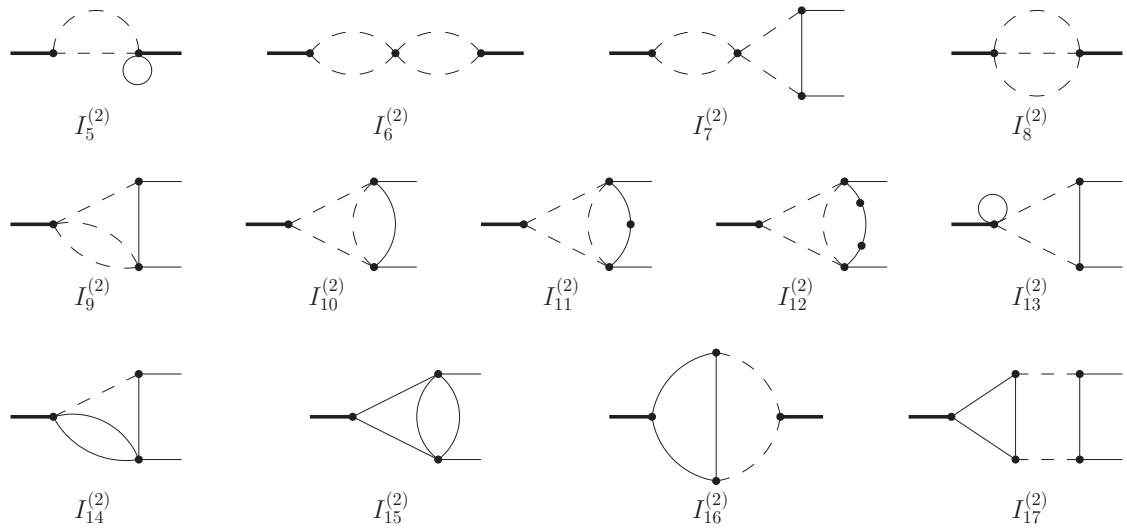


Figure D.3: Additional two-loop master integrals for the singlet contribution. The same coding as in Fig. D.2 is adopted. A dot on a line denotes a squared propagator.

of Feynman parameters. The result for $I_3^{(2)}$ can be extracted from the expression for the corresponding off-shell integral given in Ref. [142]. The result for $I_4^{(2)}$ can be extracted from the result for $L_+(1,1,1,1,1)$ given in Ref. [109]. Both results have been checked numerically with a one-fold Mellin-Barnes [135, 136] representation, using the program `MB` [141] (cf. Appendix B for $I_3^{(2)}$).

For the calculation of the two-loop singlet contribution, we need thirteen additional master integrals. They are depicted in Fig. D.3. The results are

$$I_5^{(2)} = V_E(0,1,0,0,1,1,0) = -m_Q^2 \left(\frac{\mu^2}{m_Q^2}\right)^{2\epsilon} \frac{\Gamma(\epsilon-1)\Gamma^2(1-\epsilon)\Gamma(\epsilon)}{\Gamma(2-2\epsilon)(-4-i\varepsilon)^\epsilon}\,, \tag{D.6}$$

$$I_6^{(2)} = V_E(1,0,1,0,1,1,0) = \left(\frac{\mu^2}{m_Q^2}\right)^{2\epsilon} \frac{\Gamma^4(1-\epsilon)\Gamma^2(\epsilon)}{\Gamma^2(2-2\epsilon)(-4-i\varepsilon)^{2\epsilon}}\,, \tag{D.7}$$

$$\begin{aligned} I_7^{(2)} &= V_E(1,1,1,0,1,1,0) \\ &= \frac{1}{m_Q^2}\left(\frac{\mu^2}{m_Q^2}e^{-\gamma_E}\right)^{2\epsilon} \left\{\left(\ln 2 - i\frac{1}{2}\pi\right)\frac{1}{\epsilon} + \frac{5}{6}\pi^2 + 4\ln 2 - 3\ln^2 2\right. \\ &\quad -i\pi\,(2-3\ln 2) + \left(\frac{10}{3}\pi^2 - \frac{23}{6}\pi^2\ln 2 + \zeta_3 + 12\ln 2 - 12\ln^2 2 + \frac{14}{3}\ln^3 2\right. \\ &\quad \left.\left. -i\pi\left(6 - \frac{3}{4}\pi^2 - 12\ln 2 + 7\ln^2 2\right)\right)\epsilon + \mathcal{O}\left(\epsilon^2\right)\right\}\,, \end{aligned} \tag{D.8}$$

$$I_8^{(2)} = V_E(0,0,1,1,0,1,0) = 4m_Q^2 \left(\frac{\mu^2}{m_Q^2}\right)^{2\epsilon} \frac{\Gamma^3(1-\epsilon)\Gamma(2\epsilon-1)}{\Gamma(3-3\epsilon)(-4-i\varepsilon)^{2\epsilon}}\,, \tag{D.9}$$

$$\begin{aligned} I_9^{(2)} &= V_E(0,1,1,1,0,1,0) \\ &= \left(\frac{\mu^2}{m_Q^2}e^{-\gamma_E}\right)^{2\epsilon} \left\{\frac{1}{2\epsilon^2} + \frac{5}{2\epsilon} + \frac{19}{2} + \frac{5}{12}\pi^2 - 4\ln 2 + i2\pi \right. \\ &\quad \left. + \left(\frac{65}{2} - \frac{11}{12}\pi^2 + \frac{11}{3}\zeta_3 - 28\ln 2 + 8\ln^2 2 + i\pi\left(14 - 8\ln 2\right)\right)\epsilon + \mathcal{O}\left(\epsilon^2\right)\right\}\,, \end{aligned} \tag{D.10}$$

$$\begin{aligned} I_{10}^{(2)} &= V_E(0,1,0,1,1,1,0) \\ &= \left(\frac{\mu^2}{m_Q^2}e^{-\gamma_E}\right)^{2\epsilon} \left\{\frac{1}{2\epsilon^2} + \left(\frac{5}{2} - 2\ln 2 + i\pi\right)\frac{1}{\epsilon} - 4.819(6) + 4.118(8)\,i \right. \\ &\quad \left. + \mathcal{O}\left(\epsilon\right)\right\}, \end{aligned} \tag{D.11}$$

$$\begin{aligned} I_{11}^{(2)} &= V_E(0,2,0,1,1,1,0) \\ &= -\frac{1}{m_Q^2}\left(\frac{\mu^2}{m_Q^2}e^{-\gamma_E}\right)^{2\epsilon} \left\{0.339(2) + 2.177(2)\,i + \mathcal{O}\left(\epsilon\right)\right\}\,, \end{aligned} \tag{D.12}$$

$$I_{12}^{(2)} = V_E(0,3,0,1,1,1,0) = \frac{1}{m_Q^4}\left(\frac{\mu^2}{m_Q^2}e^{-\gamma_E}\right)^{2\epsilon} \left\{-\frac{1}{2}\ln 2 + i\frac{1}{4}\pi + \mathcal{O}\left(\epsilon\right)\right\}\,, \tag{D.13}$$

$$\begin{aligned} I_{13}^{(2)} &= V_F(1,1,1,0,1,0,0) \\ &= \left(\frac{\mu^2}{m_Q^2}e^{-\gamma_E}\right)^{2\epsilon} \left\{\left(\ln 2 - i\frac{1}{2}\pi\right)\frac{1}{\epsilon} + \frac{1}{3}\pi^2 + 3\ln 2 - \ln^2 2 - i\pi\left(\frac{3}{2} - \ln 2\right) \right. \\ &\quad + \left(\pi^2 - \frac{1}{2}\pi^2\ln 2 + \zeta_3 + 7\ln 2 - 3\ln^2 2 + \frac{2}{3}\ln^3 2 \right. \\ &\quad \left. \left. -i\pi\left(\frac{7}{2} - \frac{1}{12}\pi^2 - 3\ln 2 + \ln^2 2\right)\right)\epsilon + \mathcal{O}\left(\epsilon^2\right)\right\}\,, \end{aligned} \tag{D.14}$$

$$
\begin{aligned}
I_{14}^{(2)} &= V_F(0,1,1,1,0,1,0) = L_-^{(2)}(1,0,1,1,1) \\
&= \left(\frac{\mu^2}{m_Q^2}e^{-\gamma_E}\right)^{2\epsilon}\left\{\frac{1}{2\epsilon^2}+\frac{5}{2\epsilon}+\frac{19}{2}-\frac{5}{12}\pi^2+\left(\frac{65}{2}+\frac{7}{12}\pi^2-\pi^2\ln 2-\frac{65}{6}\zeta_3\right)\epsilon\right. \\
&\quad +\left(\frac{211}{2}+\frac{43}{4}\pi^2-5\pi^2\ln 2-2\ln^2 2\pi^2+\frac{11}{6}\zeta_3-\frac{1097}{720}\pi^4+\ln^4 2+24a_4\right)\epsilon^2 \\
&\quad \left.+\mathcal{O}\left(\epsilon^3\right)\right\}, \qquad \text{(D.15)}
\end{aligned}
$$

$$
\begin{aligned}
I_{15}^{(2)} &= V_F(0,1,0,1,1,1,0) = \frac{1}{2}\left(L_+^{(2)}(0,1,1,1,1)+L_-^{(2)}(0,1,1,1,1)\right) \\
&= \left(\frac{\mu^2}{m_Q^2}e^{-\gamma_E}\right)^{2\epsilon}\left\{\frac{1}{2\epsilon^2}+\frac{5}{2\epsilon}+\frac{19}{2}-\frac{7}{12}\pi^2+\left(\frac{65}{2}-\frac{35}{12}\pi^2+4\pi^2\ln 2-\frac{43}{3}\zeta_3\right)\epsilon\right. \\
&\quad +\left(\frac{211}{2}-\frac{133}{12}\pi^2+20\pi^2\ln 2-8\pi^2\ln^2 2-\frac{215}{3}\zeta_3+\frac{47}{80}\pi^4-4\ln^4 2\right. \\
&\quad \left.\left.-96a_4\right)\epsilon^2+\mathcal{O}\left(\epsilon^3\right)\right\}, \qquad \text{(D.16)}
\end{aligned}
$$

$$
\begin{aligned}
I_{16}^{(2)} &= V_F(1,0,1,1,1,1,0) \\
&= \frac{1}{m_Q^2}\left(\frac{\mu^2}{m_Q^2}e^{-\gamma_E}\right)^{2\epsilon}\left\{-\frac{1}{2}\pi^2\ln 2+\frac{21}{8}\zeta_3-i\frac{1}{8}\pi^3+\mathcal{O}\left(\epsilon\right)\right\}, \qquad \text{(D.17)}
\end{aligned}
$$

$$
\begin{aligned}
I_{17}^{(2)} &= V_F(1,1,1,1,1,1,0) \\
&= -\frac{1}{m_Q^4}\left(\frac{\mu^2}{m_Q^2}e^{-\gamma_E}\right)^{2\epsilon}\left\{\frac{1}{4}\pi^2\ln 2+\frac{21}{16}\zeta_3-i\frac{1}{16}\pi^3+\mathcal{O}\left(\epsilon\right)\right\}, \qquad \text{(D.18)}
\end{aligned}
$$

where the $i\varepsilon$ stems from the usual Feynman prescription. $I_5^{(2)}$–$I_7^{(2)}$ and $I_{13}^{(2)}$ are products of one-loop integrals and are thus quite easy to calculate. $I_8^{(2)}$ and $I_9^{(2)}$ are recursively one-loop, i.e. the two-loop integral can be calculated by the successive evaluation of two one-loop integrals. For $I_7^{(2)}$, $I_9^{(2)}$ and $I_{13}^{(2)}$ we used a one-fold Mellin-Barnes representation for the triangle integral, which could be solved analytically. For $I_{10}^{(2)}$–$I_{12}^{(2)}$ we found a two-fold Mellin-Barnes representation. $I_{14}^{(2)}$ and $I_{15}^{(2)}$ belong to the $L_\pm^{(2)}$-integrals and can thus be reduced further. In the latter case, we used partial fractioning to make this reduction possible. $I_{16}^{(2)}$ can be determined from the result given in Ref. [143].

The errors of the numerical values in Eqs. (D.11) and (D.11) correspond to twice

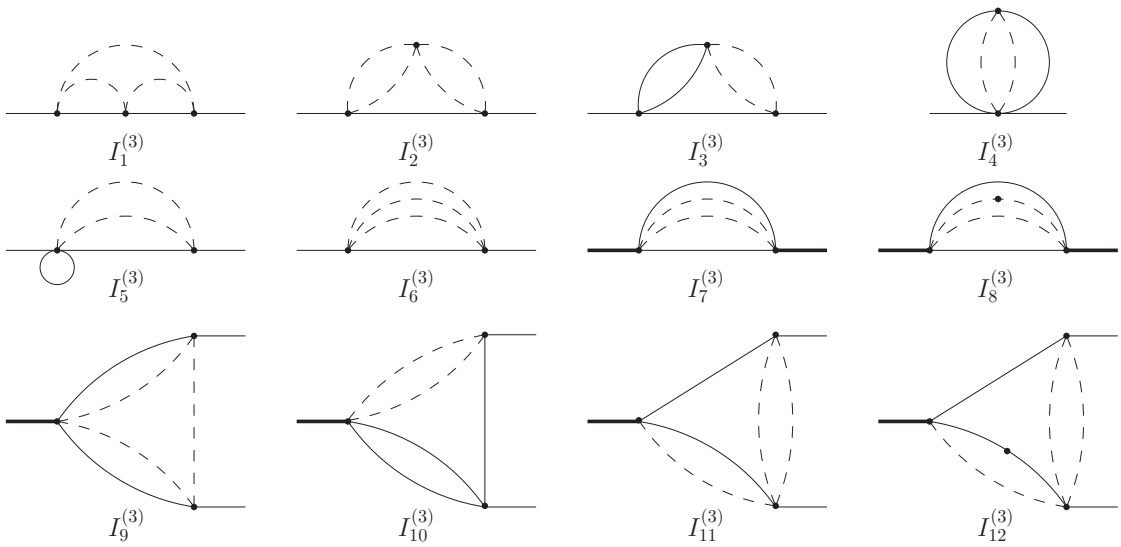


Figure D.4: Three-loop master integrals for fermionic non-singlet contribution. The same coding as in Fig. D.2 is adopted. A dot on a line denotes a squared propagator.

the Vegas error given by `MB`. Note that we were able to find an analytical results for the singlet contributions even though we only have numerical results for the $\mathcal{O}(\epsilon^0)$ terms of $I_{10}^{(2)}$ and $I_{11}^{(2)}$. This was possible since we found relations between some terms by requiring the results for the singlet contributions to be finite. We have checked that these relations hold for our numerical values.

If one uses the additional recurrence relations discussed in Section A.4, the number of master integrals is reduced by eight (four for each topology). The integrals which are no longer needed are $I_7^{(2)}$, $I_9^{(2)}$, $I_{11}^{(2)}$–$I_{15}^{(2)}$ and $I_{17}^{(2)}$.

## D.3 Three-loop integrals

The twelve master integrals needed for the three-loop fermionic non-singlet contribution are shown in Fig. D.4. They read

$$\begin{aligned} I_1^{(3)} &= J_+^{(3)}(0,1,0,1,1,0,1,0,1) \\ &= m_Q^2 \left(\frac{\mu^2}{m_Q^2} e^{-\gamma_E}\right)^{3\epsilon} \left\{ \frac{1}{3\epsilon^3} + \frac{5}{3\epsilon^2} + \left(4 + \frac{3}{4}\pi^2\right)\frac{1}{\epsilon} - \frac{10}{3} + \frac{11}{4}\pi^2 + \frac{25}{3}\zeta_3 \right. \\ &\quad + \left(-\frac{302}{3} + 2\pi^2 + \frac{89}{3}\zeta_3 + \frac{3059}{1440}\pi^4\right)\epsilon + \left(-734 - \frac{69}{2}\pi^2 + 16\zeta_3 \right. \\ &\quad \left. \left. + \frac{9751}{1440}\pi^4 + \frac{107}{4}\pi^2\zeta_3 + \frac{2309}{5}\zeta_5\right)\epsilon^2 + \mathcal{O}\left(\epsilon^3\right) \right\}, \end{aligned} \tag{D.19}$$

$$
\begin{aligned}
I_2^{(3)} &= J_+^{(3)}(0,1,1,1,0,1,1,0,0) \\
&= -m_Q^2 \left(\frac{\mu^2}{m_Q^2}\right)^{3\epsilon} \frac{\Gamma^4(1-\epsilon)\Gamma^2(\epsilon)}{\Gamma^2(2-2\epsilon)} \frac{\Gamma(3\epsilon-1)\Gamma(3-6\epsilon)}{\Gamma(3-4\epsilon)}\,, \qquad \text{(D.20)}
\end{aligned}
$$

$$
\begin{aligned}
I_3^{(3)} &= L_+^{(3,n_l)}(0,0,1,1,1,1,0,1,0) \\
&= m_Q^2 \left(\frac{\mu^2}{m_Q^2} e^{-\gamma_E}\right)^{3\epsilon} \left\{ \frac{2}{3\epsilon^3} + \frac{10}{3\epsilon^2} + \left(\frac{26}{3} + \frac{1}{2}\pi^2\right)\frac{1}{\epsilon} + 2 + \frac{9}{2}\pi^2 + \frac{14}{3}\zeta_3 \right. \\
&\quad + \left(-\frac{398}{3} + \frac{53}{2}\pi^2 - 16\pi^2 \ln 2 + \frac{238}{3}\zeta_3 + \frac{287}{720}\pi^4\right)\epsilon + \left(-1038 + \frac{259}{2}\pi^2\right. \\
&\quad -160\pi^2 \ln 2 + \frac{128}{3}\pi^2 \ln^2 2 + \frac{1862}{3}\zeta_3 + \frac{323}{720}\pi^4 + \frac{7}{2}\pi^2\zeta_3 + \frac{478}{5}\zeta_5 \\
&\quad \left.\left. + \frac{64}{3}\ln^4 2 + 512 a_4\right)\epsilon^2 + \mathcal{O}\left(\epsilon^3\right) \right\}, \qquad \text{(D.21)}
\end{aligned}
$$

$$
\begin{aligned}
I_4^{(3)} &= J_+^{(3)}(0,0,0,1,1,0,1,0,1) \\
&= m_Q^4 \left(\frac{\mu^2}{m_Q^2}\right)^{3\epsilon} \frac{\Gamma^2(1-\epsilon)\Gamma(\epsilon)\Gamma^2(2\epsilon-1)\Gamma(3\epsilon-2)}{\Gamma(4\epsilon-2)\Gamma(2-\epsilon)}\,, \qquad \text{(D.22)}
\end{aligned}
$$

$$
\begin{aligned}
I_5^{(3)} &= J_+^{(3)}(0,1,0,1,0,0,1,0,1) \\
&= m_Q^4 \left(\frac{\mu^2}{m_Q^2}\right)^{3\epsilon} \Gamma(\epsilon-1) \frac{\Gamma^2(1-\epsilon)\Gamma(\epsilon)}{\Gamma(2-2\epsilon)} \frac{\Gamma(2\epsilon-1)\Gamma(3-4\epsilon)}{\Gamma(3-3\epsilon)}\,, \qquad \text{(D.23)}
\end{aligned}
$$

$$
\begin{aligned}
I_6^{(3)} &= J_+^{(3)}(0,0,1,1,1,0,1,0,0) \\
&= m_Q^4 \left(\frac{\mu^2}{m_Q^2}\right)^{3\epsilon} \frac{\Gamma^3(1-\epsilon)\Gamma(2\epsilon-1)\Gamma(3\epsilon-2)\Gamma(5-6\epsilon)}{\Gamma(3-3\epsilon)\Gamma(4-4\epsilon)}\,, \qquad \text{(D.24)}
\end{aligned}
$$

$$
\begin{aligned}
I_7^{(3)} &= J_-^{(3)}(0,0,0,1,1,0,1,0,1) \\
&= m_Q^4 \left(\frac{\mu^2}{m_Q^2} e^{-\gamma_E}\right)^{3\epsilon} \left\{ \frac{1}{3\epsilon^3} + \frac{1}{2\epsilon^2} + \left(-\frac{17}{36} + \frac{1}{12}\pi^2\right)\frac{1}{\epsilon} - 6.6827387(1) \right. \\
&\quad \left. - 56.300353(1)\epsilon - 209.48231(1)\epsilon^2 + \mathcal{O}\left(\epsilon^3\right) \right\}, \qquad \text{(D.25)}
\end{aligned}
$$

$$
\begin{aligned}
I_8^{(3)} &= J_-^{(3)}(0,0,0,2,1,0,1,0,1) \\
&= -m_Q^2 \left(\frac{\mu^2}{m_Q^2} e^{-\gamma_E}\right)^{3\epsilon} \left\{ \frac{1}{3\epsilon^3} + \frac{2}{3\epsilon^2} + \left(-\frac{8}{3} + \frac{5}{6}\pi^2\right) \frac{1}{\epsilon} + 10.797602(1) \right. \\
&\quad \left. + 62.250613(1)\epsilon + \mathcal{O}\left(\epsilon^2\right) \right\}, \qquad \text{(D.26)}
\end{aligned}
$$

$$
\begin{aligned}
I_9^{(3)} &= J_-^{(3)}(0,1,0,1,1,0,1,0,1) \\
&= m_Q^2 \left(\frac{\mu^2}{m_Q^2} e^{-\gamma_E}\right)^{3\epsilon} \left\{ \frac{1}{3\epsilon^3} + \frac{5}{3\epsilon^2} + \left(\frac{10}{3} + \frac{3}{4}\pi^2\right) \frac{1}{\epsilon} + 33.8328(4) \right. \\
&\quad \left. + 152.870(4)\epsilon + \mathcal{O}\left(\epsilon^2\right) \right\}, \qquad \text{(D.27)}
\end{aligned}
$$

$$
\begin{aligned}
I_{10}^{(3)} &= L_+^{(3,n_l)}(0,0,1,1,1,0,1,1,0) \\
&= m_Q^2 \left(\frac{\mu^2}{m_Q^2} e^{-\gamma_E}\right)^{3\epsilon} \left\{ \frac{2}{3\epsilon^3} + \frac{10}{3\epsilon^2} + \left(8 + \frac{1}{2}\pi^2\right) \frac{1}{\epsilon} + 52.5698(4) + 145.087(4)\epsilon \right. \\
&\quad \left. + 562.250(14)\epsilon^2 + \mathcal{O}\left(\epsilon^3\right) \right\}, \qquad \text{(D.28)}
\end{aligned}
$$

$$
\begin{aligned}
I_{11}^{(3)} &= J_-^{(3)}(0,1,0,1,0,1,1,0,1) \\
&= m_Q^2 \left(\frac{\mu^2}{m_Q^2} e^{-\gamma_E}\right)^{3\epsilon} \left\{ \frac{1}{2\epsilon^3} + \frac{11}{6\epsilon^2} + \left(-\frac{1}{6} + \frac{29}{24}\pi^2\right) \frac{1}{\epsilon} + 34.791(4) \right. \\
&\quad \left. + 154.08(2)\epsilon + \mathcal{O}\left(\epsilon^2\right) \right\}, \qquad \text{(D.29)}
\end{aligned}
$$

$$
\begin{aligned}
I_{12}^{(3)} &= J_-^{(3)}(0,1,0,1,0,1,1,0,2) \\
&= \left(\frac{\mu^2}{m_Q^2} e^{-\gamma_E}\right)^{3\epsilon} \left\{ \frac{1}{6\epsilon^3} + \frac{1}{2\epsilon^2} + \left(\frac{1}{6} + \frac{7}{24}\pi^2\right) \frac{1}{\epsilon} + 7.024(4) + 32.04(2)\epsilon \right. \\
&\quad \left. + \mathcal{O}\left(\epsilon^2\right) \right\}. \qquad \text{(D.30)}
\end{aligned}
$$

$I_2^{(3)}, I_4^{(3)}, I_5^{(3)}$ and $I_6^{(3)}$ can be evaluated to all orders in $\epsilon$ and for arbitrary complex powers of the propagators with the help of Feynman parameters. $I_1^{(3)}$ was calculated in Ref. [11]. We have repeated the calculation described in the reference with the program `XSummer` [144] and find complete agreement. The results for $I_3^{(3)}$–$I_6^{(3)}$ can

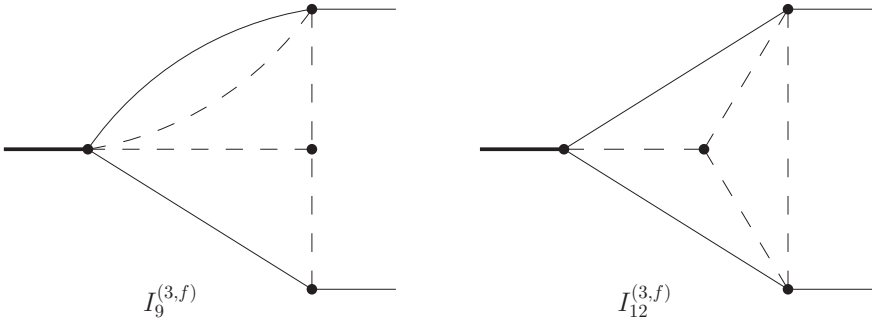


Figure D.5: $\epsilon$-finite master integrals. The same coding as in Fig. D.2 is adopted.

be found in Ref. [67]. We have checked the result for $I_3^{(3)}$ numerically with the help of a one-fold Mellin-Barnes representation and find complete agreement.

The master integrals $I_7^{(3)}$–$I_{12}^{(3)}$ have been evaluated with the help of the Mellin-Barnes method where the evaluation of the integrals has been performed with the program `MB`. $I_7^{(3)}$ and $I_8^{(3)}$ can be expressed in terms of a one-fold Mellin-Barnes representation and are thus known with a quite high precision. On the other hand, $I_{10}^{(3)}$ is represented by a two-fold and $I_9^{(3)}$, $I_{11}^{(3)}$ and $I_{12}^{(3)}$ even by a three-fold integration which results in less accurate results. The quoted uncertainties in the above equations correspond to twice the Vegas error given by `MB` for the multi-dimensional integrals and to a conservative estimate in case of the one-dimensional integrals $I_7^{(3)}$ and $I_8^{(3)}$. The pole part of $I_7^{(3)}$ agrees with the result of Ref. [145].

From Eqs. (D.19)–(D.30), one can see that we have to expand some of the master integrals to high orders in $\epsilon$. The reason for this are so-called spurious poles in the coefficient functions of these master integrals. Since the higher orders in $\epsilon$ are more complicated to calculate and are thus known with less precision, it is useful to switch to a so-called $\epsilon$-finite basis of master integrals [134].

Since $I_1^{(3)}$–$I_6^{(3)}$ are known analytically, a replacement is, of course, not necessary. Furthermore, for $I_7^{(3)}$ and $I_8^{(3)}$ the numerical precision is sufficient for our calculation. As far as the remaining four integrals are concerned, we found it convenient to replace $I_9^{(3)}$ and $I_{12}^{(3)}$ by the integrals shown in Fig. D.5. Their numerical evaluation with the help of `MB` is straightforward leading to the results

$$\begin{aligned} I_9^{(3,f)} &= J_-^{(3)}(0,1,1,1,1,0,1,0,1) \\ &= \left(\frac{\mu^2}{m_Q^2}e^{-\gamma_E}\right)^{3\epsilon}\left\{\frac{1}{6\epsilon^3}+\frac{3}{2\epsilon^2}+\left(\frac{55}{6}+\frac{3}{8}\pi^2\right)\frac{1}{\epsilon}+64.678(8)+\mathcal{O}\left(\epsilon\right)\right\}, \end{aligned} \tag{D.31}$$

$$I_{12}^{(3,f)} = J_-^{(3)}(0,1,0,1,1,1,1,0,1) = \left(\frac{\mu^2}{m_Q^2}e^{-\gamma_E}\right)^{3\epsilon}\left\{2\zeta_3\frac{1}{\epsilon}+8.1(2)+\mathcal{O}\left(\epsilon\right)\right\}. \tag{D.32}$$

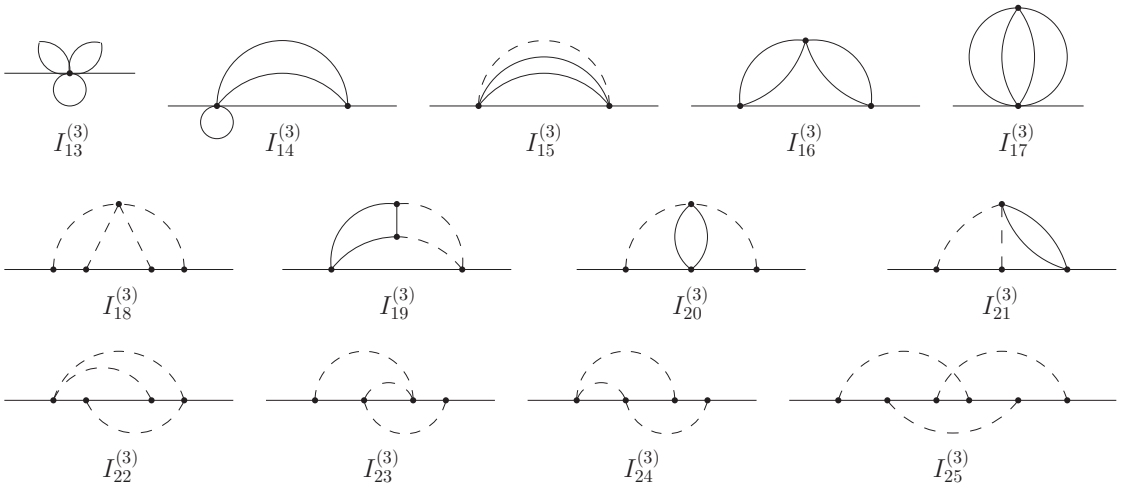


Figure D.6: Additional three-loop master integrals for quark self-energy integrals. The same coding as in Fig. D.2 is adopted.

Apart from integrals $I_1^{(3)}$–$I_6^{(3)}$, we need 13 more master integrals for the full calculation of the renormalisation constants. These are depicted in Fig. D.6. Their results are

$$I_{13}^{(3)} = J_+^{(3)}(0,0,0,0,0,0,1,1,1) = -m_Q^6 \left(\frac{\mu^2}{m_Q^2}\right)^{3\epsilon} \Gamma^3(\epsilon-1) \,, \tag{D.33}$$

$$\begin{aligned} I_{14}^{(3)} &= K_2(0,0,0,1,1,1,1,0,0) \\ &= m_Q^4 \left(\frac{\mu^2}{m_Q^2} e^{-\gamma_E}\right)^{3\epsilon} \left\{ \frac{3}{2\epsilon^3} + \frac{23}{4\epsilon^2} + \left(\frac{105}{8} + \frac{3}{8}\pi^2\right)\frac{1}{\epsilon} + \frac{275}{16} + \frac{133}{48}\pi^2 - \frac{3}{2}\zeta_3 \right. \\ &\quad + \left(-\frac{567}{32} + \frac{425}{32}\pi^2 - 8\pi^2\ln 2 + \frac{89}{4}\zeta_3 + \frac{19}{320}\pi^4\right)\epsilon \\ &\quad + \left(-\frac{14917}{64} + \frac{10105}{192}\pi^2 - 60\pi^2\ln 2 + 16\pi^2\ln^2 2 + \frac{1575}{8}\zeta_3 - \frac{941}{1152}\pi^4 \right. \\ &\quad \left. \left. -\frac{3}{8}\pi^2\zeta_3 - \frac{9}{10}\zeta_5 + 8\ln^4 2 + 192 a_4\right)\epsilon^2 + \mathcal{O}\left(\epsilon^3\right) \right\} \,, \end{aligned} \tag{D.34}$$

$$
\begin{aligned}
I_{15}^{(3)} &= K_1(0,0,0,1,1,1,0,1,0) \\
&= m_Q^4 \left(\frac{\mu^2}{m_Q^2} e^{-\gamma_E}\right)^{3\epsilon} \left\{ \frac{1}{\epsilon^3} + \frac{7}{2\epsilon^2} + \left(\frac{253}{36} + \frac{1}{4}\pi^2\right)\frac{1}{\epsilon} + \frac{2501}{216} + \frac{7}{8}\pi^2 - \zeta_3 \right. \\
&\quad + \left(\frac{59437}{1296} - \frac{257}{48}\pi^2 - \frac{7}{2}\zeta_3 + \frac{19}{480}\pi^4\right)\epsilon + \left(\frac{2831381}{7776} - \frac{23401}{288}\pi^2 \right. \\
&\quad \left. + \frac{256}{3}\pi^2 \ln 2 - \frac{7421}{36}\zeta_3 - \frac{1}{4}\pi^2\zeta_3 + \frac{133}{960}\pi^4 - \frac{3}{5}\zeta_5\right)\epsilon^2 \\
&\quad + \left(\frac{117529021}{46656} - \frac{1043441}{1728}\pi^2 + \frac{9088}{9}\pi^2 \ln 2 - \frac{3584}{9}\pi^2 \ln^2 2 - \frac{511429}{216}\zeta_3 \right. \\
&\quad + \frac{108781}{5760}\pi^4 - \frac{7}{8}\pi^2\zeta_3 - \frac{21}{10}\zeta_5 + \frac{1}{2}\zeta_3^2 + \frac{631}{120960}\pi^6 - \frac{1024}{9}\ln^4 2 \\
&\quad \left. \left. - \frac{8192}{3}a_4\right)\epsilon^3 + \mathcal{O}\left(\epsilon^4\right)\right\} , \qquad \text{(D.35)}
\end{aligned}
$$

$$
\begin{aligned}
I_{16}^{(3)} &= K_2(0,0,0,1,1,1,1,1,0) \\
&= m_Q^2 \left(\frac{\mu^2}{m_Q^2} e^{-\gamma_E}\right)^{3\epsilon} \left\{ \frac{1}{\epsilon^3} + \frac{16}{3\epsilon^2} + \left(16 + \frac{1}{4}\pi^2\right)\frac{1}{\epsilon} + 20 + 4\pi^2 - 3\zeta_3 \right. \\
&\quad + \left(-\frac{364}{3} + 32\pi^2 - 16\pi^2 \ln 2 + \frac{184}{3}\zeta_3 + \frac{163}{480}\pi^4\right)\epsilon \\
&\quad + \left(-1244 + 193\pi^2 - 168\pi^2 \ln 2 + \frac{80}{3}\pi^2 \ln^2 2 + 760\zeta_3 - \frac{197}{90}\pi^4 \right. \\
&\quad \left. \left. - \frac{87}{4}\pi^2\zeta_3 + \frac{627}{5}\zeta_5 + \frac{64}{3}\ln^4 2 + 512a_4\right)\epsilon^2 + \mathcal{O}\left(\epsilon^3\right)\right\} , \qquad \text{(D.36)}
\end{aligned}
$$

$$
\begin{aligned}
I_{17}^{(3)} &= K_2(0,0,0,0,1,1,1,1,0) \\
&= m_Q^4 \left(\frac{\mu^2}{m_Q^2} e^{-\gamma_E}\right)^{3\epsilon} \left\{ \frac{2}{\epsilon^3} + \frac{23}{3\epsilon^2} + \left(\frac{35}{2} + \frac{1}{2}\pi^2\right)\frac{1}{\epsilon} + \frac{275}{12} + \frac{23}{12}\pi^2 - 2\zeta_3 \right. \\
&\quad + \left(-\frac{189}{8} + \frac{35}{8}\pi^2 + \frac{89}{3}\zeta_3 + \frac{19}{240}\pi^4\right)\epsilon + \left(-\frac{14917}{48} + \frac{275}{48}\pi^2 - \frac{32}{3}\pi^2 \ln^2 2 \right. \\
&\quad \left. \left. + \frac{525}{2}\zeta_3 - \frac{87}{32}\pi^4 - \frac{1}{2}\pi^2\zeta_3 - \frac{6}{5}\zeta_5 + \frac{32}{3}\ln^4 2 + 256a_4\right)\epsilon^2 + \mathcal{O}\left(\epsilon^3\right)\right\} , \qquad \text{(D.37)}
\end{aligned}
$$

$$
I_{18}^{(3)} = J_+^{(3)}(0,1,1,1,0,1,1,1,1) = \frac{1}{m_Q^2}\left(\frac{\mu^2}{m_Q^2} e^{-\gamma_E}\right)^{3\epsilon} \left\{-2\pi^2\zeta_3 + 5\zeta_5 + \mathcal{O}\left(\epsilon\right)\right\} , \qquad \text{(D.38)}
$$

$$
\begin{aligned}
I_{19}^{(3)} &= K_2(1,0,0,1,0,1,1,1,1) \\
&= \left(\frac{\mu^2}{m_Q^2}e^{-\gamma_E}\right)^{3\epsilon}\left\{2\zeta_3\frac{1}{\epsilon}-\frac{1}{3}\pi^2+10\zeta_3-\frac{13}{90}\pi^4+\left(-\frac{4}{3}\pi^2+4\pi^2\ln 2\right.\right. \\
&\quad \left.\left.+24\zeta_3-\frac{13}{18}\pi^4+\frac{26}{3}\pi^2\zeta_3-\frac{85}{2}\zeta_5\right)\epsilon+\mathcal{O}\left(\epsilon^2\right)\right\}, \qquad \text{(D.39)}
\end{aligned}
$$

$$
\begin{aligned}
I_{20}^{(3)} &= K_2(1,0,1,0,1,1,1,1,0) \\
&= \left(\frac{\mu^2}{m_Q^2}e^{-\gamma_E}\right)^{3\epsilon}\left\{\frac{1}{3\epsilon^3}+\frac{7}{3\epsilon^2}+\left(\frac{31}{3}+\frac{1}{12}\pi^2\right)\frac{1}{\epsilon}+\frac{103}{3}+\frac{7}{12}\pi^2-\frac{5}{3}\zeta_3-\frac{2}{15}\pi^4\right. \\
&\quad \left.+\left(\frac{235}{3}+\frac{21}{4}\pi^2+\frac{25}{3}\zeta_3-\frac{169}{288}\pi^4+\frac{28}{3}\pi^2\zeta_3-78\zeta_5\right)\epsilon+\mathcal{O}\left(\epsilon^2\right)\right\}, \qquad \text{(D.40)}
\end{aligned}
$$

$$
\begin{aligned}
I_{21}^{(3)} &= K_2(1,0,0,1,1,1,1,0,1) \\
&= \left(\frac{\mu^2}{m_Q^2}e^{-\gamma_E}\right)^{3\epsilon}\left\{\frac{1}{6\epsilon^3}+\frac{3}{2\epsilon^2}+\left(\frac{55}{6}-\frac{7}{24}\pi^2\right)\frac{1}{\epsilon}+\frac{95}{2}-\frac{47}{24}\pi^2-\frac{29}{6}\zeta_3-\frac{4}{45}\pi^4\right. \\
&\quad +\left(\frac{1351}{6}-\frac{193}{24}\pi^2+4\pi^2\ln 2-\frac{87}{2}\zeta_3-\frac{2429}{2880}\pi^4+\frac{25}{6}\pi^2\zeta_3-\frac{49}{2}\zeta_5\right)\epsilon \\
&\quad \left.+\mathcal{O}\left(\epsilon^2\right)\right\}, \qquad \text{(D.41)}
\end{aligned}
$$

$$
\begin{aligned}
I_{22}^{(3)} &= K_2(1,1,1,1,0,0,1,1,0) \\
&= \left(\frac{\mu^2}{m_Q^2}e^{-\gamma_E}\right)^{3\epsilon}\left\{2\zeta_3\frac{1}{\epsilon}+\frac{1}{3}\pi^2+2\zeta_3-\frac{7}{90}\pi^4\right. \\
&\quad \left.+\left(\frac{14}{3}\pi^2-12\zeta_3-\frac{41}{90}\pi^4-\frac{1}{6}\pi^2\zeta_3+44\zeta_5\right)\epsilon+\mathcal{O}\left(\epsilon^2\right)\right\}, \qquad \text{(D.42)}
\end{aligned}
$$

$$
\begin{aligned}
I_{23}^{(3)} &= K_2(1,1,1,1,1,1,0,0,0) \\
&= \left(\frac{\mu^2}{m_Q^2}e^{-\gamma_E}\right)^{3\epsilon}\left\{\frac{1}{3\epsilon^3}+\frac{7}{3\epsilon^2}+\left(\frac{31}{3}+\frac{1}{12}\pi^2\right)\frac{1}{\epsilon}+\frac{103}{3}+\frac{11}{12}\pi^2+\frac{1}{3}\zeta_3-\frac{4}{45}\pi^4\right. \\
&\quad \left.+\left(\frac{235}{3}+\frac{79}{12}\pi^2+\frac{13}{3}\zeta_3-\frac{413}{1440}\pi^4+\frac{2}{3}\pi^2\zeta_3-2\zeta_5\right)\epsilon+\mathcal{O}\left(\epsilon^2\right)\right\}, \qquad \text{(D.43)}
\end{aligned}
$$

$$
\begin{aligned}
I_{24}^{(3)} &= K_2(1,1,1,0,1,0,1,1,0) \\
&= \left(\frac{\mu^2}{m_Q^2}e^{-\gamma_E}\right)^{3\epsilon}\left\{\frac{1}{6\epsilon^3}+\frac{3}{2\epsilon^2}+\left(\frac{55}{6}-\frac{7}{24}\pi^2\right)\frac{1}{\epsilon}+\frac{95}{2}-\frac{13}{8}\pi^2-\frac{17}{6}\zeta_3-\frac{1}{15}\pi^4\right. \\
&\quad \left.+\left(\frac{1351}{6}-\frac{27}{8}\pi^2-\frac{31}{2}\zeta_3-\frac{3229}{2880}\pi^4+6\pi^2\zeta_3-64\zeta_5\right)\epsilon+\mathcal{O}\left(\epsilon^2\right)\right\}, \quad \text{(D.44)}
\end{aligned}
$$

$$
I_{25}^{(3)} = K_2(1,1,1,1,1,1,1,1,0) = \frac{1}{m_Q^4}\left(\frac{\mu^2}{m_Q^2}e^{-\gamma_E}\right)^{3\epsilon}\left\{4\pi^2\ln^2 2-\frac{1}{6}\pi^4+\mathcal{O}\left(\epsilon\right)\right\}. \quad \text{(D.45)}
$$

It turns out that it is useful to choose an integral with an additional scalar product instead of $I_{25}^{(3)}$. This was done in Ref. [11] as well. In our notation this integral is given as

$$
\begin{aligned}
I_{25}^{(3,sp)} &= \left(\frac{\mu^2}{i\pi^{d/2}}\right)^3\int\frac{\mathrm{d}^dk\,\mathrm{d}^dl\,\mathrm{d}^dp}{k^2\,l^2\,p^2\left((k+l+p)^2+2q\cdot(k+l+p)\right)(k^2+2q\cdot k)} \\
&\quad\times\frac{(q\cdot l)}{(p^2+2q\cdot p)\left((k+l)^2+2q\cdot(k+l)\right)\left((l+p)^2+2q\cdot(l+p)\right)}. \quad \text{(D.46)}
\end{aligned}
$$

If this replacement is not done, the integrals $I_3^{(3)}$, $I_{15}^{(3)}$ and $I_{25}^{(3)}$ would have to be calculated to one order higher in $\epsilon$ than the results given above. The result for the additional integral is [67]

$$
I_{25}^{(3,sp)} = \frac{1}{m_Q^2}\left(\frac{\mu^2}{m_Q^2}e^{-\gamma_E}\right)^{3\epsilon}\left\{-\frac{1}{2}\pi^2\zeta_3+5\zeta_5+\mathcal{O}\left(\epsilon\right)\right\}. \quad \text{(D.47)}
$$

The analytical results for the above integrals were taken from Ref. [11] (and Ref. [146] in the case of $I_{25}^{(3)}$). We have checked the results numerically with the help of the program `MB`. However, we did find some differences. Integral $I_2^{(3)}$ does not appear in Ref. [11], although it is also needed for the calculation of the renormalisation constants. Furthermore, the result for $I_6^{(3)}$ in Ref. [11] is wrong, while the correct result can be found in Ref. [67]. As it turns out, the result given in the former reference corresponds to $J_+^{(3)}(0,1,1,1,1,0,1,0,0)$. Since there is a one-to-one correspondence between the two integrals and they are both easy to evaluate, it actually does not matter which is chosen to be the master integral.

Most of the master integrals of Ref. [11] were already calculated in Ref. [67]. However, it turns out that there are differences in the $\mathcal{O}\left(\epsilon\right)$ terms of integrals $I_{19}^{(3)}$–$I_{24}^{(3)}$. We have checked numerically that the results of Ref. [11] are correct.

# Appendix E

# Additional Formulae

### $\rho_1$ of Section 1.2.4

A crucial ingredient for our numerical analysis in Section 1.2.4 is the wave function at the origin. Currently the second order is known completely [34, 75–78] and at order $\alpha_s^3$ the quadratically [147, 148] and linearly [41, 73] enhanced logarithms and the corrections proportional to $\beta_0^3$ [45, 46] are available.

The quantity $\rho_1$ needed in Section 1.2.4 is given by

$$\begin{aligned}
\rho_1 &= 1 + \frac{\alpha_s(\mu_s)}{\pi}\left[\left(4-\frac{2}{3}\pi^2\right)\beta_0 + \frac{3}{4}a_1\right] \\
&\quad + \left(\frac{\alpha_s(\mu_s)}{\pi}\right)^2\left\{\left[-C_AC_F + \left(-2+\frac{2}{3}S(S+1)\right)C_F^2\right]\pi^2\ln(C_F\alpha_s(\mu_s))\right. \\
&\quad + \left(-\frac{5}{3}\pi^2 + 20\zeta(3) + \frac{1}{9}\pi^4\right)\beta_0^2 + \left(4-\frac{2}{3}\pi^2\right)\beta_1 + \left(\frac{5}{2}-\frac{2}{3}\pi^2\right)\beta_0 a_1 \\
&\quad \left. + \frac{3}{16}a_1^2 + \frac{3}{16}a_2 + \frac{9}{4}\pi^2 C_AC_F + \left(\frac{33}{8}-\frac{13}{9}S(S+1)\right)\pi^2C_F^2\right\} \\
&\quad + \left(\frac{\alpha_s(\mu_s)}{\pi}\right)^3\left\{\pi^2\mathcal{C}_2\ln^2\left(C_F\alpha_s(\mu_s)\right) + \pi^2\mathcal{C}_1\ln\left(C_F\alpha_s(\mu_s)\right) + \mathcal{C}_0^{\beta_0^3} + \ldots\right\},
\end{aligned} \tag{E.1}$$

with

$$\begin{aligned}
\mathcal{C}_2 &= \left(-2C_AC_F + \left(-4+\frac{4}{3}S(S+1)\right)C_F^2\right)\beta_0 - \frac{2}{3}C_A^2C_F \\
&\quad + \left(-\frac{41}{12}+\frac{7}{12}S(S+1)\right)C_AC_F^2 - \frac{3}{2}C_F^3\,,
\end{aligned} \tag{E.2}$$

$$
\begin{aligned}
\mathcal{C}_1 &= \left[\left(-3+\frac{2}{3}\pi^2\right)C_AC_F+\left(\frac{4}{3}\pi^2-\left(\frac{10}{9}+\frac{4}{9}\pi^2\right)S(S+1)\right)C_F^2\right]\beta_0 \\
&\quad+\left[-\frac{3}{4}C_AC_F+\left(-\frac{9}{4}+\frac{2}{3}S(S+1)\right)C_F^2\right]a_1+\frac{1}{4}C_A^3+\left(\frac{59}{36}-4\ln 2\right)C_A^2C_F \\
&\quad+\left(\frac{143}{36}-4\ln 2-\frac{19}{108}S(S+1)\right)C_AC_F^2+\left(-\frac{35}{18}+8\ln 2-\frac{1}{3}S(S+1)\right)C_F^3 \\
&\quad+\left(-\frac{32}{15}+2\ln 2+(1-\ln 2)\,S(S+1)\right)C_F^2T+\frac{49}{36}C_AC_FTn_l \\
&\quad+\left(\frac{8}{9}-\frac{10}{27}S(S+1)\right)C_F^2Tn_l \qquad \text{(E.3)}
\end{aligned}
$$

and

$$
\begin{aligned}
\mathcal{C}_0^{\beta_0^3} &= \\
&\beta_0^3\left[-20+\frac{22}{3}\pi^2+112\zeta(3)-\frac{7}{5}\pi^4-12\pi^2\zeta(3)-40\zeta(5)-16\zeta(3)^2+\frac{4}{105}\pi^6\right], \qquad \text{(E.4)}
\end{aligned}
$$

where $\mu_s = C_F m_q \alpha_s(\mu_s)$ is the soft scale. It is straightforward to obtain the result for general $\alpha_s(\mu)$ using standard renormalisation group analyses. In Eqs. (E.1)–(E.3) $S$ is the spin quantum number which is equal to one in our applications. The ellipses in Eq. (E.1) represent yet unknown corrections like, e.g., the pure ultrasoft contributions.

The one- and two-loop coefficients of the static potential are given by [149, 150]

$$
\begin{aligned}
a_1 &= \frac{31}{9}C_A-\frac{20}{9}T_Fn_l\,, \\
a_2 &= \left(\frac{4343}{162}+4\pi^2+\frac{22}{3}\zeta(3)-\frac{1}{4}\pi^4\right)C_A^2-\left(\frac{1798}{81}+\frac{56}{3}\zeta(3)\right)C_AT_Fn_l \\
&\quad-\left(\frac{55}{3}-16\zeta(3)\right)C_FT_Fn_l+\left(\frac{20}{9}T_Fn_l\right)^2. \qquad \text{(E.5)}
\end{aligned}
$$

### QCD $\beta$ function

The first three coefficients of the $\beta$ function read [151, 152]

$$\begin{aligned}
\beta_0 &= \frac{1}{4}\left(\frac{11}{3}C_A - \frac{4}{3}T_F n_f\right), \\
\beta_1 &= \frac{1}{16}\left(\frac{34}{3}C_A^2 - \frac{20}{3}C_A T_F n_f - 4C_F T_F n_f\right), \\
\beta_2 &= \frac{1}{64}\Bigg(\frac{2857}{54}C_A^3 - \frac{1415}{27}C_A^2 T_F n_f - \frac{205}{9}C_A C_F T_F n_f + 2\,C_F^2 T_F n_f \\
&\qquad + \frac{158}{27}C_A T_F^2 n_f^2 + \frac{44}{9}C_F T_F^2 n_f^2\Bigg).
\end{aligned} \tag{E.6}$$

### $Z_m^{\overline{\rm DR}}$ of Section 2.2.2

$Z_m^{\overline{\rm DR}}$ has been computed in Ref. [102] to three and in Ref. [98] even to four-loop order, where it is given in terms of the corresponding anomalous dimension. It is convenient to decompose $Z_m^{\overline{\rm DR}}$ in terms of the different loop contributions as

$$Z_m^{\overline{\rm DR}} = 1 + \left(\frac{e^{\gamma_E}}{4\pi}\right)^{-\epsilon}\delta\tilde{z}^{(1)} + \left(\frac{e^{\gamma_E}}{4\pi}\right)^{-2\epsilon}\delta\tilde{z}^{(2)} + \left(\frac{e^{\gamma_E}}{4\pi}\right)^{-3\epsilon}\delta\tilde{z}^{(3)} + \ldots, \tag{E.7}$$

where the ellipses denote terms of higher order in perturbation theory.

The individual contributions read

$$\delta\tilde{z}^{(1)} = -\frac{\alpha_s^{\overline{\rm DR}}}{\pi}C_F\frac{3}{4}\frac{1}{\epsilon}, \tag{E.8}$$

$$\begin{aligned}
\delta\tilde{z}^{(2)} &= \left(\frac{\alpha_s^{\overline{\rm DR}}}{\pi}\right)^2\left[\left(\frac{11}{32}C_A C_F + \frac{9}{32}C_F^2 - \frac{1}{8}C_F T_F n_f\right)\frac{1}{\epsilon^2}\right. \\
&\qquad \left. + \left(-\frac{91}{192}C_A C_F - \frac{3}{64}C_F^2 + \frac{5}{48}C_F T_F n_f\right)\frac{1}{\epsilon}\right] \\
&\quad + \frac{\alpha_s^{\overline{\rm DR}}}{\pi}\frac{\alpha_e}{\pi}C_F^2\frac{3}{16}\frac{1}{\epsilon} \\
&\quad + \left(\frac{\alpha_e}{\pi}\right)^2\left(\frac{1}{16}C_A C_F - \frac{1}{8}C_F^2 - \frac{1}{16}C_F T_F n_f\right)\frac{1}{\epsilon},
\end{aligned} \tag{E.9}$$

$$
\begin{aligned}
\delta\tilde{z}^{(3)} \;=\; & \left(\frac{\alpha_s^{\overline{\rm DR}}}{\pi}\right)^3 \left\{ \left( -\frac{121}{576}C_A^2C_F - \frac{33}{128}C_AC_F^2 - \frac{9}{128}C_F^3 + \frac{11}{72}C_AC_FT_Fn_f \right.\right. \\
& \left. + \frac{3}{32}C_F^2T_Fn_f - \frac{1}{36}C_FT_F^2n_f^2 \right)\frac{1}{\epsilon^3} + \left( \frac{1613}{3456}C_A^2C_F + \frac{295}{768}C_AC_F^2 + \frac{9}{256}C_F^3 \right. \\
& \left. - \frac{59}{216}C_AC_FT_Fn_f - \frac{29}{192}C_F^2T_Fn_f + \frac{5}{216}C_FT_F^2n_f^2 \right)\frac{1}{\epsilon^2} \\
& + \left[ -\frac{10255}{20736}C_A^2C_F + \frac{133}{768}C_AC_F^2 - \frac{43}{128}C_F^3 + \left( \frac{281}{2592} + \frac{1}{4}\zeta_3 \right) C_AC_FT_Fn_f \right. \\
& \left. \left. + \left( \frac{23}{96} - \frac{1}{4}\zeta_3 \right) C_F^2T_Fn_f + \frac{35}{1296}C_FT_F^2n_f^2 \right] \frac{1}{\epsilon} \right\} \\
& + \left(\frac{\alpha_s^{\overline{\rm DR}}}{\pi}\right)^2 \frac{\alpha_e}{\pi} \left[ \left( -\frac{11}{192}C_AC_F^2 - \frac{15}{64}C_F^3 + \frac{1}{48}C_F^2T_Fn_f \right) \frac{1}{\epsilon^2} \right. \\
& \left. + \left( \frac{5}{256}C_A^2C_F + \frac{7}{32}C_AC_F^2 + \frac{9}{64}C_F^3 - \frac{3}{32}C_F^2T_Fn_f \right) \frac{1}{\epsilon} \right] \\
& + \frac{\alpha_s^{\overline{\rm DR}}}{\pi} \left(\frac{\alpha_e}{\pi}\right)^2 \left[ \left( -\frac{9}{64}C_AC_F^2 + \frac{9}{32}C_F^3 + \frac{9}{64}C_F^2T_Fn_f \right) \frac{1}{\epsilon^2} \right. \\
& \left. + \left( -\frac{1}{64}C_A^2C_F + \frac{7}{32}C_AC_F^2 - \frac{3}{8}C_F^3 - \frac{1}{64}C_AC_FT_Fn_f - \frac{1}{8}C_F^2T_Fn_f \right) \frac{1}{\epsilon} \right] \\
& + \left(\frac{\alpha_e}{\pi}\right)^3 \left[ \left( -\frac{1}{48}C_A^2C_F + \frac{1}{12}C_AC_F^2 - \frac{1}{12}C_F^3 + \frac{1}{24}C_AC_FT_Fn_f \right.\right. \\
& \left. - \frac{1}{12}C_F^2T_Fn_f - \frac{1}{48}C_FT_F^2n_f^2 \right)\frac{1}{\epsilon^2} + \left( \frac{1}{32}C_A^2C_F - \frac{1}{8}C_AC_F^2 + \frac{1}{8}C_F^3 \right. \\
& \left. \left. - \frac{1}{24}C_AC_FT_Fn_f + \frac{5}{48}C_F^2T_Fn_f + \frac{1}{96}C_FT_F^2n_f^2 \right)\frac{1}{\epsilon} \right] \\
& - \frac{1}{8}\left(\frac{\alpha_e}{\pi}\right)^2 \frac{\eta_1}{\pi}\frac{1}{\epsilon} + \frac{5}{36}\left(\frac{\alpha_e}{\pi}\right)^2 \frac{\eta_2}{\pi}\frac{1}{\epsilon} + \frac{1}{12}\left(\frac{\alpha_e}{\pi}\right)^2 \frac{\eta_3}{\pi}\frac{1}{\epsilon} + \frac{3}{64}\frac{\alpha_e}{\pi}\left(\frac{\eta_1}{\pi}\right)^2 \frac{1}{\epsilon} \\
& - \frac{5}{12}\frac{\alpha_e}{\pi}\left(\frac{\eta_2}{\pi}\right)^2 \frac{1}{\epsilon} + \frac{7}{96}\frac{\alpha_e}{\pi}\left(\frac{\eta_3}{\pi}\right)^2 \frac{1}{\epsilon} - \frac{1}{16}\frac{\alpha_e}{\pi}\frac{\eta_1}{\pi}\frac{\eta_3}{\pi}\frac{1}{\epsilon}\,. \qquad \text{(E.10)}
\end{aligned}
$$

# Bibliography


[1] Tevatron Electroweak Working Group, arXiv:hep-ex/0703034.

[2] M. Martinez and R. Miquel, Eur. Phys. J. C **27** (2003) 49 [arXiv:hep-ph/0207315].

[3] A. H. Hoang *et al.*, Eur. Phys. J. directC **2** (2000) 1 [arXiv:hep-ph/0001286].

[4] A. H. Hoang, arXiv:hep-ph/0412160.

[5] A. Pineda and A. Signer, Nucl. Phys. B **762** (2007) 67 [arXiv:hep-ph/0607239].

[6] B. A. Kniehl, A. Onishchenko, J. H. Piclum and M. Steinhauser, Phys. Lett. B **638** (2006) 209 [arXiv:hep-ph/0604072].

[7] P. Marquard, J. H. Piclum, D. Seidel and M. Steinhauser, Nucl. Phys. B **758** (2006) 144 [arXiv:hep-ph/0607168].

[8] K. G. Chetyrkin and M. Steinhauser, Phys. Rev. Lett. **83** (1999) 4001 [arXiv:hep-ph/9907509].

[9] K. G. Chetyrkin and M. Steinhauser, Nucl. Phys. B **573** (2000) 617 [arXiv:hep-ph/9911434].

[10] K. Melnikov and T. van Ritbergen, Phys. Lett. B **482** (2000) 99 [arXiv:hep-ph/9912391].

[11] K. Melnikov and T. van Ritbergen, Nucl. Phys. B **591** (2000) 515 [arXiv:hep-ph/0005131].

[12] S. P. Martin and M. T. Vaughn, Phys. Lett. B **318** (1993) 331 [arXiv:hep-ph/9308222].

[13] L. V. Avdeev and M. Y. Kalmykov, Nucl. Phys. B **502** (1997) 419 [arXiv:hep-ph/9701308].

[14] P. Marquard, L. Mihaila, J. H. Piclum and M. Steinhauser, arXiv:hep-ph/0702185.

[15] B. Odom, D. Hanneke, B. D'Urso and G. Gabrielse Phys. Rev. Lett. **97** (2006) 030801.

[16] G. W. Bennett *et al.* [Muon G-2 Collaboration], Phys. Rev. D **73** (2006) 072003 [arXiv:hep-ex/0602035].

[17] G. Gabrielse, D. Hanneke, T. Kinoshita, M. Nio and B. Odom, Phys. Rev. Lett. **97** (2006) 030802.

[18] F. Jegerlehner, arXiv:hep-ph/0703125.

[19] W. E. Caswell and G. P. Lepage, Phys. Lett. B **167** (1986) 437.

[20] G. T. Bodwin, E. Braaten and G. P. Lepage, Phys. Rev. D **51** (1995) 1125 [Erratum-ibid. D **55** (1997) 5853] [arXiv:hep-ph/9407339].

[21] N. Brambilla *et al.*, arXiv:hep-ph/0412158.

[22] M. Beneke and V. A. Smirnov, Nucl. Phys. B **522** (1998) 321 [arXiv:hep-ph/9711391].

[23] V. A. Smirnov, *Applied asymptotic expansions in momenta and masses*, Springer Tracts Mod. Phys. **177** (2002) 1.

[24] E. Eichten and B. R. Hill, Phys. Lett. B **234** (1990) 511.

[25] A. Pineda and J. Soto, Nucl. Phys. Proc. Suppl. **64** (1998) 428 [arXiv:hep-ph/9707481].

[26] M. E. Luke, A. V. Manohar and I. Z. Rothstein, Phys. Rev. D **61** (2000) 074025 [arXiv:hep-ph/9910209].

[27] V. B. Berestetskii, E. M. Lifshitz and L. P. Pitaevskii, *Quantum Electrodynamics*, Butterworth-Heinemann, Oxford, 1982.

[28] A. H. Hoang and T. Teubner, Phys. Rev. D **58** (1998) 114023 [arXiv:hep-ph/9801397].

[29] A. H. Hoang and T. Teubner, Phys. Rev. D **60** (1999) 114027 [arXiv:hep-ph/9904468].

[30] K. Melnikov and A. Yelkhovsky, Nucl. Phys. B **528** (1998) 59 [arXiv:hep-ph/9802379].

[31] O. I. Yakovlev, Phys. Lett. B **457** (1999) 170 [arXiv:hep-ph/9808463].

[32] M. Beneke, A. Signer and V. A. Smirnov, Phys. Lett. B **454** (1999) 137 [arXiv:hep-ph/9903260].

[33] T. Nagano, A. Ota and Y. Sumino, Phys. Rev. D **60** (1999) 114014 [arXiv:hep-ph/9903498].

[34] A. A. Penin and A. A. Pivovarov, Nucl. Phys. B **550** (1999) 375 [arXiv:hep-ph/9810496].

[35] I. I. Y. Bigi, M. A. Shifman, N. G. Uraltsev and A. I. Vainshtein, Phys. Rev. D **50** (1994) 2234 [arXiv:hep-ph/9402360].

[36] M. Beneke and V. M. Braun, Nucl. Phys. B **426** (1994) 301 [arXiv:hep-ph/9402364].

[37] M. Beneke, Phys. Lett. B **434** (1998) 115 [arXiv:hep-ph/9804241].

[38] I. I. Y. Bigi, M. A. Shifman, N. Uraltsev and A. I. Vainshtein, Phys. Rev. D **56** (1997) 4017 [arXiv:hep-ph/9704245].

[39] W. A. Bardeen, A. J. Buras, D. W. Duke and T. Muta, Phys. Rev. D **18** (1978) 3998.

[40] A. H. Hoang, A. V. Manohar, I. W. Stewart and T. Teubner, Phys. Rev. D **65** (2002) 014014 [arXiv:hep-ph/0107144].

[41] A. H. Hoang, Phys. Rev. D **69** (2004) 034009 [arXiv:hep-ph/0307376].

[42] A. A. Penin, A. Pineda, V. A. Smirnov and M. Steinhauser, Nucl. Phys. B **699** (2004) 183 [arXiv:hep-ph/0406175].

[43] B. A. Kniehl, A. A. Penin, V. A. Smirnov and M. Steinhauser, Nucl. Phys. B **635** (2002) 357 [arXiv:hep-ph/0203166].

[44] A. A. Penin and M. Steinhauser, Phys. Lett. B **538** (2002) 335 [arXiv:hep-ph/0204290].

[45] A. A. Penin, V. A. Smirnov and M. Steinhauser, Nucl. Phys. B **716** (2005) 303 [arXiv:hep-ph/0501042].

[46] M. Beneke, Y. Kiyo and K. Schuller, Nucl. Phys. B **714** (2005) 67 [arXiv:hep-ph/0501289].

[47] V. S. Fadin and V. A. Khoze, JETP Lett. **46** (1987) 525 [Pisma Zh. Eksp. Teor. Fiz. **46** (1987) 417].

[48] A. H. Hoang and C. J. Reißer, Phys. Rev. D **71** (2005) 074022 [arXiv:hep-ph/0412258].

[49] A. H. Hoang and C. J. Reißer, Phys. Rev. D **74** (2006) 034002 [arXiv:hep-ph/0604104].

[50] R. J. Guth and J. H. Kühn, Nucl. Phys. B **368** (1992) 38.

[51] D. Eiras and M. Steinhauser, Nucl. Phys. B **757** (2006) 197 [arXiv:hep-ph/0605227].

[52] F. A. Chishtie and V. Elias, Phys. Lett. B **521** (2001) 434 [arXiv:hep-ph/0107052].

[53] J. C. Collins, A. V. Manohar and M. B. Wise, Phys. Rev. D **73** (2006) 105019 [arXiv:hep-th/0512187].

[54] D. Binosi and L. Theussl, Comput. Phys. Commun. **161** (2004) 76 [arXiv:hep-ph/0309015].

[55] W. H. Furry, Phys. Rev. **51** (1937) 125.

[56] C. Itzykson and J. B. Zuber, *Quantum Field Theory*, McGraw-Hill, New York, 1980.

[57] P. Baikov, private communication.

[58] P. Nogueira, J. Comput. Phys. **105** (1993) 279.

[59] T. Seidensticker, unpublished.

[60] R. Harlander, T. Seidensticker and M. Steinhauser, Phys. Lett. B **426** (1998) 125 [arXiv:hep-ph/9712228].

[61] T. Seidensticker, arXiv:hep-ph/9905298.

[62] M. Steinhauser, Comput. Phys. Commun. **134** (2001) 335 [arXiv:hep-ph/0009029].

[63] K. G. Chetyrkin and F. V. Tkachov, Nucl. Phys. B **192** (1981) 159.

[64] P. A. Baikov, Phys. Lett. B **385** (1996) 404 [arXiv:hep-ph/9603267].

[65] P. A. Baikov, Nucl. Instrum. Meth. A **389** (1997) 347 [arXiv:hep-ph/9611449].

[66] V. A. Smirnov and M. Steinhauser, Nucl. Phys. B **672** (2003) 199 [arXiv:hep-ph/0307088].

[67] S. Laporta and E. Remiddi, Phys. Lett. B **379** (1996) 283 [arXiv:hep-ph/9602417].

[68] S. Laporta, Int. J. Mod. Phys. A **15** (2000) 5087 [arXiv:hep-ph/0102033].

[69] P. Marquard and D. Seidel, unpublished.

[70] G. Källen and A. Sarby, K. Dan. Vidensk. Selsk. Mat.-Fis. Medd. 29, N17 (1955) 1.

[71] A. Czarnecki and K. Melnikov, Phys. Rev. Lett. **80** (1998) 2531 [arXiv:hep-ph/9712222].

[72] M. Beneke, A. Signer and V. A. Smirnov, Phys. Rev. Lett. **80** (1998) 2535 [arXiv:hep-ph/9712302].

[73] B. A. Kniehl, A. A. Penin, M. Steinhauser and V. A. Smirnov, Phys. Rev. Lett. **90** (2003) 212001 [Erratum-ibid. **91** (2003) 139903(E)] [arXiv:hep-ph/0210161].

[74] K. G. Chetyrkin, J. H. Kühn and M. Steinhauser, Comput. Phys. Commun. **133** (2000) 43 [arXiv:hep-ph/0004189].

[75] J. H. Kühn, A. A. Penin and A. A. Pivovarov, Nucl. Phys. B **534** (1998) 356 [arXiv:hep-ph/9801356].

[76] A. A. Penin and A. A. Pivovarov, Phys. Lett. B **435** (1998) 413 [arXiv:hep-ph/9803363].

[77] A. A. Penin and A. A. Pivovarov, Nucl. Phys. B **549** (1999) 217 [arXiv:hep-ph/9807421].

[78] K. Melnikov and A. Yelkhovsky, Phys. Rev. D **59** (1999) 114009 [arXiv:hep-ph/9805270].

[79] C. Anastasiou and A. Lazopoulos, JHEP **0407** (2004) 046 [arXiv:hep-ph/0404258].

[80] G. 't Hooft and M. J. G. Veltman, Nucl. Phys. B **44** (1972) 189.

[81] P. Breitenlohner and D. Maison, Commun. Math. Phys. **52** (1977) 11.

[82] W. Bernreuther, R. Bonciani, T. Gehrmann, R. Heinesch, T. Leineweber and E. Remiddi, Nucl. Phys. B **723** (2005) 91 [arXiv:hep-ph/0504190].

[83] S. A. Larin, Phys. Lett. B **303** (1993) 113 [arXiv:hep-ph/9302240].

[84] W. Bernreuther, R. Bonciani, T. Gehrmann, R. Heinesch, T. Leineweber, P. Mastrolia and E. Remiddi, Nucl. Phys. B **712** (2005) 229 [arXiv:hep-ph/0412259].

[85] A. H. Hoang and P. Ruiz-Femenía, Phys. Rev. D **73** (2006) 014015 [arXiv:hep-ph/0511102].

[86] E. Braaten and S. Fleming, Phys. Rev. D **52** (1995) 181 [arXiv:hep-ph/9501296].

[87] W. Bernreuther, R. Bonciani, T. Gehrmann, R. Heinesch, P. Mastrolia and E. Remiddi, Phys. Rev. D **72** (2005) 096002 [arXiv:hep-ph/0508254].

[88] A. I. Onishchenko and O. L. Veretin, arXiv:hep-ph/0302132.

[89] N. Gray, D. J. Broadhurst, W. Grafe and K. Schilcher, Z. Phys. C **48** (1990) 673.

[90] D. J. Broadhurst, N. Gray and K. Schilcher, Z. Phys. C **52** (1991) 111.

[91] R. Delbourgo and V. B. Prasad, J. Phys. G **1** (1975) 377.

[92] W. Siegel, Phys. Lett. B **84** (1979) 193.

[93] D. M. Capper, D. R. T. Jones and P. van Nieuwenhuizen, Nucl. Phys. B **167** (1980) 479.

[94] W. Siegel, Phys. Lett. B **94** (1980) 37.

[95] D. Stöckinger, JHEP **0503** (2005) 076 [arXiv:hep-ph/0503129].

[96] W. Hollik and D. Stöckinger, Phys. Lett. B **634** (2006) 63 [arXiv:hep-ph/0509298].

[97] I. Jack, D. R. T. Jones and K. L. Roberts, Z. Phys. C **62** (1994) 161 [arXiv:hep-ph/9310301].

[98] R. V. Harlander, D. R. T. Jones, P. Kant, L. Mihaila and M. Steinhauser, JHEP **0612** (2006) 024 [arXiv:hep-ph/0610206].

[99] J. C. Collins, *Renormalization*, Cambridge University Press, Cambridge, 1984.

[100] M. E. Peskin and D. V. Schroeder, *An Introduction to Quantum Field Theory*, Westview Press, Boulder, 1995.

[101] I. Jack, D. R. T. Jones, S. P. Martin, M. T. Vaughn and Y. Yamada, Phys. Rev. D **50** (1994) 5481 [arXiv:hep-ph/9407291].

[102] R. Harlander, P. Kant, L. Mihaila and M. Steinhauser, JHEP **0609** (2006) 053 [arXiv:hep-ph/0607240].

[103] J. A. M. Vermaseren, S. A. Larin and T. van Ritbergen, Phys. Lett. B **405** (1997) 327 [arXiv:hep-ph/9703284].

[104] R. Z. Roskies, E. Remiddi and M. J. Levine in *Quantum Electrodynamics*, edited by T. Kinoshita, World Scientific, Singapore, 1990.

[105] L. F. Abbott, Nucl. Phys. B **185** (1981) 189.

[106] L. F. Abbott, Acta Phys. Polon. B **13** (1982) 33.

[107] T. van Ritbergen, A. N. Schellekens and J. A. M. Vermaseren, Int. J. Mod. Phys. A **14** (1999) 41 [arXiv:hep-ph/9802376].

[108] T. Kinoshita and M. Nio, Phys. Rev. D **73** (2006) 013003 [arXiv:hep-ph/0507249].

[109] D. J. Broadhurst, Z. Phys. C **54** (1992) 599.

[110] J. S. Schwinger, Phys. Rev. **73** (1948) 416.

[111] A. Petermann, Helv. Phys. Acta **30** (1957) 407.

[112] C. M. Sommerfield, Phys. Rev. **107** (1957) 328.

[113] W. M. Yao *et al.* [Particle Data Group], J. Phys. C **33** (2006) 1, URL: http://pdg.lbl.gov.

[114] R. Escribano and E. Massó, Nucl. Phys. B **429** (1994) 19 [arXiv:hep-ph/9403304].

[115] W. Bernreuther, R. Bonciani, T. Gehrmann, R. Heinesch, T. Leineweber, P. Mastrolia and E. Remiddi, Phys. Rev. Lett. **95** (2005) 261802 [arXiv:hep-ph/0509341].

[116] J. Fleischer and O. V. Tarasov, Phys. Lett. B **283** (1992) 129.

[117] S. Laporta and E. Remiddi, Phys. Lett. B **301** (1993) 440.

[118] S. Laporta and E. Remiddi, Phys. Lett. B **265** (1991) 182.

[119] J. Heitger, A. Juttner, R. Sommer and J. Wennekers [ALPHA Collaboration], JHEP **0411** (2004) 048 [arXiv:hep-ph/0407227].

[120] E. Eichten and B. R. Hill, Phys. Lett. B **243** (1990) 427.

[121] A. F. Falk, B. Grinstein and M. E. Luke, Nucl. Phys. B **357** (1991) 185.

[122] B. A. Ovrut and H. J. Schnitzer, Nucl. Phys. B **179** (1981) 381.

[123] A. Czarnecki and A. G. Grozin, Phys. Lett. B **405** (1997) 142 [arXiv:hep-ph/9701415].

[124] A. G. Grozin and M. Neubert, Nucl. Phys. B **508** (1997) 311 [arXiv:hep-ph/9707318].

[125] G. Amorós, M. Beneke and M. Neubert, Phys. Lett. B **401** (1997) 81 [arXiv:hep-ph/9701375].

[126] K. G. Chetyrkin and A. G. Grozin, Nucl. Phys. B **666** (2003) 289 [arXiv:hep-ph/0303113].

[127] A. G. Grozin, arXiv:hep-ph/0008300.

[128] A. G. Grozin, Springer Tracts Mod. Phys. **201** (2004) 1.

[129] P. A. Baikov and V. A. Smirnov, Phys. Lett. B **477** (2000) 367 [arXiv:hep-ph/0001192].

[130] J. A. M. Vermaseren, arXiv:math-ph/0010025, URL: http://www.nikhef.nl/~form.

[131] C. Bauer, A. Frink and R. Kreckel, arXiv:cs.sc/0004015.

[132] R. H. Lewis, *Fermat's User Guide*, URL: http://www.bway.net/~lewis.

[133] M. Tentyukov and J. A. M. Vermaseren, arXiv:cs.sc/0604052.

[134] K. G. Chetyrkin, M. Faisst, C. Sturm and M. Tentyukov, Nucl. Phys. B **742** (2006) 208 [arXiv:hep-ph/0601165].

[135] V. A. Smirnov, Phys. Lett. B **460** (1999) 397 [arXiv:hep-ph/9905323].

[136] J. B. Tausk, Phys. Lett. B **469** (1999) 225 [arXiv:hep-ph/9909506].

[137] L. M. Brown and R. P. Feynman, Phys. Rev. **85** (1952) 231.

[138] V. A. Smirnov, *Evaluating Feynman integrals*, Springer Tracts Mod. Phys. **211** (2004).

[139] H. Cheng and T. T. Wu, *Expanding Protons: Scattering at High Energies*, MIT Press, Cambridge, MA, 1987.

[140] C. Anastasiou and A. Daleo, JHEP **0610** (2006) 031 [arXiv:hep-ph/0511176].

[141] M. Czakon, Comput. Phys. Commun. **175** (2006) 559 [arXiv:hep-ph/0511200].

[142] A. I. Davydychev and M. Y. Kalmykov, Nucl. Phys. B **699** (2004) 3 [arXiv:hep-th/0303162].

[143] M. Y. Kalmykov and O. Veretin, Phys. Lett. B **483** (2000) 315 [arXiv:hep-th/0004010].

[144] S. Moch and P. Uwer, Comput. Phys. Commun. **174** (2006) 759 [arXiv:math-ph/0508008].

[145] S. Groote, J. G. Körner and A. A. Pivovarov, Eur. Phys. J. C **36** (2004) 471 [arXiv:hep-ph/0403122].

[146] S. Laporta and E. Remiddi, Phys. Lett. B **356** (1995) 390.

[147] B. A. Kniehl and A. A. Penin, Nucl. Phys. B **577** (2000) 197 [arXiv:hep-ph/9911414].

[148] A. V. Manohar and I. W. Stewart, Phys. Rev. D **63** (2001) 054004 [arXiv:hep-ph/0003107].

[149] M. Peter, Nucl. Phys. B **501** (1997) 471 [arXiv:hep-ph/9702245].

[150] Y. Schröder, Phys. Lett. B **447** (1999) 321 [arXiv:hep-ph/9812205].

[151] O. V. Tarasov, A. A. Vladimirov and A. Y. Zharkov, Phys. Lett. B **93** (1980) 429.

[152] S. A. Larin and J. A. M. Vermaseren, Phys. Lett. B **303** (1993) 334 [arXiv:hep-ph/9302208].

# Acknowledgements

First of all, I would like to thank my supervisors Prof. Bernd Kniehl and Prof. Matthias Steinhauser for giving me the opportunity to work on this interesting topic. In particular, I thank Prof. Steinhauser for numerous discussion through which I have learned a lot about particle physics in general and multi-loop calculations in particular. I thank Prof. Jochen Bartels for agreeing to be the second referee for the disputation.

I am indebted to Stefan Bekavac, Joachim Brod, Martin Främke, Alexander Kune and Peter Marquard for carefully reading parts of the manuscript.

I thank Andrey Grozin, Peter Marquard, Luminita Mihaila, Andrei Onishchenko and Dirk Seidel for fruitful collaborations. I am grateful to Pavel Baikov, Mikhail Kalmykov and Vladimir Smirnov for helpful discussions and useful advice.

Throughout my dissertation, I have profited a lot from discussions (not always about physics) with several colleagues. In particular, I am thankful to Stefan Bekavac, Joachim Brod, Michael Faisst, Frank Fugel, Philipp Kant, Torben Kneesch, Philipp Maierhöfer, Falk Metzler, Andreas Scharf, Markus Schulze and Florian Schwennsen. Furthermore, I thank all members of the II. Institut für Theoretische Physik in Hamburg and the Institut für Theoretsiche Teilchenphysik in Karlsruhe for creating a very pleasant and inspiring working environment.

Last, but certainly not least, möchte ich mich bei meiner ganzen Familie, insbesondere bei meinen Eltern und meinem Bruder, und meinen Freunden für die andauernde Unterstützung während meines gesamten Studiums bedanken.